FATIGUE RESISTANCE OF ASPHALT MIXTURES AFFECTED BY WATER VAPOR MOVEMENT

A Dissertation

by

YUNWEI TONG

Submitted to the Office of Graduate and Professional Studies of
Texas A&M University
in partial fulfillment of the requirements for the degree of

DOCTOR OF PHILOSOPHY

Chair of Committee,	Robert L. Lytton
Committee Members,	Dallas. N. Little
	Jon A. Epps
	Anastasia Muliana
	Rong Luo
Head of Department,	Robin Autenrieth

December 2013

Major Subject: Civil Engineering

ABSTRACT

This dissertation has two key objectives: the first objective is to develop a method of predicting and quantifying the amount of water that can enter into a pavement system by vapor transport; the second objective is to identify to which extent the fatigue crack growth of pavement would result from such moisture accumulation. To fulfill these two objectives, a diffusion model was first established to illustrate the wetting process of the surface asphalt layer due to the vapor migration from subgrade soil into the upper layer. Secondly, in order to quantify the degree of moisture damage induced by water vapor diffusion, fine aggregate mixture specimens were fabricated and conditioned at different levels of relative humidity in closed vacuum desiccators that allows little temperature fluctuation. Moreover, the moisture conditioned specimens were tested using a newly developed repeated direct tension test method to evaluate the fatigue crack growth. The RDT test greatly reduced the stress state complexity within the specimens by evenly distributing stress over the cross section area of the cylindrical specimen. Compared to the previous torsional test, the newly proposed test protocol was more efficient in characterizing the moisture susceptibility of the asphalt mixture. A major finding in this dissertation is that the higher level of RH in as asphalt surface layer will induce significantly higher crack growth rates.

ACKNOWLEDGEMENTS

I would like to take this opportunity to express my deepest appreciation to my committee chair, Dr. Robert L. Lytton, for his continued support in my research. Dr. Lytton's enthusiastic and serious attitude towards research set up a lift-time example for me. I would have never realized my potential or developed a strong passion to be a researcher in the area of pavement material characterization and modeling without Dr. Lytton's long-term support. My appreciation also goes to my committee members, Dr. Dallas N. Little, Dr. Jon A. Epps, Dr. Anastasia Muliana and Dr. Rong Luo, for their guidance and support throughout the course of this research. It has been a privilege and pleasure to work with all of them.

Many thanks go to all my friends at Texas A&M University for their encouragement, willingness to help and support. My sincere appreciation to Jeff Perry for the many hours of lab testing with me. I also thank my colleagues and friends who have supported me throughout the process, especially Xue Luo and Yuqing Zhang for helping me develop my technology skills.

Finally, thanks to my parents for their encouragement and to my wife for her love and patience.

NOMENCLATURE

AC	Asphalt Concrete
ASCE	American Society of Civil Engineer
CAM	Christensen Anderson Marasteanu
DMA	Dynamic Mechanical Analyzer
DPSE	Dissipated Pseudo Strain Energy
FAM	Fine Aggregate Mix
FFT	Fast Fourier Transform
HMA	Hot Mix Asphalt
MRL	Materials Reference Library
pF	Unit of Suction
PG	Performance Graded
RDT	Repeated Direct Tension
RH	Relative Humidity
RPSE	Recoverable Pseudo Strain Energy
SGC	Superpave Gyratory Compactor
SHRP	Strategic Highway Research Program
TRB	Transportation Research Board
TI	Thornthwaite Index
TXDOT	Texas Department of Transportation
WMA	Warm Asphalt Mix

TABLE OF CONTENTS

Page

LIST OF FIGURES

Page

LIST OF TABLES

Page

CHAPTER I

INTRODUCTION

Asphalt concrete is a composite material composed of binder, aggregates and air, and can be considered as a particular composite with two dominant phases: relatively coarse aggregates and a matrix phase comprised of asphalt mastic and air. Asphalt mastic, which is significantly softer than the coarse aggregate phase, coats and bonds these granular particles together and provides tensile strength to the composite. However, because the affinity of the aggregates for water is far greater than it is for the asphalt binder, the presence of moisture tends to soften the asphalt mastic and strip the asphalt binder from the aggregate surface, which significantly reduces the tensile strength of asphalt mixture and consequently accelerates the pavement deterioration. Moisture damage, which is influenced by a variety of factors such as: materials types, mixture design, environment and traffic, can be defined as progressive degradation of asphalt mixture material due to the presence of water. The occurrence of moisture damage in asphalt material is a rather complex phenomenon, which involves chemical, physical, mechanical and thermodynamic processes (Caro et al. 2008a). Moisture damage generally occurs either within the asphalt mastic (cohesive failure) due to water weakening the material or it can occur at the asphalt-aggregate interface (adhesive failure) by water penetrating into the asphalt-aggregate interface (Lytton et al. 2005). Since the asphalt mastic acts as glue to coat and bond the coarse aggregate together, subsequently, in order for the moisture to reach the interface between the coarse

aggregates and asphalt, water must work its way through the matrix phase at first. Therefore, it is believed that the moisture damage initiates with the asphalt mastic weakening and then water progresses into the asphalt-aggregate interface to induce adhesive failure.

Moisture damage starts with the water transport into the pavement systems. It is generally agreed upon that water enters a pavement system by two major mechanisms: 1) surface water percolates into the pavement system, and 2) subsurface water is drawn up into a pavement system by capillary rise (Masad et al. 2007). In addition to the above two commonly accepted mechanisms, there is another important mechanism of transporting water into the pavement, which is by subsurface vapor diffusion. Although it remains unclear to what extent the permeation of water vapor from the subsurface will affect the asphalt mixture performance, the moisture vapor in asphalt mixture plays an essential role in inducing moisture related premature degradation. For example, the pavement distress survey conducted by Hicks (1991) indicates that 30% to 50% of the pavements in the state of Arizona have experienced moisture-related distress such as premature rutting, cracking and raveling although Arizona has a semiarid/desert climate. Specifically, stripping of the asphalt pavement after the placement of a seal coat has occurred on approximately 50% of the asphalt pavements in Arizona, which could potentially be a result of water vapor build-up in the asphalt layer beneath the seal coat. Another example of the water-vapor-induced moisture damage has been identified in the state of Washington, where severe stripping was observed after a seal coat was placed, which was due to the moisture accumulation in the underlying asphalt layer (Kandhal et

al. 1989, Kandhal and Rickards 2001) Although water vapor in the pavement surface layer produces moisture damage, little information is available that addresses the movement of moisture in the vapor phase into the pavement system and its destructive effects on pavement performance.

Fatigue cracking is the most common distress in asphalt pavement. Numerous research has been conducted by different researchers to estimate the fatigue life of pavement. It is found that three major approaches were adopted widely by researchers to model the development of fatigue cracking. The first one is commonly used strain-based models, which uses a relation between the radial strain at the bottom of the asphalt concrete layer and the number of load applications to crack appearance in the pavement. The representative research for the strain-based modeling was conducted by Monismith et al (1971). At that time, this research was essential in modeling the fatigue cracking in the laboratory. The second approach is the dissipated energy approach introduced by Van Dijk (1977). This approach is still a phenomenal method, which requires statistical regression analysis. The third is the fracture and damage mechanics based method, which adopted the fundamental concept from mechanics and make necessary modification for different materials. This approach is the most promising approach since it can offer a consistent indication of the fatigue cracking in the specimens. Therefore, this research adopts the fracture mechanics based approach in evaluating the fatigue cracking of asphalt mixture. The detailed formulations is discussed in the Chapter V. However, it has to be recognized that some shift factors have to be adopted to calibrate these models based on observed field performance. Ideally laboratory fatigue tests

should simulate field conditions, however, this is impossible to do in the real life. The reason is that there are so many variables in the field that cannot be easily considered in laboratory testing, such as specimen fabrication, compound loading, random rest periods, and the multi stress state. Some laboratory tests simulate some of these variables but not all of them at the same time (Ghuzlan and Carpenter 2002).

Warm-mix asphalt (WMA) represents a group of technologies that allow reduced mixing and placement temperatures thereby enabling reduced fuel consumption, enhanced compaction, increased economical haul distances and an extended paving season. WMA technologies can be broadly grouped into two categories: 1) *Chemical Modifiers* that rely on a variety of different mechanisms, such as surfactants to help coat the aggregate at lower temperatures or waxes that decrease the viscosity above their melting point; and 2) *Foaming Processes* that introduce small amounts of water into the plant that turns into steam, expanding the binder phase and reducing mix viscosity (Estakhri, et al. 2010). Warm-mix asphalt is usually produced at temperatures 20 C° to 50 C° lower than hot-mix asphalt. As a result, this decrease in temperature reduces the binder aging during the production and hence increases the resistance of asphalt mixture to fatigue cracking. However, lower mixing temperature reduces the binder absorption into aggregate and thus makes the water much easier to penetrate into the asphalt-aggregate interface, which leads to the reduction of bonding between aggregate and asphalt and consequently makes the WMA more susceptible to the moisture damage. Furthermore, both the Foaming and Evotherm DAT technologies discussed in this dissertation introduce water into the mixture during the production process. Although it

is generally assumed that the water foaming effect disappears due to the evaporation in four hours after the production, it is highly possible that moisture can be trapped in mixture without access to escape. As a consequence, the existence of moisture in the mixtures tends to intensify the stripping of asphalt binder from the aggregate surface, and thus can accelerate the fatigue cracking propagation in WMA.

From the financial perspective, the degradation of asphalt pavements induced by the moisture in the U.S. results in additional vehicle costs over $54 billion annually (Copeland 2005, Abu Al-Rub et al. 2010). Considering the increased pressure that the DOT agencies are facing due to the shortfall in transportation funding, the demand for the asphalt pavement to perform as expected with minimal moisture related premature failure becomes more and more pressing. Conversely, more than 42 million tons of WMA have been placed in 2011 without a fundamental understanding of its moisture-related performance. Therefore, for the purpose of accurately evaluate the performance of WMA and later incorporate it as a sustainable alternative into the roadway industry, a systematic study of the moisture susceptibility and fatigue resistance of WMA is necessary.

Objectives and Tasks

The goal of this research is to address the problems mentioned above pertaining to the modeling of moisture transport in pavement systems and quantifying its destructive effects on asphalt mixtures. The research will focus on achieving the following objectives:

1) Develop a water vapor diffusion model in pavement systems to characterize the vapor transport in pavement;
2) Design an lab experiment to moisture condition FAM based on the proposed water vapor diffusion model;
3) Develop a controlled-stress RDT test method and perform these tests on the FAM specimens using the DMA;
4) Apply a mechanistic based approach to analyze the fatigue crack growth for both dry and moisture conditioned specimens;
5) Apply this new test and data analysis method to the WMA to evaluate its moisture susceptibility.
6) Validate this mechanistic based approach by testing a different set of specimens using a different testing method.

TASK 1. Conduct Information Search

The objective of this task is to conduct an extensive literature review to gather information on available water transport models and current moisture susceptibility evaluation methods. This research performed literature searches on the following aspects:

1) Methods for the modeling of water movement in pavement;
2) Current moisture conditioning methods for asphalt mixtures;
3) Testing protocols and procedures used to evaluate the moisture susceptibility of asphalt mixture;
4) Effects of moisture on the fracture performance of the asphalt mixtures.

TASK 2. Establish Moisture Diffusion Model in Pavement

A model has been developed in this task to relate the water vapor diffusion to the pavement wetting process and to demonstrate water vapor movement in pavements. This model will help better understand the water presence in pavements and will provide a method of incorporating water vapor diffusion in pavement design. The following developments and modifications are taken into accounts during the modeling:

1) Develop a water vapor diffusion model based on the Fick's second law;
2) Water vapor diffusion coefficient will be modeled and incorporated into the model;
3) Determine the relative humidity in pavement;
4) Develop a model to account for the wind effect on the relative humidity development in pavement.

TASK 3. Develop Experimental Design

The objective of this task is to develop a comprehensive laboratory experiment plan corresponding to the developed water diffusion model for pavement. Furthermore, the experimental plan will be used to characterize the material properties of asphalt mixture. This experiment plan will consider a number of variables in the experiment, including binders, aggregates, WMA additives and levels of relative humidity. Specifically, the following work will be conducted:

1) Prepare materials including aggregates, binder and WMA additives, and fabricate asphalt mixtures specimens in the lab;

2) Design a moisture condition method corresponding to the developed water vapor diffusion model in pavement
3) Perform the laboratory tests according to the testing protocol designed in Task 4 on different asphalt mixtures that vary by asphalt binder, aggregate, WMA additives and levels of RH;
4) Conduct performance tests, predict the testing results using the proposed models and validate the models based on the comparisons between modeling and testing.

TASK 4. Testing Protocols Design

The objectives of this task are to provide a systematic testing protocol and analyzing formulations to rapidly and accurately evaluate the moisture susceptibility of asphalt mixtures. The following is the proposed testing protocols:

1) A controlled-stress RDT test protocol will be developed to perform the tests using the DMA;
2) Both nondestructive and destructive RDT laboratory tests will be conducted in sequence on WMA and HMA specimens as planned. Corresponding fracture properties of the specimens as the Paris' Law coefficients, damage density and crack size distribution will be determined based on the test data.
3) Validate this newly developed RDT by conducting a different test on a set of different specimens.

TASK 5. Document Findings and Recommendations

All findings and recommendations of this study, including the literature review, theoretical development, experimental design, test protocol and data analysis, will be

documented in the Ph.D. Dissertation. The major research findings will be summaries in a number of technical papers for presentation in international conferences and for potential publication in learned scientific journals.

Dissertation Outline

This dissertation is composed of seven chapters. Chapter I discusses the importance of the moisture damage, details the research objective and each individual tasks, and provides the general framework for this research.

Chapter II delivers a literature review on moisture damage including a discussion of the current status of the moisture damage in U.S., factors that influence moisture damage, the mechanisms of moisture transport, the modes of moisture damage, the available treatments used to alleviate moisture damage, and the current laboratory tests used to assess moisture damage.

Chapter III provides details about the specimens fabrication process including the material used to prepare the asphalt mix samples in the laboratory, the mix design and gradations, the mixing and compaction procedures and the In addition, Chapter III includes the details about the air void measurements in the laboratory.

The mechanisms of water transport by diffusion are discussed in Chapter IV, including the laboratory measurements of water vapor diffusivity, the suction model used to establish the relative humidity profile in the pavement and the wind influence on the relative humidity profile in pavement. In addition, the laboratory setup for the specimens' moisture conditioning is discussed in this chapter.

Chapter V details the development of the mechanistic based fracture model for fine aggregate mixture testing. The formulation of fatigue crack growth subject to repeated direct tension is established to determine the mean crack radius at every load cycle of the RDT test. The test protocols required to obtain all the required parameters to the model, and the comparison of the mixtures according to the Paris' Law fracture parameters are presented in this chapter.

Chapter VI. A different set of specimens were tested to validate the fracture model are included in Chapter VII.

Finally, Chapter VIII summarizes the main findings, provides conclusions and recommendations, and includes proposed future research work.

CHAPTER II

BACKGROUND ON MOISTURE DAMAGE

An extensive literature review is presented in this chapter to gather information on the magnitude of moisture damage in U.S., the inherent reasons of moisture damage, the available water transport models and current moisture susceptibility evaluation methods.

The Extent of Moisture Damage

Moisture damage is a national issue. In 2004, the Colorado Department of Transportation conducted a survey of 55 agencies in U.S. and it is found that moisture damage is a concern in majority of the surveyed agencies. As illustrated in the Figure 1, more than 80% of the agencies reported moisture related damage in pavement (Hicks et al. 2003).

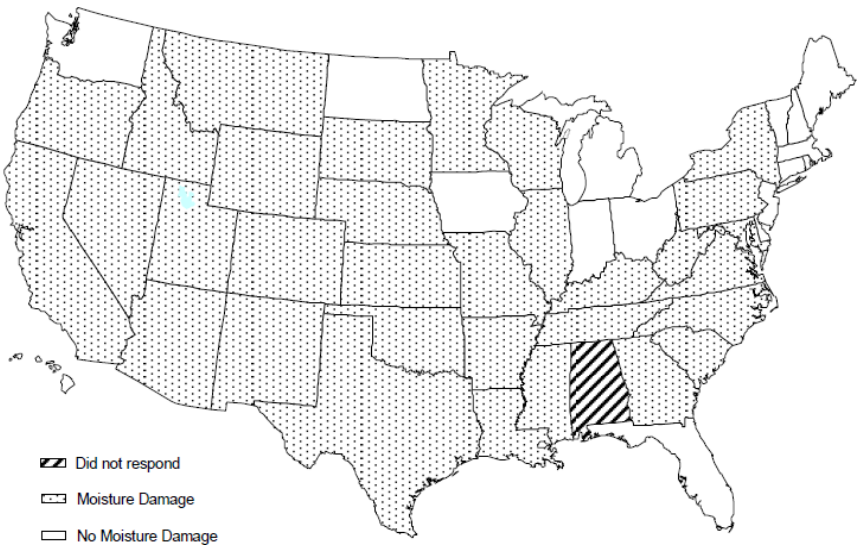

Figure 1. Extent of Moisture Damage in U.S.

As shown in the Figure 2, approximately 40% of the surveyed agencies reported that more than 30% of their pavement experienced moisture related distress and another 40% of agencies experienced 10% to 20 percent of moisture damage. This survey further demonstrated that moisture damage is a national topic even if it is in the arid area such as Arizona and west Texas.

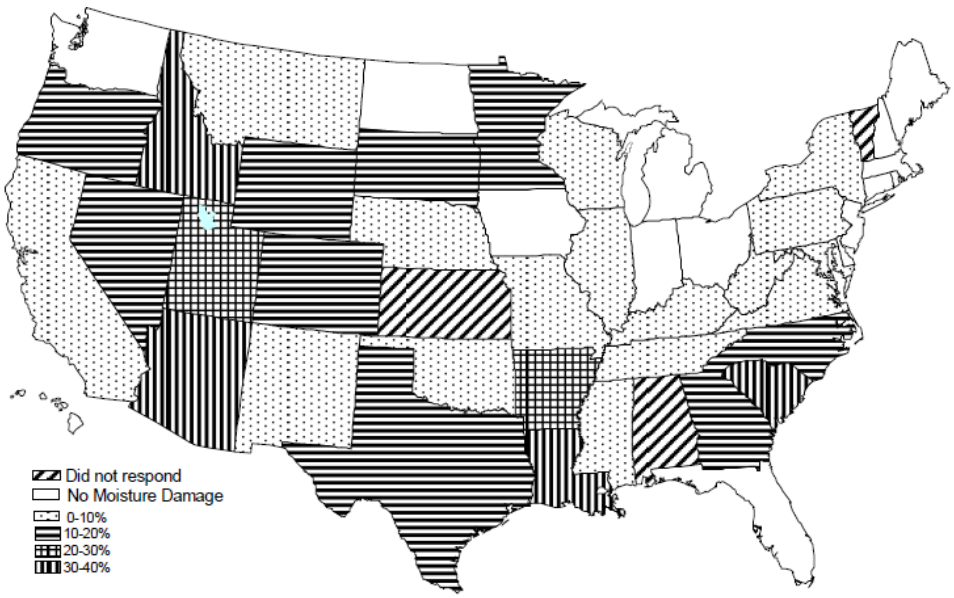

Figure 2. Percent of Pavement Experiencing Moisture Related Distress

As show in the Figure 3, the survey results revealed that 82% of the agencies require some sort of anti-strip treatment. Of those that treat, 56% treat with liquids, 15% with liquid or lime, and 29% with lime.

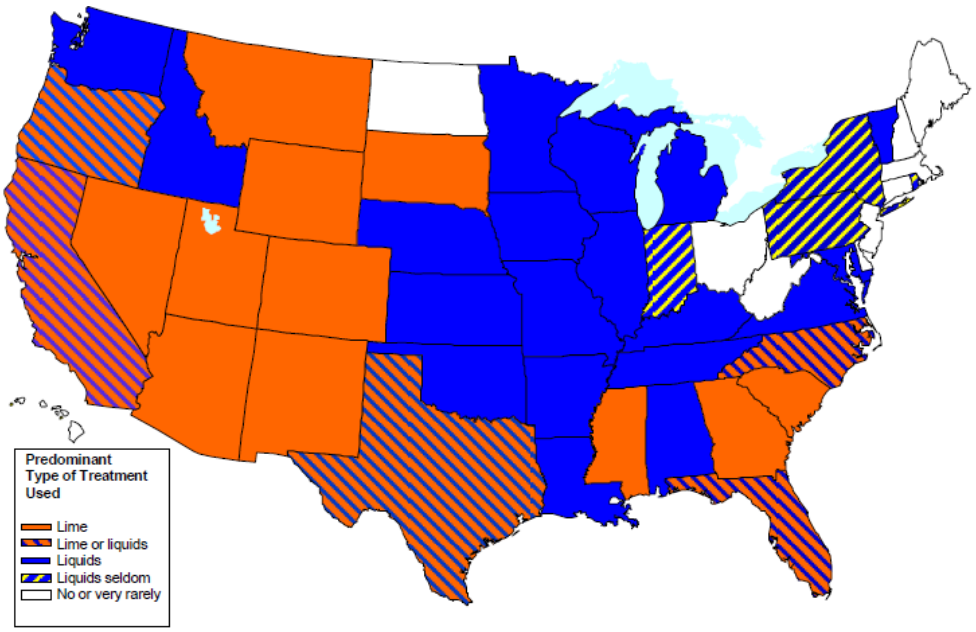

Figure 3. Treatment for Moisture Damage

As demonstrated in the Figure 4, majority of the states adopts the tensile test (AASHTO T283, ASTM D4867, or similar) to characterize the moisture susceptibility of asphalt mixture. Approximately, 10% of the state uses the compressive test for moisture susceptibility evaluation (Hicks et al. 2003).

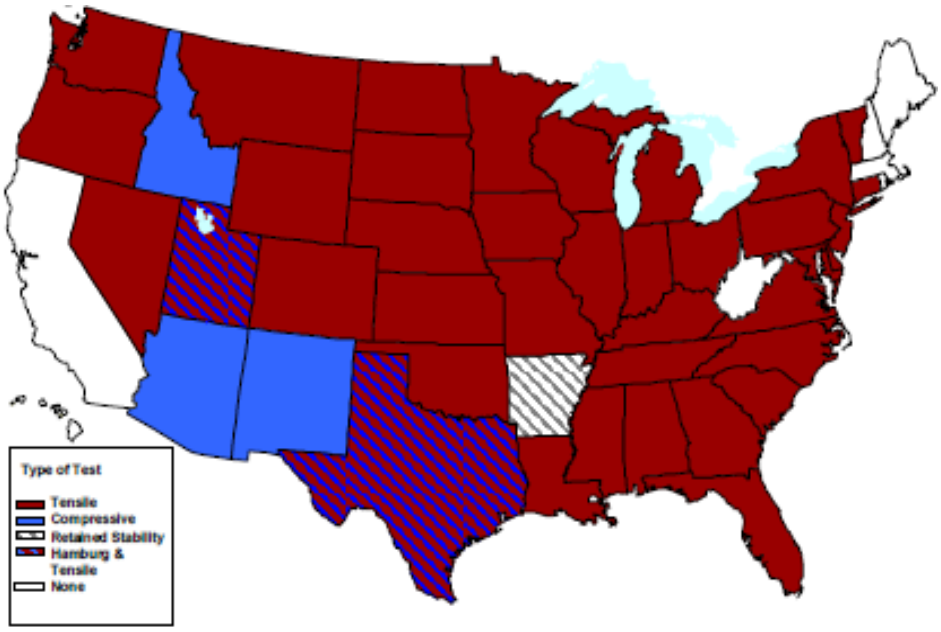

Figure 4. Characterization of Moisture Damage

The Intrinsic Reasons for Moisture Damage

The reason that water can work its way into the surface between asphalt and aggregate stems from fundamental concept called surface energy.

Surface energy quantifies the disruption of intermolecular bonds that occur when a surface is created. To simplify, the surface energy in a thermodynamic sense is the reversible work required to create a unit area of new surface. For example, a material of unit cross sectional area is subjected to a tensile stress and if this material is entirely brittle, the energy consumed on the sample is dissipated only through propagation of a crack by creating two new surfaces.

Therefore, a tensile force can be applied to divide the materials into dissimilar parts. For a completely brittle interface of unit cross sectional area, the energy expended

is the sum of the individual surface energies for the two materials involved, minus an interfacial energy (Pocius 1997). Dupré, in 1867, proposed the following formulas for computing work of adhesion and Gibbs free energy of adhesion between two materials.

$$W^a = \gamma_i + \gamma_j - \gamma_{ij} \quad (1)$$

where, W^a is the work of adhesion, γ_i is the surface energy of the *ith* material and γ_{ij} is the interfacial energy between the two materials in contact.

Following the form suggested by Fowkes (Fowkes 1964), the surface energy of a single phase is given by,

$$\gamma_i = \gamma_i^{LW} + \gamma_i^{AB} \quad (2)$$

where, LW denotes Lifshitz-van der Waals, and AB denotes acid-base.

It follows that the free energy of cohesion and adhesion likewise constitutes two components. Therefore, the Gibbs free energy of cohesion is,

$$\Delta G_i^c = -2\gamma_i = \Delta G_i^{cLW} + \Delta G_i^{cAB} \quad (3)$$

And the Gibbs free energy of adhesion is,

$$\Delta G_{ij}^a = \gamma_{ij} - \gamma_i - \gamma_i = \Delta G_{ij}^{aLW} + \Delta G_{ij}^{aAB} \quad (4)$$

The van der Waals forces represent the interaction between two symmetric molecules. For the LW component, the Berthelot geometric mean rule therefore holds,

$$\Delta G_{ij}^{aLW} = -2\sqrt{\gamma_i^{LW}\gamma_j^{LW}} \quad (5)$$

The AB component cannot be treated in the same, and was derived empirically by Van Oss et al. (*23*),

$$\Delta G_{ij}^{aAB} = -2\left(\sqrt{\gamma_i^+ \gamma_j^-} + \sqrt{\gamma_i^- \gamma_j^+}\right) \quad (6)$$

Van Oss and his co-workers presented the full version of the Young-Dupré equation by inserting ΔG^{LW} and ΔG^{AB},

$$-\Delta G^a = W^a = \gamma_L^{Tot}(1+\cos(\theta)) = 2\left(\sqrt{\gamma_L^{LW}\gamma_S^{LW}} + \sqrt{\gamma_L^+\gamma_S^-} + \sqrt{\gamma_L^-\gamma_S^+}\right) \quad (7)$$

where, L represents the liquid and S the solid under consideration. Equation (13) allows three unknown surface energy components to be solved for if the contact angles of three liquids with different and known polarities are measured on the unknown surface. These polarities have been defined as monopolar basic, monopolar acidic, bipolar (basic and acidic), or apolar.

If the surface energy components for each individual material is known, this principal has a significant practical application in predicting the work of adhesion between two materials such as asphalt and aggregate. Correspondingly, the cohesive energy can be predicted within the asphalt. By adapting the Dupré equation, the adhesive bond energy between asphalt and aggregate in the presence of water is:

$$\Delta G_{ikj} = \gamma_{ij} - \gamma_{ik} - \gamma_{jk} \quad (8)$$

where, subscript i refers to asphalt, j refers to aggregate, and k refers to water. With the components of the free energy of interfacial interaction additive, the adhesive bond energy is computed as:

$$\Delta G_{ikj}^a = \Delta G_{ikj}^{aLW} + \Delta G_{ikj}^{aAB} \quad (9)$$

Van Oss et al. (1988 and 1991) proposed the following complete formula to compute the adhesive bond energy between asphalt and aggregate in the presence of water.

$$\Delta G_{ikj}^{a} = 2\left[\begin{array}{l}\sqrt{\gamma_i^{LW}\gamma_k^{LW}} + \sqrt{\gamma_j^{LW}\gamma_k^{LW}} - \sqrt{\gamma_i^{LW}\gamma_j^{LW}} - \gamma_k^{LW} + \\ \sqrt{\gamma_k^{+}}\left(\sqrt{\gamma_i^{-}} + \sqrt{\gamma_j^{-}} - \sqrt{\gamma_k^{-}}\right) + \\ \sqrt{\gamma_k^{-}}\left(\sqrt{\gamma_i^{+}} + \sqrt{\gamma_j^{+}} - \sqrt{\gamma_k^{+}}\right) - \sqrt{\gamma_i^{+}\gamma_j^{-}} - \sqrt{\gamma_i^{-}\gamma_j^{+}}\end{array}\right] \quad (10)$$

When the liquid is water, this interaction is called the "hydrophobic interaction" where the adhesive bond strength is less than zero. This indicates the interaction between aggregate and asphalt becomes repulsion, which is the driving force for water to displace asphalt from the surface of aggregate (Oss et al. 1988).

Because the affinity of aggregates for water is far greater than their affinity for the asphalt binder, the presence of moisture tends to soften the asphalt mastic and strip the asphalt binder from the aggregate surface, which significantly reduces the tensile strength of asphalt mixture and consequently accelerates the pavement deterioration.

Mechanism of Moisture Damage

This topic has been extensively discussed by other authors and therefore the intent is not to provide a comprehensive report about this subject, but rather to present a concise summary of the major moisture damage mechanisms.

Due to the complexity of the stripping phenomenon, defining the mechanisms and causes of stripping remains a difficult task. Numerous mechanisms have been proposed for stripping including detachment, displacement, spontaneous emulsification, film rupture, pore pressure, and hydraulic scouring.

As demonstrated in the Figure 5, it is known that asphalt films are not impervious. Therefore penetration of the asphalt film by water would permit moisture to get to the asphalt-aggregate interface and provide opportunity for a detachment and displacement mechanism to become active. Detachment can be generally defined as the separation of an asphalt film from an aggregate surface by a thin film of water without an obvious break in the mastic. Displacement can be defined as the removal of asphalt mastic from the aggregate by water. It is also highly likely that the detachment mechanism may precede the displacement mechanism (Caro et al. 2008a).

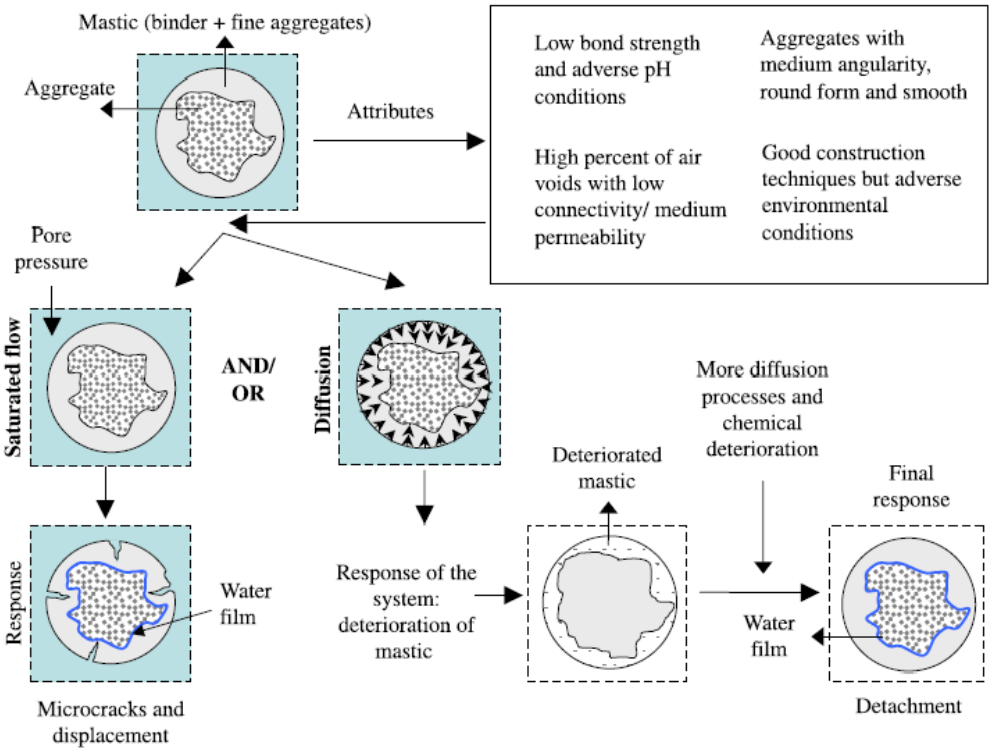

Figure 5. Moisture Damage Mechanisms: Displacement and Detachment

Spontaneous emulsification happens when an inverted emulsion of water droplets in asphalt cement forms rather than the converse. It is found that this process can be intensified under traffic on mixtures laden with free water.

Film rupture can initiate stripping when film fissures occur at sharp aggregate contact due to dust particles on the aggregate surface. The rupture may occur because of the construction loads and operating traffic during construction, or could be environmentally induced by freeze-thaw cycling. Once a break in the film occurs, moisture that presence of dust enhance the formation may lead to rupturing. (Kiggundu and Roberts 1988).

Hydraulic scouring is caused compression phenomenon around by the occurrence of a capillary tension a moving heavy traffic wheel on a saturated HMA structure. Defects such as surface ravening can occur once the asphalt is stripped off the aggregate. Furthermore, dust mixed with rain water and, in the presence of traffic, can enhance the abrasion of asphalt films from the aggregate.

It is reported that some asphalt pavement distresses are directly related to the presence of water in the pavement. Furthermore, the pavement distress can be accelerated by the occurrence of moisture damage in the asphalt mixture. Therefore, it is essential to accurately characterize the moisture susceptibility of asphalt mixture.

The Problems in Moisture Damage Characterization

Problems in Characterization of Water Transport in Pavement Systems

Moisture can enter into pavement systems by three different mechanisms. However, a literature review suggests that the majority of the research in characterizing moisture

damage of asphalt mixture focuses on the hypothesis that surface infiltrated water is the main mechanism of water movement in pavement (Masad et al. 2007). This is a reasonable assumption in the area that has a high level of rainfall. However, in the hot and dry area with minimal rainfall, moisture related distresses are still widely observed in the pavement systems. Hence, it is necessary to develop a method of predicting and quantifying the amount of water that can enter into a pavement system by other means. Carpenter et al (1974) constructed a map of the expected suction levels in the subgrade below a pavement by relating the equilibrium suction to the Thornthwaite moisture index. The obtained subgrade PF values for pavement subgrade reveals that the soil vapor pressure is generally near saturation (100% relative humidity). Consequently, the subgrade soil beneath the pavement can be treated as water vapor saturated material. Due to the existence of the relative humidity gradients between the subgrade soil and air above the pavement surface, vapor can transport from the subgrade soil into the pavement layers by diffusion process. With better understanding of water movement in pavement, some research efforts have been performed to study the moisture diffusion in the pavement systems.

Cheng et al (2002) measured the water vapor diffusion and water holding capacity in different asphalt binders by monitoring the gravimetric increase of specimens subject to controlled relative humidity in Universal Sorption Device (USD). It was found in this research that the asphalt has a great potential for holding water due to the water vapor diffusion. Sasaki et al. (2006) examined the water vapor transfer from air into the pavement system and the water storage mechanisms which produce moisture damage in

asphalt mixtures. All specimens used in this research were taken from a surface course, which is practically impermeable to liquid water. The specimens were conditioned in a temperature/humidity programmed-control chamber and only the top surface was allowed for the moisture to in/out. The findings of this study showed that the pavement asphalt mixture absorb and desorb significant amount of water on a daily basis through vapor-state permeation via connected microspores. This research conceptually indicates that water vapor diffuse much faster into the asphalt moisture than the water in liquid phase (Cheng et al. 2002). Kassem et al. (2006) developed an experimental method for measuring moisture diffusion coefficients in asphalt mastics by placing the specimens in a water bath and measuring the total suction changes in the asphalt mixture. The water diffusion coefficient was achieved by using thermocouple psychrometers to measure the relative humidity in asphalt mixtures under well-defined boundary conditions. It is found that the water diffusion coefficients were related to percent air voids in asphalt mixtures. Furthermore, the testing results showed that water diffused faster into asphalt mixtures, which are reported to have poor resistance to moisture damage. Arambula et al. (2007) experimentally explored the cause of moisture damage in dry region due to the capillary rise. The results of her research suggest that the capillary rise phenomenon makes the water more accessible to the asphalt binder in the mixture. As the water rise to reach into the air voids of asphalt mixture, given the relative humidity gradient between the voids filled with water and asphalt-aggregate interface, moisture would be driven by this gradient to diffuse through the asphalt mastic and ultimately reach the asphalt-aggregate interface. Arambula et al. (2010) developed an efficient technique to measure the water

diffusion coefficient for different asphalt mixture materials by periodically monitor the weight of cylindrical specimens-plastic ensembles that are subject to a controlled RH room. This research shows that the water vapor diffusion coefficients play a significant role in drive the moisture movement in asphalt mixture (Arambula et al. 2010). Vasconcelos et al. (2011) experimentally determine the diffusion of water in different fine aggregate mixtures (FAM) using simple gravimetric sorption measurements. The results indicate that the moisture diffusion coefficient depends on the types of aggregate and asphalt binder. For any given asphalt binder, the moisture uptake increases as the Specific Surface Ares (SSA) of aggregate increases, which also results in higher water diffusion in the asphalt mixture.

Although the past research indicates that water diffusion can be a significant mechanism of water transport in asphalt mixture, there is little information to reflect how the vapor diffusion from subsurface contributes the wetting process of pavement in the field. Furthermore, it is not clear to what extent the permeation of water vapor will affect the mechanical performance of asphalt mixtures. Hence, it is necessary to model the relative humidity changes in the asphalt pavement layer with time due to the subsurface water vapor diffusion. Moreover, it is essential to develop an efficient performance based test to evaluate the water vapor diffusion effects, which would provide the basis to incorporate the moisture diffusion effect in the future pavement design.

Problems in Current Moisture Conditioning Method

The prediction of moisture induced damage to asphalt mixture begins with conditioning the testing specimens with proper methods. At present, there is a series of moisture

conditioning methods available, which are categorized as follows:

- Static immersion method-specimens are immersed in the water for a period of time
- Vacuum saturation method-apply partial vacuum pressure to the specimens in vacuum container

Freeze-thaw cycles can be combined with the moisture conditioning to simulate the climatic change in the cold areas. For this widely used vacuum saturation method, in order to accelerate the moisture intrusion into the specimens, a vacuum of ranging from 250 mm to 700 mm Hg partial pressure (13-70 kpa absolute pressure) is usually applied. The concern is that a vacuum pressure as high as 700 mm Hg could potentially disturb the structure of the specimens and cause strength reduction in the specimens. Therefore, this concern needs to be addressed before applying high vacuum in conditioning specimens. Another concern is that the current conditioning method using liquid water can only be justified if there is adequate liquid water to enter the pavement. However, in places with little rainfall, these current moisture conditioning methods do not represent the true water transport mechanism in the field. Therefore, other conditioning alternative needs to be considered to simulate the true field situation.

Problems in Current Water Damage Characterization Tests

The accurate characterization of moisture damage is essential in predicting the service life of pavement. Caro et al. (2008b) conducted extensive literature reviews concerning moisture damage characterization and modeling. His study suggests that the majority of current practices for evaluating moisture damage in asphalt mixture focus on

comparative measures (wet-versus-dry comparison) such as the widely used quantitative Tensile Strength Ratio (TSR) test, which compares the tensile strength of the moisture conditioned specimen to the tensile strength of the controlled dry specimens. TSR test is simple and straightforward to demonstrates the moisture effect on the reduction of the tensile strength, however several research projects performed by different researches point outs that TSR results has no good correlation with pavement performance in the field. Kanitpong and Bahia (2006) evaluated the relationship between the performance of asphalt pavement in the field and the TSR values obtained from the laboratory measurement on the original asphalt mixtures used in the later pavement construction. In this study, the Pavement Distress Index (PDI), which is a measurement of pavement distress level, was used to describe the pavement condition and indicate the need for pavement maintenance or rehabilitation. It was found that there is no direct relationship between the TSR values and the filed pavement performance as indicated by the PDI. Solaimanian et al (2006) performed three different tests including ASTM D4867 test on the eleven different asphalt mixtures with known field performance. Only six out of the eleven mixtures show some correlation between TSR results and field performance. TSR and other similar tests attempt to quantify the overall asphalt mixture's resistance to moisture damage but ignore the fundamental material properties, which are the keys to evaluate the pavement performance.

As the need for more accurate and efficient characterization method to relate the moisture damage to fundamental material properties, the concept of using surface free energy was brought into the pavement community. Surface free energy, which indicates

the material surface physical chemistry characteristics, can be used to evaluate adhesive fracture and moisture susceptibility characteristics within the asphalt-aggregate system. The surface free energy of a solid (or a liquid) is defined as the work needed to create new elemental area under a vacuum condition. The thermodynamic changes in the surface free energies of adhesion and cohesion are related to separation of the interface between the asphalt and the aggregate or fracture within the binder or mastic. Hence, surface energy of asphalt binders and aggregates is one of the most essential and fundamental material property that significantly affects the performance of asphalt mixes and it is very important to be able to measure the surface free energies of asphalt and aggregate, which are required to calculate the work of adhesion and cohesion. Cheng et al. (2001) proposed to use the surface energy measurement for both asphalt and aggregate to select the most compatible asphalt-aggregate system. The better compatibility between asphalt and aggregate means the mixture has better resistance to fatigue and moisture damage. Bhasin et al. (2006) proposed to use the adhesive bond energy ratio to evaluate the moisture damage of asphalt mixture. The energy ration formula is expressed as follows:

$$R^{Total} = \frac{\left|\Delta G_{AS}\right|}{\left|\Delta G_{WAS}\right|} \tag{11}$$

where R is the energy ratio; ΔG_{AS} is the adhesive bond energy between the asphalt and the aggregate; ΔG_{WAS} is typically negative and represents the adhesive bond energy between the asphalt, aggregate and water.

Based on the known field performance date, a higher R value usually stands for the better resistance to moisture damage in the field. Little and Bhasin (2006) refined the model in the as follows:

$$R^{Total} = \frac{\left|\Delta G_{AS} - \Delta G_{AA}\right|}{\left|\Delta G_{WAS}\right|} \tag{12}$$

where ΔG_{AA} is the cohesive bond energy of the asphalt.

The reasoning behind the model in Equation 12 is that the asphalt will wet the aggregate surface better if the cohesive bond energy of the asphalt is less than the work of adhesion. Therefore, the surface energy has a great potential in selecting compatible asphalt-aggregate combination. However, a single-parameter moisture damage ratio (MDR) model is not sufficient to characterizing the moisture damage of asphalt mixture due to its complexity. As a result, multi-parameter MDR, which characterizes the moisture damage by combining more than one material property, should be adopted to account for the physical, chemical and mechanical process induced by moisture.

Lytton et al. (1993) developed a comprehensive microfracture model to backcalculate the fracture parameters and to develop a relationship for predicting the number of load cycles to crack initiation. In this model, the energy balance approach is proposed to evaluate the asphalt mixture' stiffness reduction as a function of the parameters A and n, of Paris' law, the surface energy density, the microcrack length, and the dissipated energy. By comparing the fracture parameters for both dry and wet specimen, one can estimate the fatigue life reduction due to the moisture. This research laid the ground for the future development of more comprehensive microfracture model.

Lytton et al (2005) derived another mechanistic model to evaluate the fatigue crack growth of asphalt mixture by using Paris law. The final model is formulated as follows:

$$R = \frac{r(N)}{K^{\frac{1}{2n+1}}} = \left[(2n+1)^{1+1} \left(\frac{E_R b}{4\pi E_1 \Delta G_f} \right)^n N \right]^{\frac{1}{2n+1}} \quad (13)$$

Where E_R is the reference modulus of asphalt mixture; K is a constant for each material that is inversely proportional to the square of the tensile strength of the asphalt mixture G_f is the adhesive bond energy between asphalt and aggregate; N is the number of loading cycles; n is the Paris' law parameter; $b = \frac{\partial W_R}{\partial \ln N}$ is the dissipated pseudostrain energy per unit volume of the intact material per load cycle; E_1 can be obtained by fitting the relaxation modulus vs. time.

Equation 13 combines mixture physical, chemical and mechanical properties to calculate the crack growth in both dry and wet specimens. This model was widely adopted by other researchers to evaluate the moisture damage of for both the asphalt mixture and asphalt mastic (Masad et al. 2006, Arambula et al. 2007).

To sum up, although there is a wide variety of approach to characterize the moisture damage of asphalt mixture, there is a lack of agreement in selecting the most efficient and accurate methodology. Therefore, it is necessary to develop a comprehensive model, which can efficiently and repeatedly evaluate the moisture damage of asphalt mixture from the fundamental material property.

CHAPTER III

MATERIAL PROPERTIES AND SPECIMENS FABRICATION

The experiments were designed to evaluate the effect of moisture, aging, air voids, and different WMA additives on the asphalt mixture fatigue resistance. Materials, specimen fabrication, specimen aging and moisture conditioning for each experiment are discussed in this section.

HMA Materials and Mix Design

The material selection, material properties, and corresponding mix designs are introduced in this section.

Asphalt Binders and Aggregates

Four different binders were selected based on the experimental testing plan shown in table 1. The first two binders used were AAM and AAD, which are from the Strategic Highway Research Program (SHRP) Materials Reference Library (MRL) and represent a range of properties expected in unmodified binders used in the United States. The specific gravity values for AAD and AAM are 1.028 and 1.034, respectively. The Valero and NuStar binders were also used in the expanded testing plan and their PG grades are listed in the Table 1. The newly developed RDT, which was discussed in the Chapter V in details, is used to characterize the fatigue properties of FAM.

Table 1. Material Library and Experimental Testing Plan for HMA

Mix Type	Conditioning
1.Hanson Aggregates+PG76-22[NuStar] 2.Hanson Aggregates+PG64-16[Valero] 3.Texas Limestone+SHRP AAD-1 4.Texas Limestone+SHRP AAM-1	0 and 6 weeks aging; 0% and 100% RH; Different Level of Air Voids
Tests	**Equipment**
Nondestructive Uniaxial Tensile Dynamic Modulus	DMA
Destructive Uniaxial Tensile Dynamic Modulus	
Nondestructive Uniaxial Tensile Creep	
Nondestructive Uniaxial Tensile Dynamic Modulus	
Destructive Uniaxial Tensile Dynamic Modulus	

Gradation and Binder Content

The TxDOT Type C gradation was chosen for the mix design and the detailed information is listed in Table 2.

Table 2. Hanson Limestone Full Aggregate Mixture Gradation.

Sieve No.	Sieve Size (mm)	Cumulative Passing %
1"	25	100
3/4"	19	99.6
3/8"	9.5	74
No. 4	4.75	58.1
No. 8	2.36	37.3
No. 30	0.6	19.7
No. 50	0.3	8.1
No. 200	0.075	2.8

As summarized in the Appendix A, the design procedure for the FAM only considers the granular material of the HMA mixture passing the No. 16 (1.18 mm) sieve. Then the FAM gradation curve was developed for the material passing No. 16 and the same proportions for each aggregate passing the No. 16 (1.18 mm) sieve was maintained. The corresponding aggregate gradation for FAM is presented in Table 3.

Table 3. Corresponding Gradation for FAM

Sieve No.	Individual Retaining %
No. 30	27.31
No. 50	42.8
No. 100	11.44
No. 200	8.12
Pan (-No. 200)	10.33

The optimal binder content for the full aggregate mixture was determined to be 4.7 percent by the weight of the mixture according to the 2004 Texas Department of Transportation (TxDOT) Tex-204-F specification (TxDOT 2004). The binder content of the FAM specimens was determined using the aggregate surface area method based on the optimum binder content of the corresponding full aggregate mixture. The aggregate surface area method assumes that the asphalt binder is proportionally distributed on the aggregate surface area. The following equations was developed to quantify the binder content of FAM.

$$CR_i = 3\left(\frac{1}{r_i D_i} + \frac{1}{r_{i-1} D_{i-1}}\right) \tag{14}$$

where CR_i = specific surface area of the particles with diameters in the range between sieve sizes D_i and D_{i-1}; r_i = effective density of aggregate, kg/m^3.

The assumption of perfectly spherical aggregate was calibrated using a volume factor K, which was obtained using the following equation:

$$V_i = KM\frac{4}{3}\pi\left[\frac{1}{2}(D_i + D_{i-1})\right]^3 \quad (15)$$

where V_i = measured volume of aggregate retained on the i_{th} sieve; M = number of aggregate particles retained on the i_{th} sieve; and K = volume factor.

The volume factor K was then used to calibrate the CR_i:

$$CR_i = 3K\left(\frac{1}{r_i D_i} + \frac{1}{r_{i-1} D_{i-1}}\right) \quad (16)$$

It can be seen that the specific surface area factor is related to aggregate particle size, effective density of aggregate, and volume factor. Once the binder content is determined, then the fabrication of asphalt mixture should follow the corresponding Specification in each state. The optimum binder content for both mixtures was determined according to TxDOT Tex-204-F test procedures and specifications. The optimum binder content was 10.7 percent by weight of the mixture.

WMA Materials and Mix Design

Asphalt Binders and Aggregates

Two different mixes were designed for testing. The first one is a lab compacted lab molded mix, which used the Lion asphalt with PG64-22 and the non-absorptive quartzite

aggregate. The second one is the lab compacted plant mix, which used the Pelican asphalt with PG70-22 and the absorptive limestone. The details concerning the materials are listed in the Table 4.

Table 4. Material Library for WAM

Mix No.	Materials	
	Asphalt Binder	**Aggregate**
1	Pelican PG70-22	Absorptive Limestone Centex Dolomite)
2	Lion PG 64-22	Non-Absorptive Quartzite (Jones Mill)

Gradation and Binder Content

The lab mix is a type of Superpave D mixture, which was designed based on the TxDOT 2004 specification. The full aggregate mixture gradation is shown in Table 5. The corresponding aggregate gradation for FAM is presented in Table 6.

Table 5. Aggregate Gradation for Lab Mix

Sieve No.	Cum. Passing %
3/4"	100
1/2"	100
3/8"	93.1
No. 4	64.6
No. 8	40.7
No. 16	26.2
No. 30	14.6
No. 50	8.5
No. 200	3.5

Table 6. Corresponding Gradation for FAM

Sieve Size	Individual Retaining %
No. 16	0
No. 30	44.23
No. 50	23.46
No. 200	18.85
Pan	13.46

The plant mix materials is from the upgraded project construction of FM973 and all the related information is summarized in the Table7. The gradation information is listed in the Table 8.

Table 7. Summary of WMA Field Project

Field Project	FM973
Construction Dates	28-Nov-11
WMA Technologies	Evotherm DAT, Foaming
Mix Design Information	TxDOT Type C
	Binder: PG 70-22 Aggregate: Centex Limestone Optimal Binder Content: 5.2%
Production Temperature	HMA: 320°F
	Evotherm: 275°F
	Foaming: 275°F
Placement Temperature	HMA: 275°F
	Evotherm: 240°F
	Foaming: 235°F
Lab Curing (2 hours)	HMA: 275°F
at Temperature	Evotherm: 240°F
	Foaming: 275°F

The plant mix materials is from the upgraded project construction of FM973 and all the related information is summarized in the Table7. The gradation information is listed in the Table 8.

Table 8. Aggregate Gradation for Field Mix

Sieve No.	Cumulative Retaining %
#200	5.30%
#100	8.60%
#50	16.10%
#30	21.10%
#16	26.80%
#8	36.20%
#4	53.90%
3/8"	82.00%
1/2"	93.60%
3/4"	100%
1"	100%

DMA Specimen Fabrication

The basic FAM specimen fabrication procedure involves aggregate batching, binder-aggregate mixing, short-term oven aging, compaction, sawing and coring, and volumetric analysis to determine the specimen air void content. These processes were conducted according to the 2004 TxDOT specification. The first step in the preparation of the specimens consisted of mixing and compacting, using the Superpave gyratory compactor (SGC) to obtain a 6 inches diameter cylindrical sample with an approximate height of 3.5 inches, as shown in Figure 6. This procedure was similar to the one used to prepare regular HMA specimens. The upper and lower parts of the cylinders were sawed in order to produce a new cylinder 6 inches in diameter and 2 inches in height. This compacted sample was cored into small DMA cylindrical specimens 0.5 inch in diameter and 2 inches in height as illustrated in the Figure 7. Each specimen was properly labeled

and prepared for testing. The detailed procedure of preparing specimens for testing was discussed in the Appendix A.

Figure 6. SGC Compactor

Figure 7. DMA Cylindrical Specimen

Then, the FAM specimens for the DMA were tested to determine their air void contents. Since the DMA specimens were cored from samples with a 6 inches diameter made by the SGC, the DMA specimens cored from the outer circle of the 6-inch diameter specimen had a larger air void content than those cored from the inner circle, which was consistent with what was observed in the pilot testing. This indicates that the closer to the center of the 6 inches diameter gyratory specimen, the lower the air void content. This pattern was found in both samples made with the NuStar PG76-22 binder and samples made with the Valero PG64-16 binder, as shown in Figure 8 and 9, respectively.

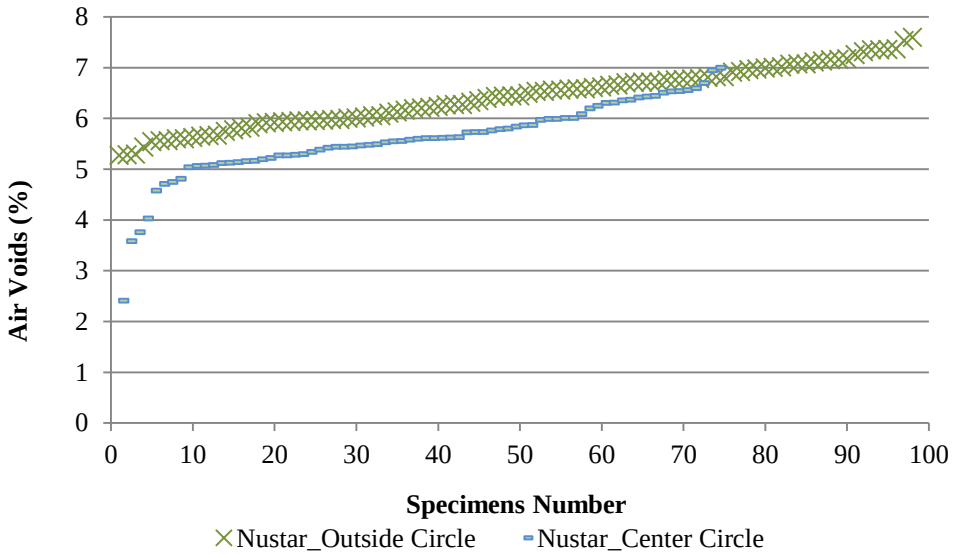

Figure 8. NuStar with Hanson Limestone Specimens' Air Voids Distribution

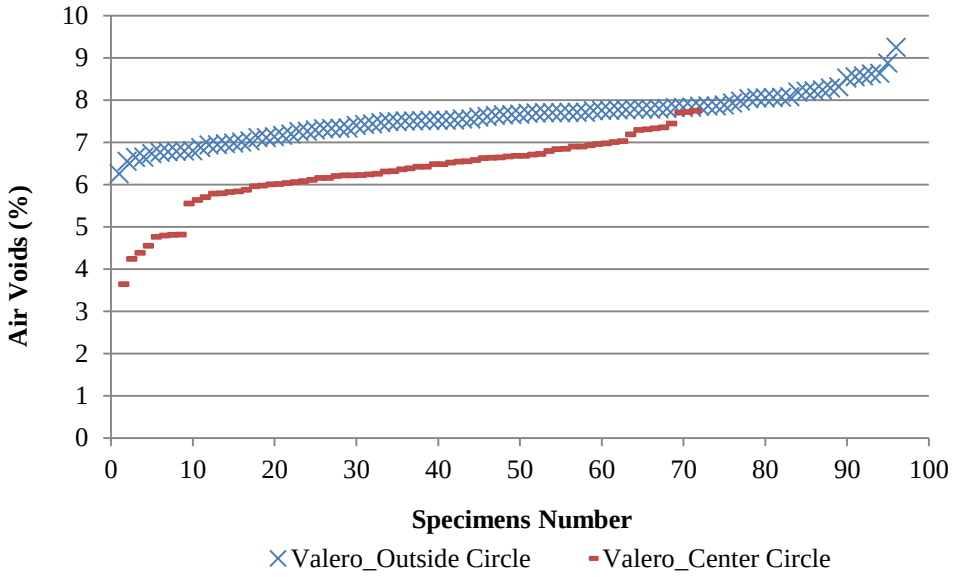

Figure 9. Valero with Hanson Limestone Specimens' Air Voids Distribution

Specimens Conditioning

Specimens Aging

For all of the FAM specimens, two laboratory aging periods of 0 and 6 weeks were used for specimens aging. Basically, the specimens are placed in the desiccators with the heated air at 60°C in the chamber. Since the desiccators are open to the air in the environmentally controlled room, the air circulates freely around the specimens in an environmentally temperature-controlled room and accelerates oxidation of the binder in the mixtures. Figure 10 illustrates the apparatus used for specimens aging.

Figure 10. DMA Specimens Aging in Desiccators

Based on the investigation on the water vapor diffusion and RH profiles in asphalt pavements, a laboratory experiment was designed to condition FAM specimens at different RH levels and to perform the controlled-stress repeated direct tension (RDT) tests on the FAM specimens using the DMA. This section will present the details of specimen fabrication, specimen conditioning, and test procedures.

Specimens Moisture Conditioning

In this research, a new moisture conditioning method was developed. According to the RH profiles established for the asphalt pavements in the Chapter IV, two RH levels, 0 percent and 100 percent, were selected in this study to condition FAM specimens. A constant RH level can be achieved in the vacuum desiccator using a chemical solution

whose affinity for water regulates the water vapor pressure in the closed system with little temperature fluctuation. The RH level in the vacuum desiccator corresponds to the specific solution that is chosen to use in the vacuum desiccator. Therefore, desiccant was used to achieve 0 percent RH level, and distilled water was used to achieve 100 percent RH level. Then the FAM specimens were placed in the vacuum desiccator with the specific RH, as shown in Figure 11.

Figure 11. DMA Specimens Conditioning in Desiccators

The weight of the specimens were monitored for over a period of six month. It is found that the weight of the specimens tends to stabilize around four month. After the specimens' weight are stable, the specimens were wrapped with plastic wrap to prevent the moisture from evaporation.

CHAPTER IV

VAPOR DIFFUSION IN PAVEMENT*

Water vapor movement within the pavement layers is a diffusion process and occurs along the temperature and vapor concentration gradients. Carpenter et al (1974) constructed a map of the expected suction levels in the subgrade below a pavement by relating the equilibrium suction to the Thornthwaite moisture index. The average obtained subgrade pF values in Texas is around 3.6, which is equal to 99.6 percent RH (Carpenter et al. 1974). This designated suction map demonstrates that the RH in clay subgrades is always near 100 percent, which is constantly higher than the RH in the air above the pavement. Because of this, gradient water vapor always diffuses upward. Goss et al. (2007) conducted in-situ measurements of RH in a dry Tanzanian soil in a 3-month period, and the results indicate that the RH in this particular soil type stays above 96 percent with little fluctuation at a depth of 6 cm below the surface. This finding demonstrates that the upward water vapor diffusion occurs continuously due to the RH gradient between the soil and air. Another finding of this investigation is that evaporation only affects the RH of the first 3 cm of the soil and does not progress into

* "Modeling Water Vapor Diffusion in Pavement and Its Influence on Fatigue Crack Growth of Fine Aggregate Mixture" by Y. Tong, R. Luo, and R. L. Lytton. Presented at the 92nd Annual Meeting of the Transportation Research Board, January 2013, Washington, D.C., and accepted for publication in the 2013 series of the Transportation Research Record: Journal of the Transportation Research Board (forthcoming).

the deeper soils, which indicates that the deeper part of the soil acts as an efficient reservoir to recharge the water from the subsurface. Consequently, subgrade soil beneath the pavement can be treated as water vapor saturated material. In cold weather, the temperature gradients facilitate the vapor movement upward from underlying layers and thus produce nearly saturated vapor pressure in the pavement surface layer. In hot weather, although the pavement surface temperature is higher than the underlying layer, a temperature gradient which tends to drive the water vapor moving downward, the existing RH gradients override the tendency of the downward movement of the water vapor driven by the temperature gradient.

Another factor that needs to be addressed is the effect of wind on the water vapor diffusion process. When there is no wind, the RH in the air above the pavement surface remains steady. However, if there is a wind blowing across the pavement surface, it removes the water vapor rapidly in the air above the pavement surface. This generates a steeper RH gradient between the air and the asphalt surface layer and increases the rate with which the RH increases in the asphalt

Formulation of Water Vapor Diffusion

Suction in soil can be defined in terms of the free energy or the relative vapor pressure (relative humidity) with which soil particles hold water. Analogous to the soil structure, asphalt mixtures are porous media that have the ability to attract and retain water. The water vapor movement in pavement can be modeled by Fick's second law, which is generally used to model a diffusion process driven by concentration gradients. In order to model the water vapor diffusion in pavement, the following assumptions are made: (a)

the water vapor flow is a transient state and moves only upward, and (b) the water vapor absorption in pavement is linear across the pavement. Therefore, the diffusion process in pavement is governed by a differential equation controlled by a single diffusivity coefficient D as shown in:

$$\frac{\partial u}{\partial t} = D\frac{\partial^2 u}{\partial x^2} \tag{17}$$

where u = the suction at the specified depth of pavement on a logarithmic scale, pF; D = the water vapor diffusion coefficient of the asphalt mixture, mm 2/s; x = the distance downward from the surface of the HMA layer, cm; and t = the service time since placement of HMA, s. Boundary conditions are set as follows:

$$u\left(x = d, t\right) = u_d \tag{18}$$

$$\frac{\partial u}{\partial x}\left(x = 0, t\right) = 0 \tag{19}$$

where u_d = the suction in the granular base material.

The coefficient of water vapor diffusivity is modeled using the equation as follows:

$$M_{abs}(t) = M_{\max}(1 - e^{-\frac{3Dt}{\left(d/2\right)^2}}) \tag{20}$$

where M_{abs} = the mass increase of specimens with the increase of time; M_{Max} = the maximum mass that the specimen can gain; α = the exponential rate of water diffusion; D = the diffusivity of water vapor in FAM, m2/s; and d = the diameter of the specimen, m.

Using the Laplace transform, the solution to the equation is given as follows:

$$u(x,t) = u_d + \frac{4}{\pi}(u_d - u_0)\left\{\sum_{n=1}^{\infty}\frac{(-1)^n}{(2n-1)} * e^{-(2n-1)\frac{\pi^2 Dt}{4d^2}} * cos\left[\frac{(2n-1)\pi\sqrt{D}x}{2d}\right]\right\} \quad (21)$$

where u_0 = initial suction in the asphalt mixture, pF. Another term, $E(t)$ is added to the solution in to account for the water vapor evaporation at the pavement surface:

$$E(t) = -(u_d - u_0) * e^{(h*x+h^2Dt)} * erfc(\frac{x}{2\sqrt{Dt}} + h\sqrt{Dt}) \quad (22)$$

where h = coefficient of vapor transfer; and $erfc(x) = \frac{2}{\sqrt{\pi}}\int_x^{\infty} e^{-t^2} dt$.

The total suction at a given depth beneath the surface of an asphalt layer can be converted to relative humidity at a given temperature using the formulation as follows:

$$u = \log_{10}\left[-\left(\frac{RT}{mg}\ln\left(\frac{RH}{100}\right)\right)\right] \quad (23)$$

where R = universal gas constant; T = absolute temperature; m = molecular mass of water vapor; and g = gravitational acceleration at the earth's surface.

This suction model does not consider the wind effect on water vapor diffusion in the pavement. In order to incorporate the wind influence into this water vapor diffusion model, the flux boundary condition, including wind speed at the pavement surface, is formulated using the equation as follows:

$$\frac{\partial u}{\partial x} = f(u) * (u_a - u_s) \quad (24)$$

where $\frac{\partial u}{\partial x}$ = the rate of potential evaporation; u_a = the suction in the air; u_s = the suction at the pavement surface; and $f(u)$ = a function that depends on the wind above the surface of the pavement and can be expressed using the equation in as follows:

$$f(u) = h*(1+\alpha_m) \tag{25}$$

where h = the coefficient of vapor transfer at the boundary surface; and α_m = the mass exchange coefficient of water vapor due to the wind at the surface. Specifically, the equation indicates that the wind speed increases the water vapor mass exchange at the surface, α_m:

$$\alpha_m = K\sqrt{\frac{V}{L}} \tag{26}$$

where V = the wind speed, m/s; and L = the length over which the wind blows. The largest α_m occurs if the wind blows across the width of the highway, m.

The K can be expressed as:

$$K = 0.662\lambda_m(P_{rm})^{1/3}(\frac{1}{\nu})^{1/2} \tag{27}$$

where P_{rm} = Prandtl number for air; ν = kinematic viscosity of air, m2/s; and λ_m = a constant at the air temperature of 20°C and is taken as $2.54\times10^{-3} kg/(s^{-1}\times m^2)$.

By substituting the Equation in 27 into the Equation 26, α_m was calculated based on wind data available for Texas from the National Climatic Data Center.

Determination of Relative Humidity in Asphalt Pavements

Based on the above formulation of water vapor diffusion, a schematic illustration of the water vapor movement in the asphalt surface layer was established in order to determine the relative humidity in asphalt pavements, as presented in Figure 1. The thickness of the asphalt layer was set at 10 cm, and the suction in the newly placed asphalt layer was set at 7 pF, which is equivalent to 0 percent RH. Then three pavement locations in three different climatic zones with distinct air RH levels were selected for the analysis according to available in-situ weather data. Information on the three climatic zones is shown in Table 9. The Thornthwaite Index (TI) was used to approximate the suction profiles of the subgrade soils and the base course material immediately beneath the surface layer (Thornthwaite 1948). As indicated in Table 9, the suction in the base course material for the three locations in Texas was set at approximately 3 pF by relating the TI to the equilibrium suction level in the subgrade along the centerline of the pavement. The coefficient of vapor transfer from the pavement into the air was held constant as 0.54 cm-1, which is a widely used number in evaluating water vapor evaporation of soil (Mitchell 1980, Sood 2005). Subsequently, with all the know parameters listed in the Table 9, the RH profiles of asphalt pavements in the three climatic zones were determined based on the formulation of water vapor diffusion developed in the previous section.

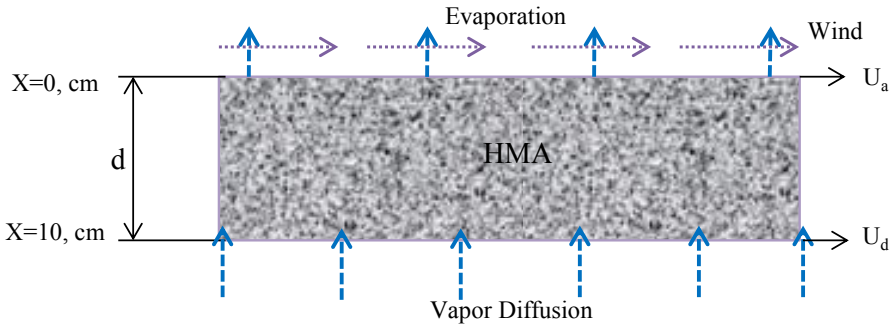

Figure 12. Water Vapor Diffusion in Pavement

Table 9. Inputs for Pavement HMA Layer Suction Prediction Model

Locations	West Texas	Central Texas	East Texas
Average Air RH (%)	10	50	74
Base Suction (pF)	4.0	3.6	3.2
Water Vapor Diffusivity (m^2/s)			2.12×10^{-11}
Coefficient of Vapor Transfer (cm^{-1})			0.54
Initial Asphalt Mixture (Oven Dry) pF			7.0

Figure 13 presents the RH profiles determined without considering the effect of the wind. As illustrated in Figure 13, as service time increases, the asphalt surface layer gradually wets up after placement due to the moisture movement from the subgrade soil into the base course and then into the surface layer. The closer to the pavement surface, the lower the relative humidity in the asphalt layer. The moisture builds up in the asphalt

mixture at such a fast rate that the RH in the surface asphalt layer reaches 95 percent in approximately 180 days, and this RH level remains constant within the asphalt layer. These modeling results illustrate that the pavement surface layer attains nearly saturation vapor pressure within a relatively short period of 180 days. This high RH level may lead to an accelerated pavement deterioration rate.

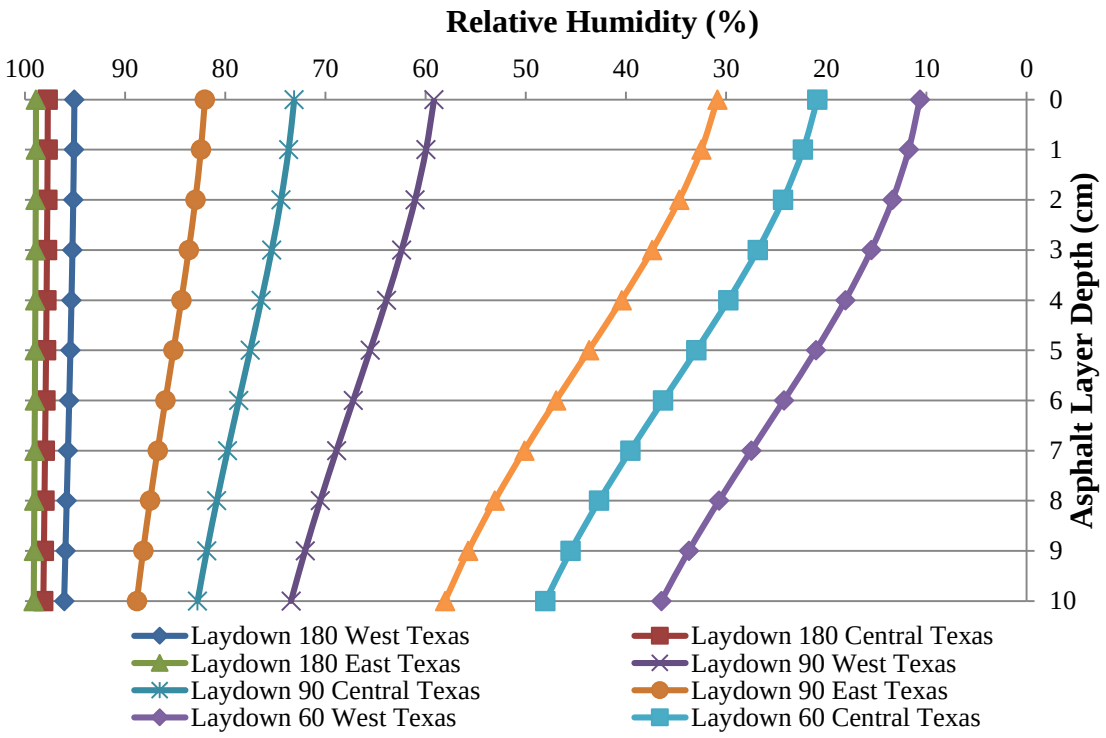

Figure 13. Asphalt Layer RH Changes with Time

When considering the effect of wind on water vapor movement in asphalt pavements, Equation 25 was used to calculate the mass exchange coefficient of water vapor due to the wind at the surface. When the wind speed ranged from 3.6 m/s to 8.9 m/s, the value of α_m ranged from 0.126 to 0.184. A commonly used empirical number of

α_m, which is 0.146, was also identified in the literature (Wilson 1990). This demonstrates that the value of α_m calculated using the formulation closely matched the widely used empirical value.

Table 10. Measured Diffusion Coefficients for Different Materials.

Material	Reference	Diffusion Coefficient (m^2/s)
Mixture	(Kassem et al. 2006)	$1 \times 10^{E-11}$ to $2 \times 10^{E-11}$
	Arambula et al. (2010)	$2.54 \times 10^{E-10}$ (Vapor)
	(Kringos et al. 2008)	$3 \times 10^{E-13}$
Binder	(Cheng et al. 2002)	$2 \times 10^{E-11}$ to $6 \times 10^{E-11}$
DMA	(Vasconcelos et al. 2011)	$7.83 \times 10^{E-13}$ to $4.90 \times 10^{E-12}$

When incorporating the modified $f(u)$ in the suction model to account for the wind effect, the increased coefficient of vapor transfer h at the boundary accelerated the water vapor movement from the base, which resulted in rapid wetting of the pavement surface layer. As shown in Figure 14, the solid curves represent the RH profiles in the asphalt pavement without the wind effect, while the dashed curves exhibit the RH profiles in the asphalt layer as the wind blows across the pavement at a speed of 3.6 m/s, which is a common wind speed recorded in Texas. It can be clearly observed that the

water vapor diffusion was accelerated due to the wind blowing across the pavement in all three climatic locations in Texas and that the asphalt layer reached water vapor saturation at a faster rate than when not considering the wind effect.

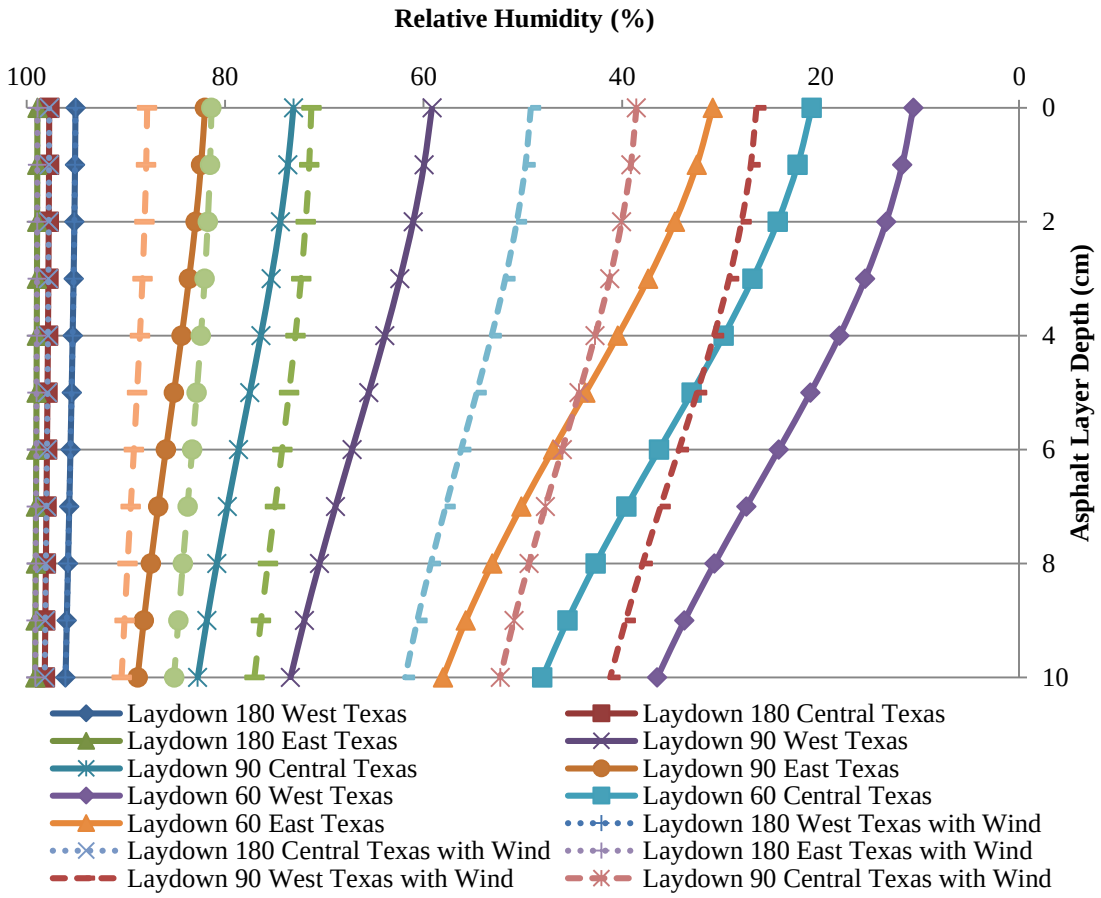

Figure 14. Asphalt Layer RH Changes with the Impact of Wind

Quantify Water Vapor Diffusion Coefficients

By monitoring the weight of the specimens, as shown in Figure 15 and Figure 16, the water vapor diffusivity was obtained. From the measured data calculation, the water diffusivity in the FAM specimen with the Valero binder ranged from D = 2.12E^{-11} m^2/s to D = 3.04E^{-11} m^2/s, and the water vapor diffusivity in the specimen with the NuStar binder ranged from D = 2.29E^{-11} m^2/s to D = 2.85E^{-11} m^2/s, both of which were within reasonable ranges compared to the literature data listed in Table 10. It was also observed that vapor diffused faster than liquid water in pavement.

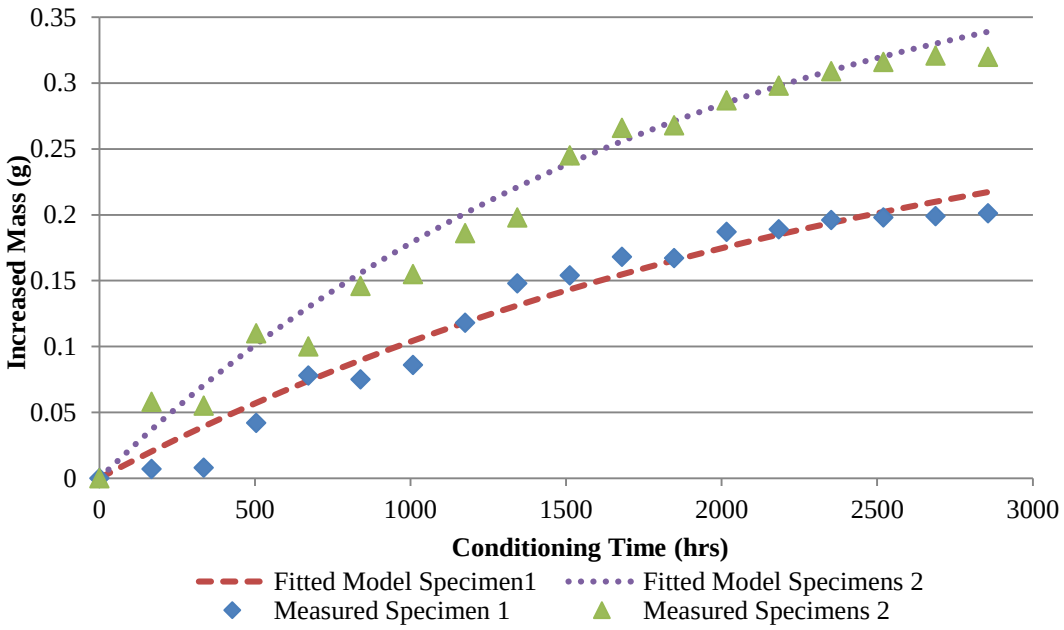

Figure 15. Moisture Uptake vs. Time for Specimens with Valero Binder

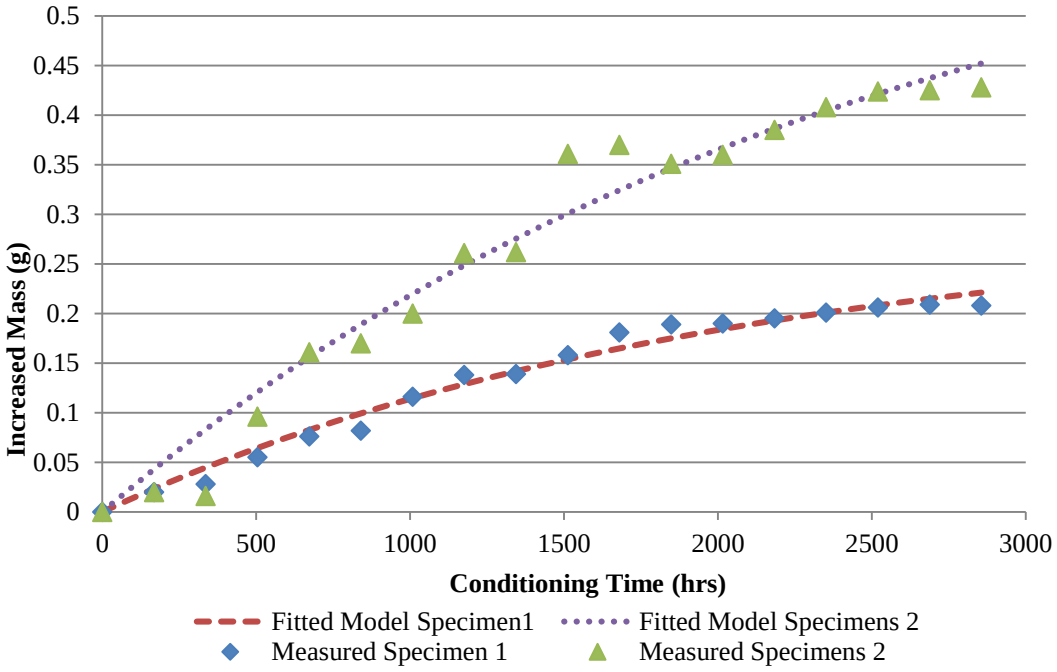

Figure 16. Moisture Uptake vs. Time for Specimens with NuStar Binder

CHAPTER V

CHARACTERIZAION OF FATIGUE CRACK GROWTH*

This research adopted an energy based methodology to characterize the fatigue properties of asphalt mixture. The DPSE represents the amount of energy expended for the fatigue damage in a loading cycle and the RPSE represents the amount of energy recovered in a loading cycle. The DPSE contains both the energy for fatigue cracking and the energy for permanent deformation. For the purpose of accurately characterizing fatigue cracking, the energy used for cracking is separated from permanent deformation by separating the DPSE for fatigue cracking from that for permanent deformation. Differentiating these two parts DPSE requires studying the energy distribution in developing these two types of damage. The following chapter discussed the theoretical development in details.

Balance Equations

Based on the understanding of the primary, secondary, and tertiary stages of the RDT test on FAM specimens, the crack propagation in the tertiary stage was analyzed to determine the fatigue properties of the FAM specimens subject to different conditioning.

---

* "Modeling Water Vapor Diffusion in Pavement and Its Influence on Fatigue Crack Growth of Fine Aggregate Mixture" by Y. Tong, R. Luo, and R. L. Lytton. Presented at the 92nd Annual Meeting of the Transportation Research Board, January 2013, Washington, D.C., and accepted for publication in the 2013 series of the Transportation Research Record: Journal of the Transportation Research Board (forthcoming).

The formulation of fatigue crack growth was established to determine the mean crack radius at every load cycle of the RDT test. This formulation was developed based on the strain energy equivalence principle, which states that different types of energy, which is the dissipated strain energy, recoverable strain energy, and the total of both in the bulk asphalt mixture specimen are equivalent to their counterparts in the intact material. When the FAM specimens were subjected to a tensile force, only the intact material could sustain the stress, while the cracked area or air void could not take any stress. The stress and strain measured from the DMA test were merely the apparent representations of what actually happened in the FAM specimens and were named apparent stress and apparent strain, respectively. The energy, stress, and strain of the intact material were defined as the true energy, true stress, and true strain, all of which had to be inferred from the test measurements by applying the force and energy equivalence equations.

Based on the relationship between the apparent material properties and the intact material properties, the force equivalence was formulated using the equation as follows:

$$\sigma^A A = \sigma^T \left(A - S \right) \tag{28}$$

where σ^A = the apparent stress, and the superscript A stands for "apparent"; A = the total cross-section area of the specimen; σ^T = the true stress of the intact material, and the superscript T stands for "true"; and S = the area of cracks or voids. The above force equivalence states that the force on the whole cross-section σ^A should be equal to that in the intact cross-section σ^T .

In addition to the force equivalence, the dissipated pseudo strain energy (DPSE) balance and the recoverable pseudo strain energy (RPSE) balance were adopted from the literature and were formulated using the Equations 29 and 30, respectively.

$$DPSE^{A} = DPSE^{T} \tag{29}$$

$$\mathrm{RPSE}^{A}V = \mathrm{RPSE}^{T}V - \mathrm{RPSE}^{T}\left(\frac{2}{3}M_N\pi^2{c_N}^3 - \frac{2}{3}M_O\pi^2{c_O}^3\right) + \gamma\left(2M_N\pi{c_N}^2 - 2M_O\pi{c_O}^2\right) \tag{30}$$

where DPSE represents the dissipated pseudo strain energy; V = the volume of one layer of the asphalt mixture specimen, for which the thickness equals the mean film thickness; RPSE represents the recoverable pseudo strain energy; C_0 = the average air void or crack size of the specimen in the undamaged state; C_N is the average crack radius after a number of n loading cycles; M_0 is the initial number of air voids of specimen; M_N = the number of cracks after a number of n loading cycles; and γ is the surface energy. The DPSE balance was used to determine the true stress in the intact material, and the RPSE balance was employed to characterize the mean crack radius at various numbers of loading cycles.

Due to the viscoelastic nature of the asphalt mixture, a considerable amount of energy is consumed to overcome the viscosity of the material during the loading and unloading process. Therefore, Schapery's (1975) nonlinear elastic-visco-elastic correspondence principle, which utilizes the concept of pseudo strain, was adopted as a means of separating the materials' time-dependent effect. In Schapery's correspondence principle, the measured strain can be converted to the corresponding pseudo strain using the equation as follows:

$$\varepsilon^R = E_R^{-1} \int_0^t E(t-\tau) \frac{d\varepsilon(\tau)}{d\tau} d\tau \tag{31}$$

where ε^R is pseudo strain; E_R is the reference modulus; and t is time.

The DPSE, which drove the damage in the material during the loading process, was calculated using the definition of pseudo strain given above. The general form of the DPSE was expressed using the equation as follows:

$$DPSE = \int_0^t \sigma(t) \frac{d\varepsilon_R(t)}{dt} dt \tag{32}$$

Substituting the Equation 31 into Equation 32, the DPSE was derived based on the measurement from the test; the RPSE was also obtained from the DPSE.

In the controlled-stress DMA tests, the stress variation with frequency was simulated using the equation shown as follows:

$$\sigma(t) = \sigma_0 \left[1 - \cos(\omega t)\right] \tag{33}$$

where σ_0 = amplitude of stress; and ω = the radian frequency, rad/s. The corresponding strain curve in the controlled-stress tests was then simulated using the equation as follows:

$$\varepsilon(t) = \varepsilon_0 \nabla D(t) - \varepsilon_{(N)} \cos(\omega t - \varphi) \tag{34}$$

where φ is the phase angle in the undamaged material by which the strain $\varepsilon_{(N)}$ lags the stress; and ΔD = the creep compliance slope of the specimen. The pseudo strain was then formulated using the equation as follows:

$$\varepsilon^R = \sigma_0 \Delta D t + \varepsilon_N \cos(\omega t - \phi + \varphi) \tag{35}$$

where ε_N is the strain amplitude of the n[th] loading cycles; and ϕ is the phase angle of the damaged specimen.

Integrating the Equation 35 into the Equation 32, the DPSE and RPSE were determined using the Equations 36 and 37, respectively.

$$DPSE^A = \pi \frac{\left(\sigma^T\right)^2}{E_{LVE}} \sin(\varphi_0 - \varphi_{NLVE}) + (\sigma^T)^2 \Delta D \tag{36}$$

where φ_0 = phase angle of the FAM specimen on the zero loading cycle; and φ_{NLVE} = nonlinear viscoelastic phase angle of the undamaged FAM specimen that was measured in the nondestructive RDT test.

$$RPSE^A * A_{AM} \bar{t} = \frac{\left(\sigma^T\right)^2}{2E_{LVE}} A_{AM} \bar{t} - \frac{\left(\sigma^T\right)^2}{2E_{LVE}} \left(\frac{2M\pi^2 \bar{c}^3}{3} \right) + 2M\pi \bar{c}^2 G_f^a \tag{37}$$

where E_{LVE} = linear viscoelastic modulus of the FAM specimen that was measured from the undamaged RDT test; $\bar{t}$ = asphalt film thickness; A_{AM} = total area of damaged asphalt mastic; $\bar{c}$ = mean crack radius; and G_f^a = FAM adhesive bond energy.

The cumulative RPSE equivalence, yielding the mean crack radius after repeated loading cycles, was established as follows:

$$\sum_{i=1}^{N}\left(RPSE_i^A\right)V=\sum_{i=1}^{N}RPSE_i^TV-\frac{2\pi^2}{3E_{LVE}}\frac{3\cos(\phi_{(N)}-\varphi)}{4E_{LVE}}*$$
$$\left[\left(\sigma_1^T\right)^2M_0{c_0}^3+\left(\sigma_2^T\right)^2M_1{c_1}^3-\left(\sigma_2^T\right)^2M_0{c_0}^3+\cdots+\left(\sigma_N^T\right)^2M_{N-1}{c_{N-1}}^3-\left(\sigma_N^T\right)^2M_{N-2}{c_{N-2}}^3\right] \quad (38)$$
$$+2\pi G_f^a\left(M_0{c_0}^2+M_1{c_1}^2-M_0{c_0}^2+\cdots+M_{N-1}{c_{N-1}}^2-M_{N-2}{c_{N-2}}^2\right)$$

Assuming that the $\sigma_i^{T_i}$ for two consecutive cycles was equal, the mean crack radius of the FAM was formulated using the Equations 39 and 40, respectively.

$$\bar{c}=\frac{\left[\beta RPSE_N^TV-\alpha RPSE_N^A+2\nabla G_f^a\right]}{\pi M_{N-1}C_{N-1}^2}\left[\frac{2E_T}{(\sigma_N^T)^2\pi\cos(\phi_{(N)}-\varphi)}\right] \quad (39)$$

$$\alpha=\frac{\sum_{i=1}^{N}\left(\mathrm{RPSE}_i^A\right)V}{\left(\mathrm{RPSE}_N^A\right)V}\qquad\beta=\frac{\sum_{i=1}^{N}\mathrm{RPSE}_i^TV}{\mathrm{RPSE}_N^TV} \quad (40)$$

where M = number of cracks; $\sigma_i^{T_i}$ is the true stress of the material in the ith loading cycle; and E^T is the true modulus of the material.

The specific expression for the stress-controlled RDT test was formulated using the Equations 41 and 42, respectively.

$$DPSE^A=\pi\frac{\left(\sigma^A\right)^2}{E^A}\sin(\varphi_d-\varphi_{NLVE})+(\sigma^A)^2\Delta D \quad (41)$$

$$RPSE^A=\frac{(\sigma^A)^2}{E^A}\frac{3}{4}\cos(\phi_d-\varphi_{NLVE}) \quad (42)$$

where φ_{NLVE} represents the nonlinear viscoelastic phase angle of FAM; and D is creep compliance.

Test Set-up

A controlled-stress RDT test method was developed to characterize the fatigue crack growth of the FAM specimens. As illustrated in Figure 17, each FAM specimen was glued to a pair of end caps and was then mounted using clamps in the environmental chamber of the DMA equipment for testing. During the test, the DMA applied a tensile force to the FAM specimen through the top loading cell while recording the stress and strain data of the test specimen. The detailed test-up is presented in the Appendix A.

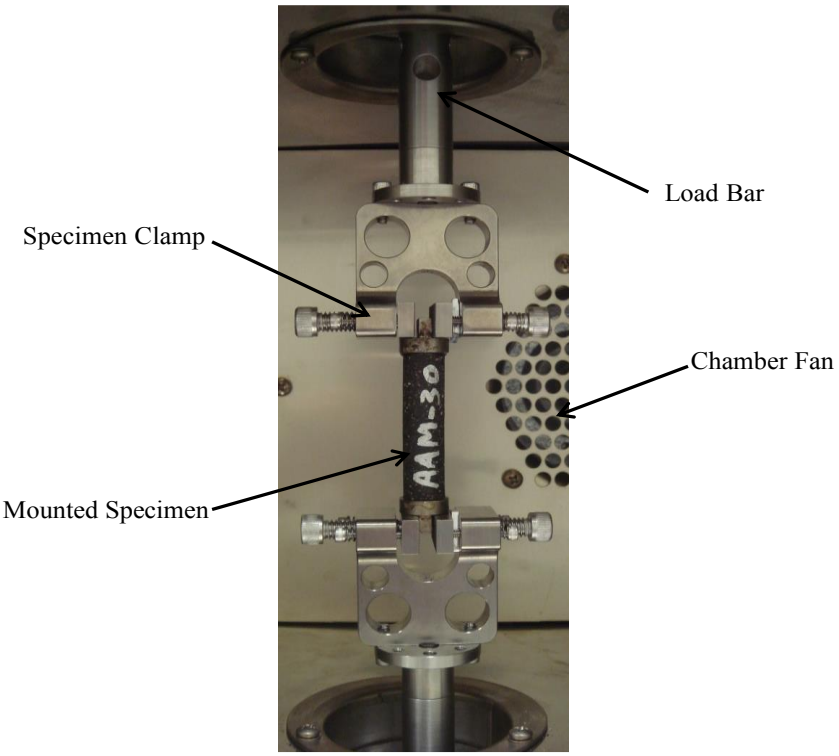

Figure 17. DMA Test Configuration

Two consecutive controlled-stress RDT tests are performed on the same asphalt mixture specimen: 1) nondestructive RDT tests with 100 load cycles at low loading

level; and 2) destructive RDT test with 1,000 load cycles. The loading frequency is set for 1 Hz in both tests. The nondestructive RDT tests are performed to determine the undamaged properties of the asphalt mixture specimen which is the reference state from which the damage introduced into the asphalt mixture could be quantified. To reduce data noise, the Fast Fourier Transform (FFT) was performed on the measured stress and strain data. As shown in Figure 18, the stress and stress curve are not smooth but the data can be smoothed by fitting the data using FFT. The test data with reduced noise were then analyzed to determine the fatigue properties of the FAM specimens, which are detailed in the following section.

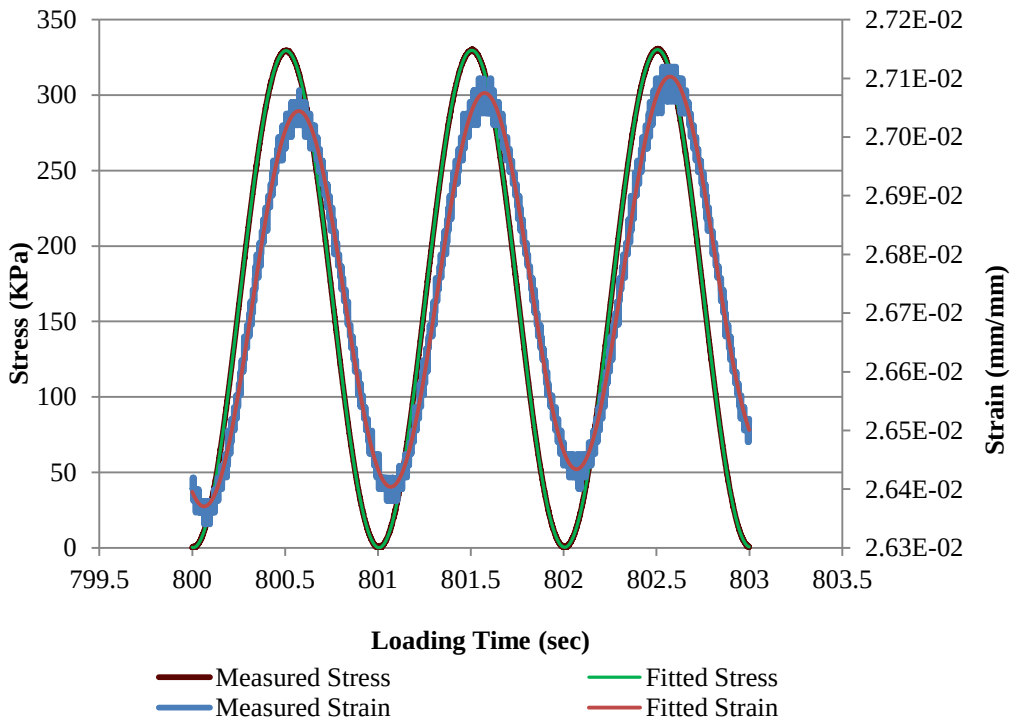

Figure 18. Stress and Strain Curve Measured from Controlled-stress RDT

Measured Magnitude and Phase Angle of Complex Modulus

Based on the measured stress and strain data, the magnitude and phase angle of the complex modulus of each specimen were determined at every loading cycle at both undamaged and damaging stress levels. The modulus magnitude was the ratio of the stress amplitude to the strain amplitude; the phase angle was the lag angle between the stress peak and the strain peak.

As demonstrated in Figure 19, when the stress amplitude was raised to a level of 332 kPa, both modulus magnitude and phase angle presented three stages, which are denoted in the figure by primary stage, secondary stage, and tertiary stage. The phenomenon of material stiffening was observed in the primary stage as illustrated in Figure 20, in which the modulus magnitude increased while the phase angle decreased as the load cycles increased. In the secondary stage, both modulus magnitude and phase angle stayed approximately constant with the increase in the number of load cycles. In the tertiary stage, the modulus magnitude decreased and the phase angle increased as the load cycles increased, which indicated the opening and propagating of cracks in the specimens.

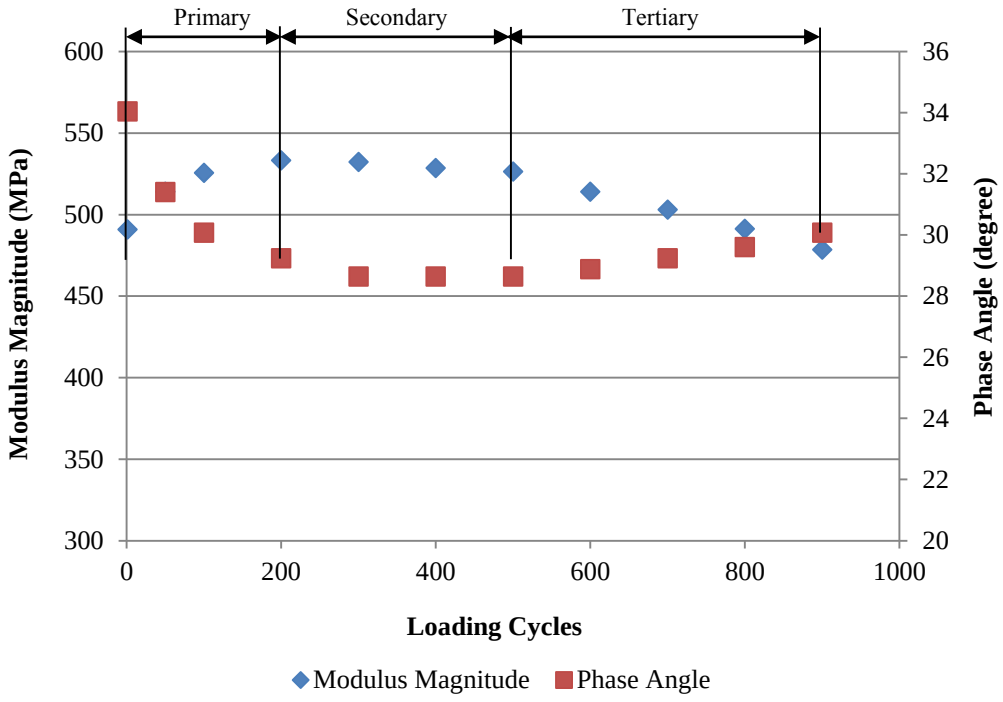

Figure 19. Measured Modulus Magnitude and Phase Angle at Stress Amplitude of 332 kPa

A possible reason for the material stiffening in the DMA test was the restructuring process in the specimen, as shown in Figure 21. The tensile force applied to the specimen stretched the asphalt mastic, which led to a thinner film thickness. The tensile strength of a FAM mixture tends to increase as the film thickness decreases (Marek and Herrin 1968). In the meantime, the aggregates are drawn together with the reduction of the cross-sectional area during the repeated tensile loading, which leads to better interlocking among aggregates.

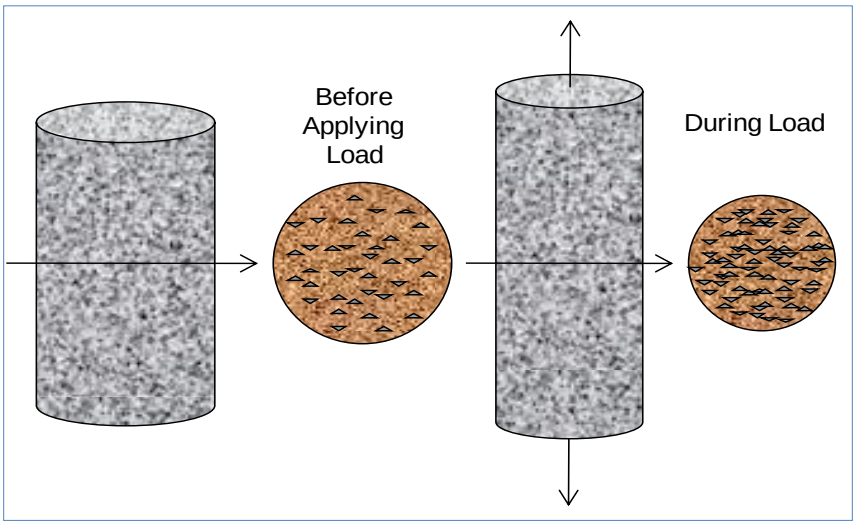

Figure 20. DMA Specimens Stiffening

Crack Growth Rate

Based on the discussion of crack growth formulation, the mean crack radius, $\overline{c}$, was calculated for each FAM specimen in every load cycle. Figure 21 illustrates the growth of $\overline{c}$ in two AAD specimens with approximately the same air void content of 3.6 percent but different RH levels (0 percent and 100 percent, respectively). For both specimens, $\overline{c}$ shows an approximate linear relationship with the number of load cycles. Therefore, a linear function was used to fit the data points of $\overline{c}$ in each specimen, as illustrated in Figure 21 and Figure 22 respectively. The high R-squared value demonstrated the goodness of the model fit. The slope of the linear model was then defined as the crack growth rate. A higher crack growth rate indicated that cracks grew faster when subjected to the same number of load cycles. The specimen labeled AAD1, which was conditioned at 100 percent, had a crack growth rate of 1.586 × 10-6 $m/cycle$,

which was roughly 50 percent higher than the crack growth rate of the specimen labeled AAD2 conditioned at 0 percent, which was 9.639 × 10-7 $m/cycle$. Similar observations were identified on AAM specimens. Figure 22 presents the calculated $\overline{c}$ of two AAM specimens, which were conditioned at 0 percent and 100 percent, respectively. The specimen labeled AAM13 with an RH level of 100 percent had a crack growth rate of 2.726 × 10-6 $m/cycle$, while the crack growth rate was 9.365 × 10-7 $m/cycle$ for the specimen that was labeled AAM18 and was conditioned at 0 percent.

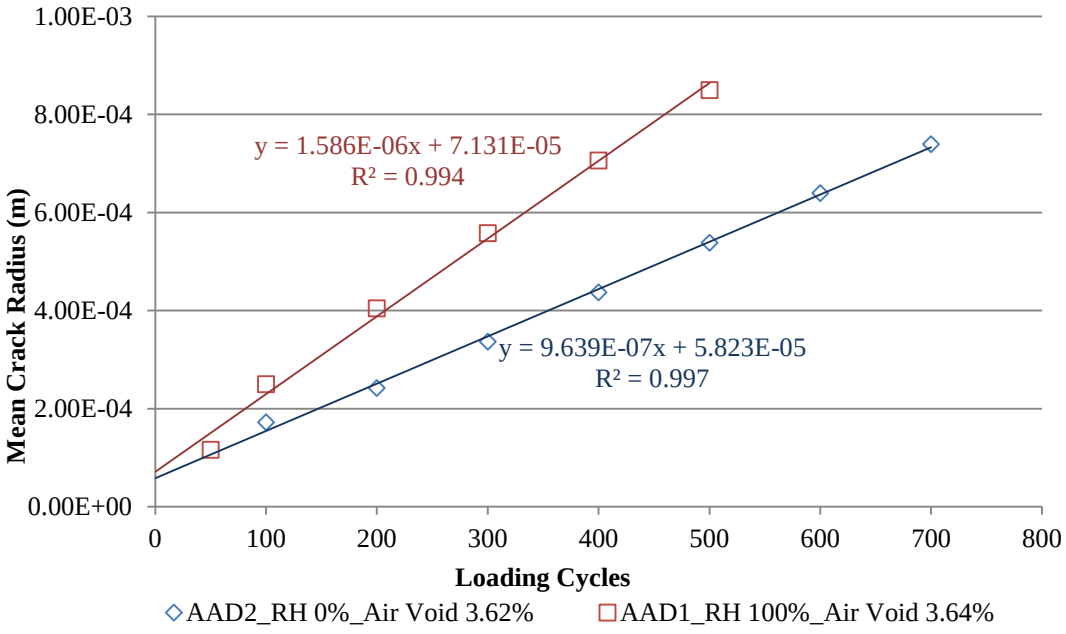

Figure 21. Crack Growth for AAM Specimens Conditioned at 0% and 100% RH

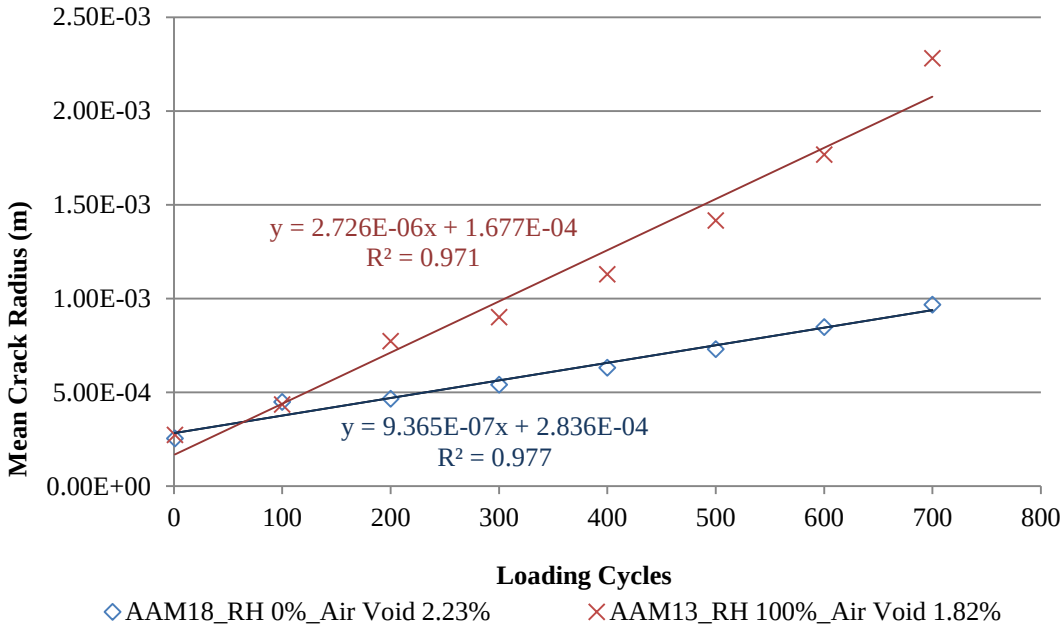

Figure 22. Crack Growth for AAD Specimens Conditioned at 0% and 100% RH

Paris' Law and Damage Density

The fundamental fracture law is Paris' law, which relates the stress intensity factor range to critical crack growth under a fatigue stress regime. There are some modifications to the Paris' Law but the fundamental concept maintains the same. The details of how it is modeled were discussed in the chapter 3 of the SHRP Report No. A-357 (Lytton et al. 1993). Lytton (2005) also used the crack growth potential to evaluate the moisture susceptibility of the asphalt mix specimens. The equation to estimate the crack growth was derived from Paris' law, which can be expressed in terms of the J-integral as follows:

$$\frac{dc}{dN} = AJ^n \tag{43}$$

where dc/dN is the crack growth per cycle; and A and N are regression coefficients determined from experiments.

The damage density of the FAM, as shown in Figure 23, can also fitted to the form using the equation as follows:

$$\phi = \phi_0 + aN^b \tag{44}$$

By modeling the damage density increase using the modified Paris' law, the fracture parameter was also obtained from the formulation using the equation as follows:

$$\varphi = \varphi_0 + A'^{\frac{1}{n'+1}} \left(\frac{1}{2A_F} \right)^{\frac{n'}{n'+1}} (cd)^{\frac{n'}{n'+1}} \frac{n'+1}{dn'+1} N^{\frac{dn'+1}{n'+1}} \tag{45}$$

Comparing Equation 44 to Equation 45, the modified Paris' law fracture parameters n′ and A′ were obtained.

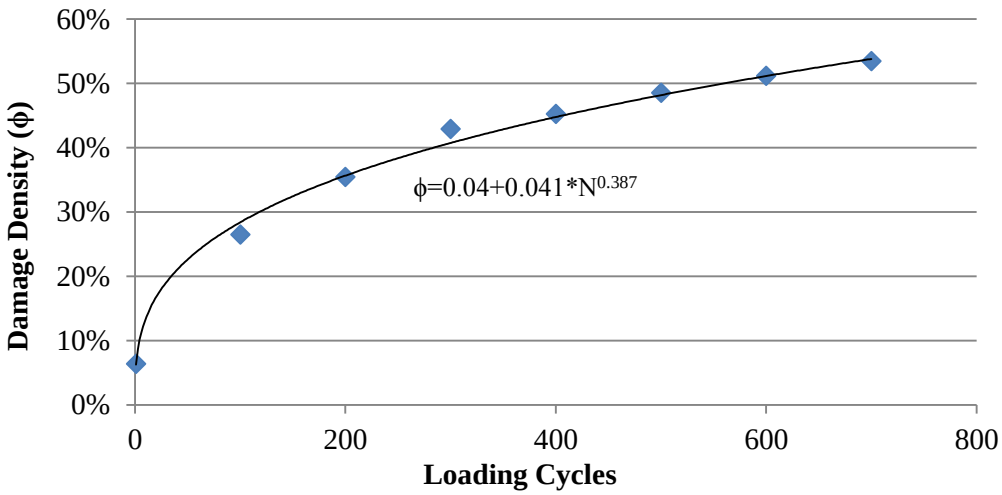

Figure 23. Damage Density vs. Loading Cycles

Surface Energy Measurement

As shown in the Equation 39, the bond energy between asphalt and aggregate is a key input for calculation the fatigue crack growth. Therefore, it is important to measure the surface energy f or both asphalt and aggregate. The detailed surface energy measuring procedure is listed in the Appendix B. Once all the surface energy components for both the asphalt and aggregate are obtained, the bond energy between the asphalt and aggregate can be calculated using the following equation:

$$\gamma_{ij} = \left(\sqrt{\gamma_i^{LW}} - \sqrt{\gamma_j^{LW}} \right)^2 + 2\left(\sqrt{\gamma_i^- \gamma_i^+} + \sqrt{\gamma_j^- \gamma_j^+} - \sqrt{\gamma_i^- \gamma_j^+} - \sqrt{\gamma_j^- \gamma_i^+} \right) \tag{46}$$

where, subscript i and j represent the aggregate and binder respectively.

And with the presence of the water, the bond energy among water, asphalt and aggregate can be calculated using the following equation:

$$\begin{aligned} \Delta G_{132} = {} & \sqrt{\gamma_1^{LW} \gamma_3^{LW}} + \sqrt{\gamma_2^{LW} \gamma_3^{LW}} - \sqrt{\gamma_1^{LW} \gamma_2^{LW}} - \gamma_3^{LW} + \\ & 2\sqrt{\gamma_3^+} \left(\sqrt{\gamma_1^-} + \sqrt{\gamma_2^-} - \sqrt{\gamma_3^-} \right) + \\ & 2\sqrt{\gamma_3^-} \left(\sqrt{\gamma_1^+} + \sqrt{\gamma_2^+} - \sqrt{\gamma_3^+} \right) - \\ & 2\sqrt{\gamma_1^+ \gamma_2^-} - 2\sqrt{\gamma_1^- \gamma_2^+} \end{aligned} \tag{47}$$

where, subscript 1, 2 and 3 represent the three materials aggregate, binder and water respectively.

As shown in the Figure 24, the bond energy varies significantly for the same aggregate with different binders. The bonder energy changes dramatically for the same binder with different aggregates. Therefore, the bond energy can be used to relate directly to the tensile strength of the asphalt mix, and it can be used to evaluate the moisture

susceptibility of asphalt mix by ranking the material. In practice, if the choice of aggregate is limited by the location, one can choose the best match binder type with the available aggregate to resist the moisture damage of asphalt mix.

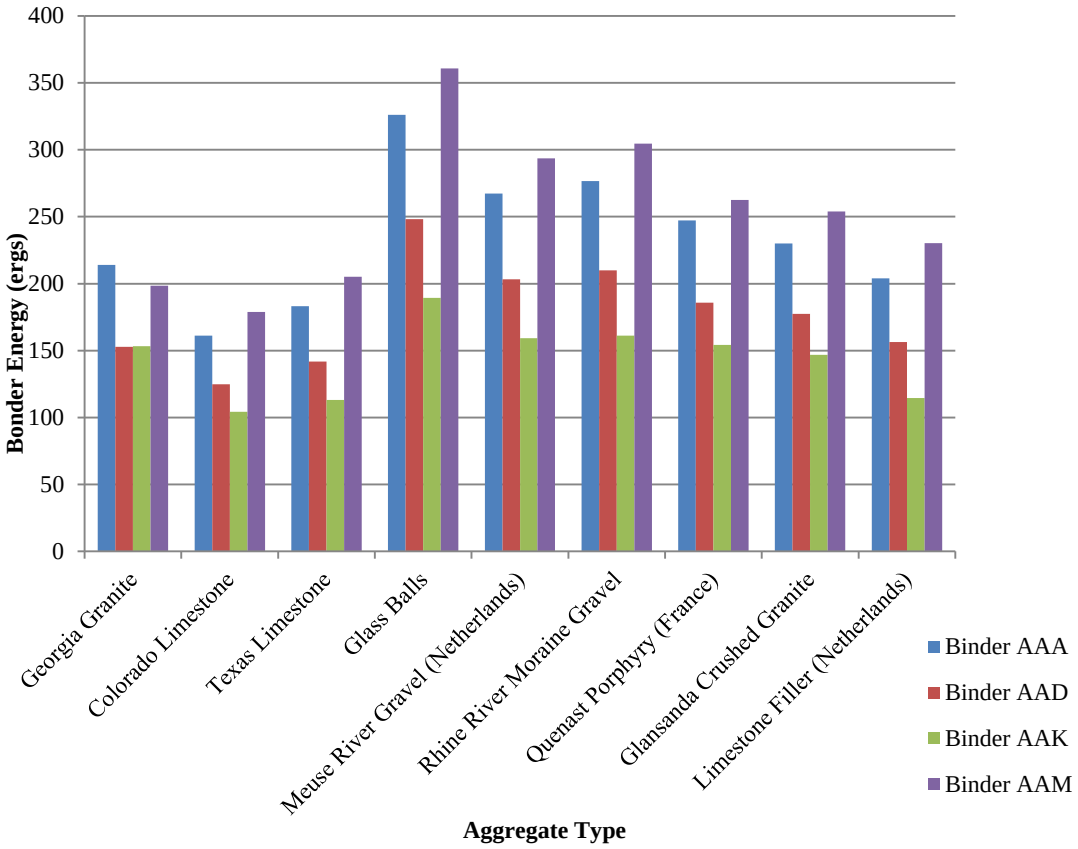

Figure 24. Bond Energy Comparison for 4 Different Binders with 9 Different Aggregates

The same reasoning can be used to evaluate the tensile strength of Warm Mix Asphalt (WMA). As shown in Figure 25, with the presence of the WMA additives, the bond energy between the aggregate and asphalt changes dramatically. This change of bond energy contributes to the tensile strength reduction of the WMA, which in return will

significantly affect the fatigue resistance of WMA. Therefore the surface energy measurements can be used directly to relate to the performance of asphalt mix. As shown in Figure 26, as the presence of water, the bond energy changes from positive value to negative value, which demonstrates that the water plays a role in deboning the composite material. For example, the bond energy for the hot mix will always be greater than the WMA, which means that the WMA is much more susceptible to moisture damage than the HMA.

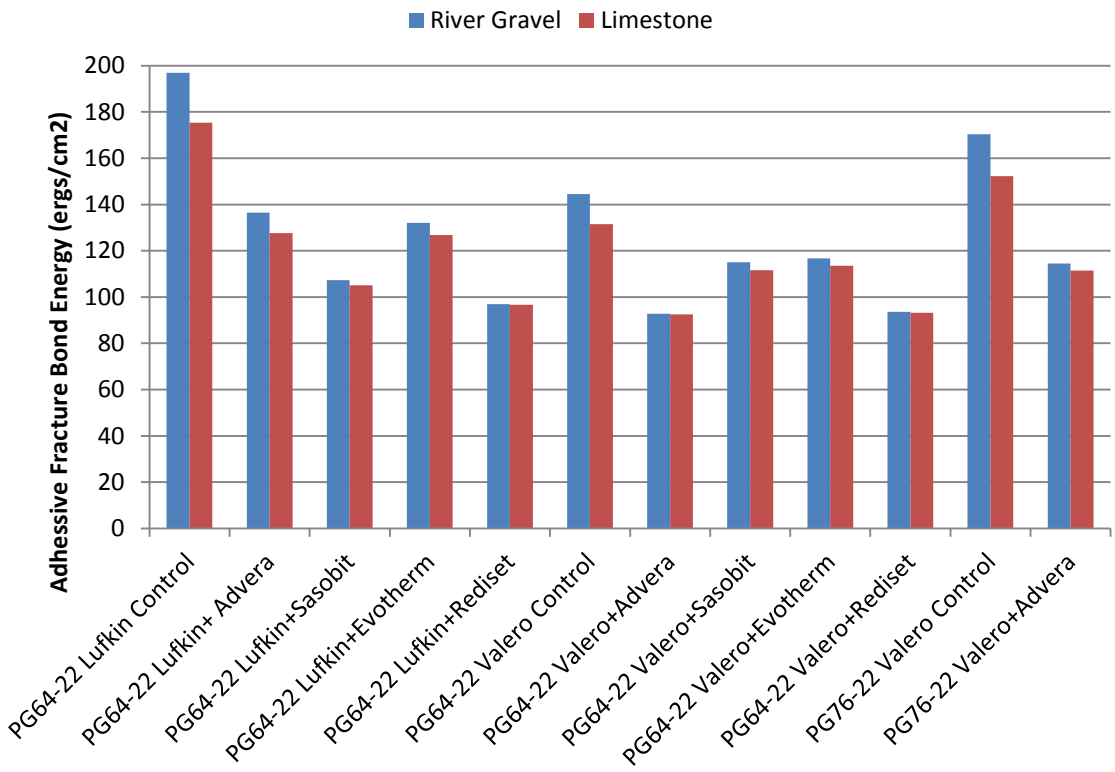

Figure 25. Bond Energy Comparison for Different Binders with Different Aggregates without Water

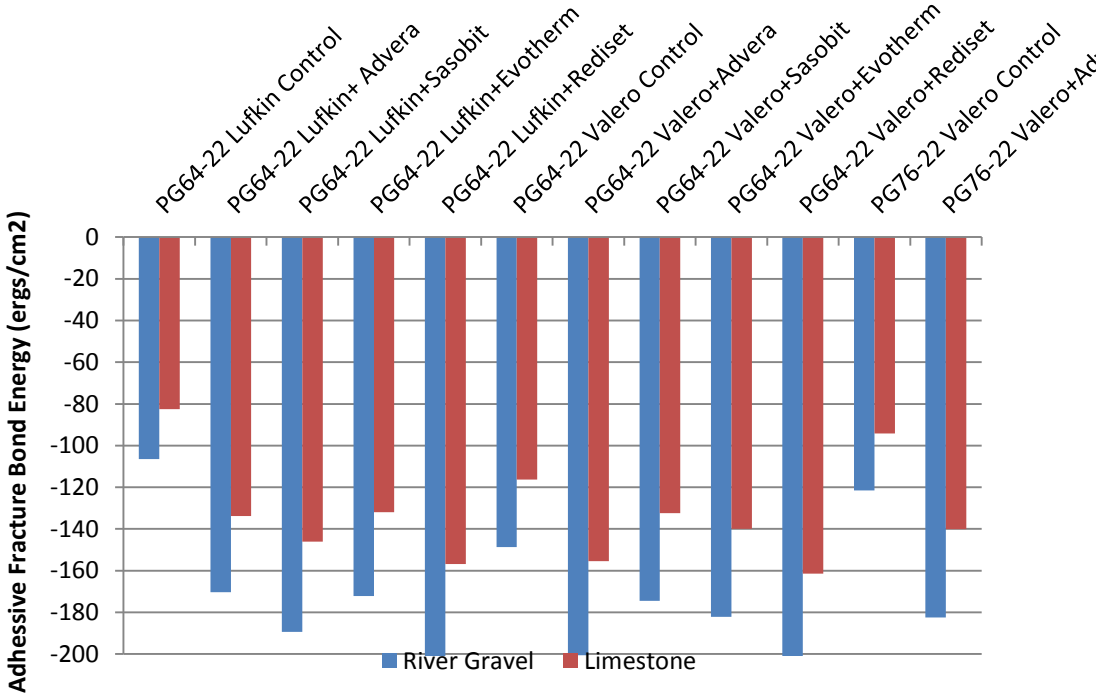

Figure 26. Bond Energy Comparison for Different Binders with Different Aggregates with Water

Another moisture damage mechanism is the cohesive fracture in asphalt mastic, which is illustrated in Figure 27. The presence of water greatly reduces the cohesive bond energy within asphalt mastic, however, the presence of additives Evotherm and sasobit can improve the moisture susceptibility to cohesive failure of WMA.

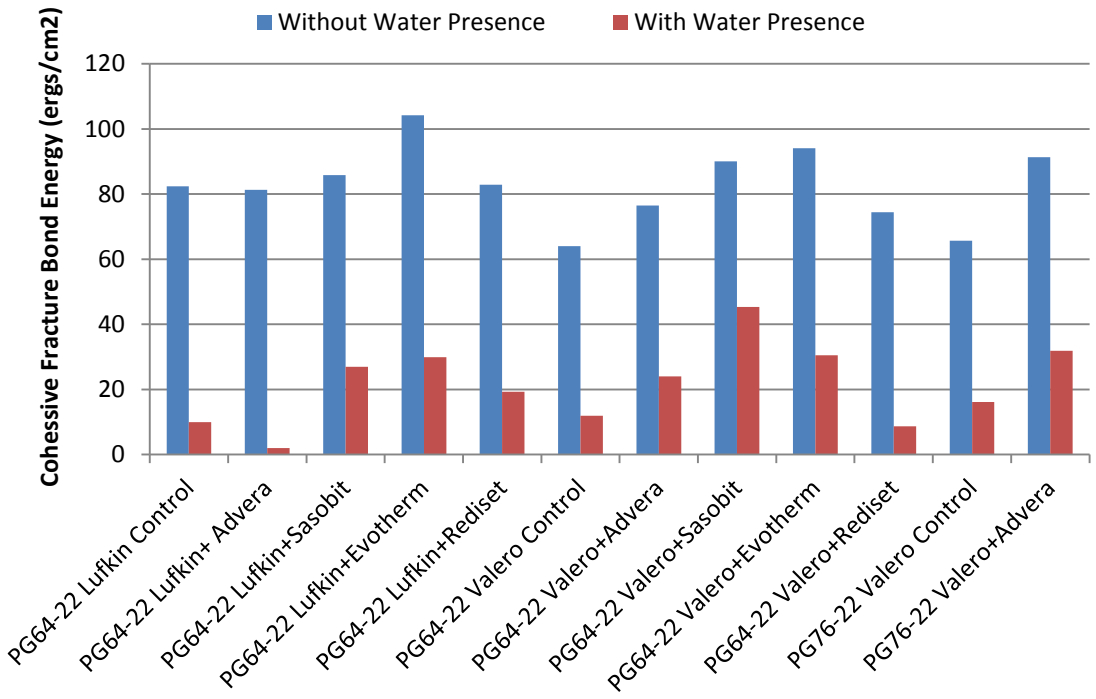

Figure 27. Cohesive Energy Comparison for Different Binders with Different Aggregates

Analysis Results

HMA Test Results

Both of the dry and wet FAM specimens fabricated with the Valero binder and NuStar binder were tested using the DMA to obtain their fatigue properties. All the analysis results are summarized in Table 11 and Table 12.

Table 11. Fracture Parameters for Specimens Fabricated with NuStar Binders

Binder	Specimen ID	Air Void %	RH %	A′	n′
NuStar PG76-22	11_A0	6.58	0	8.26E-16	2.92
	4_A0	8.05	0	4.38E-17	4.23
	14_A6	5.55	0	1.40E-29	6.09
	16_A6	6.92	0	4.08E-35	7.37
	9_A6	7.49	0	4.86E-29	5.97
	10_A6	7.64	0	1.74E-25	5.15
	5_A0	6.79	100	2.54E-42	9.02
	8_A0	7.82	100	7.25E-51	10.99
	12_A0	7.37	100	4.64E-48	11.24
	17_A0	6.1	100	4.60E-42	9.79

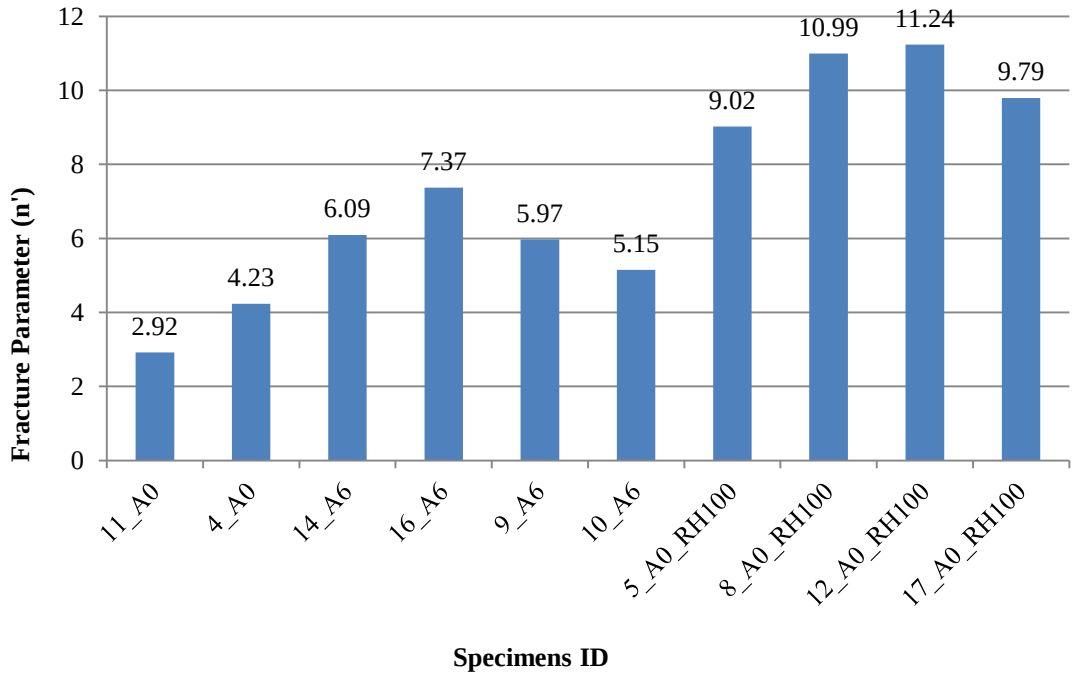

Figure 28. Fracture Parameter n' for Specimens with NuStar Binder

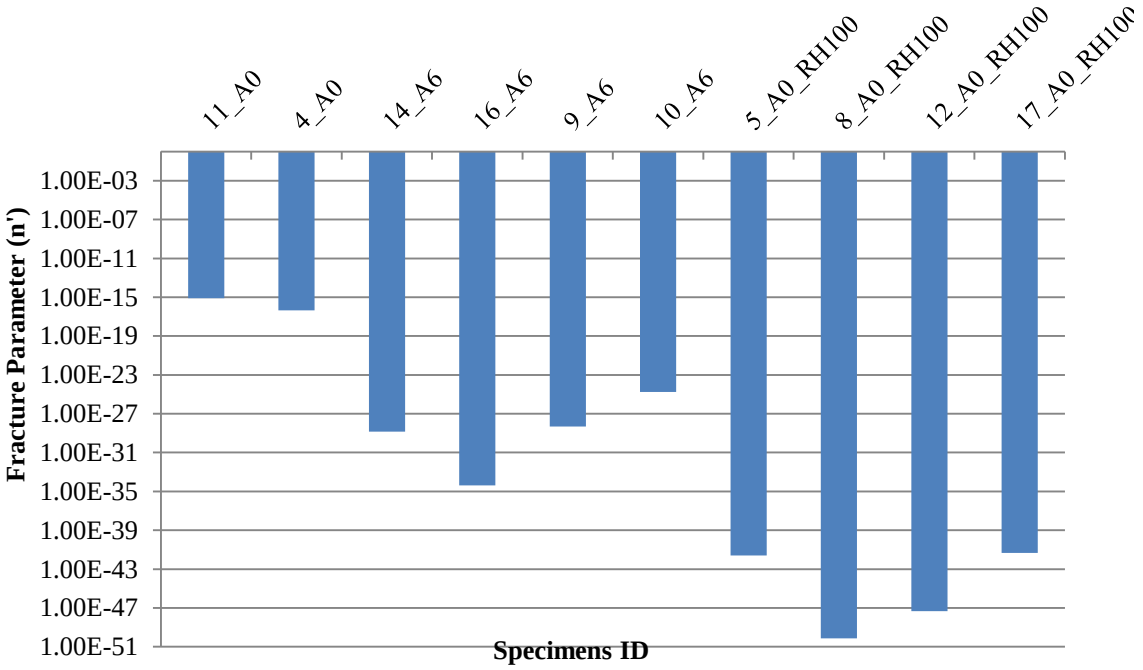

Figure 29. Fracture Parameter A' for Specimens with NuStar Binder

As is clearly observed in Figure 28, as the conditioning relative humidity increased to 100 percent, the fracture parameter n' tended to increase for FAM specimens with NuStar binder, which indicates that the saturated vapor pressure in the specimens significantly increased the fatigue potential of the asphalt mix material. As shown in the Figure 29, the modified Paris' law parameter A' tended to decrease as the condition relative humidity increased; it is believed, however, that this decrease was not adequate to offset the increase of A'. Therefore, it was concluded that the moisture presence in the asphalt due to vapor diffusion did increase the fatigue crack of the asphalt mix significantly. These findings demonstrate that cracks grow faster in specimens with a higher RH level. This fact indicates that the diffusion of subsurface water vapor accelerates the deterioration of the asphalt layer of flexible pavement. As a result, the RH level must be taken into consideration when predicting the fatigue life of any asphalt mixture and when designing asphalt pavements.

Table 12. Fracture Parameters for Specimens Fabricated with Valero Binders

Binder	Specimen ID	Air Void %	RH %	A′	n′
Valero PG64-16	7_A0	7.54	0	6.83E-16	2.96
	53_A0	8.19	0	1.29E-15	2.5
	8_A0	6.91	100	1.09E-52	11.44
	9_A0	7.35	100	1.06E-48	10.52
	54_A0	6.54	100	1.65E-40	8.42

Table 12. Continued

Binder	Specimen ID	Air Void %	RH %	A′	n′
Valero PG64-16	74_A0	7.55	100	1.36E-68	15.07
	11_A6	6.58	0	1.59E-37	7.94
	12_A6	7.37	0	2.56E-38	8.12
	15_A6	6.88	0	1.56E-26	5.4
	17_A6	7.71	0	8.91E-31	6.37

The same trend is observed for the FAM specimens with Valero binder. As demonstrated in the Figure 30, as the conditioning relative humidity increased to 100 percent, the fracture parameter n' tended to increase for Valero specimens. The fracture parameter A' tended to decrease as the condition relative humidity increased as shown in Figure 31. This fact confirms that the diffusion of subsurface water vapor is a major mechanism of water transport in pavement.

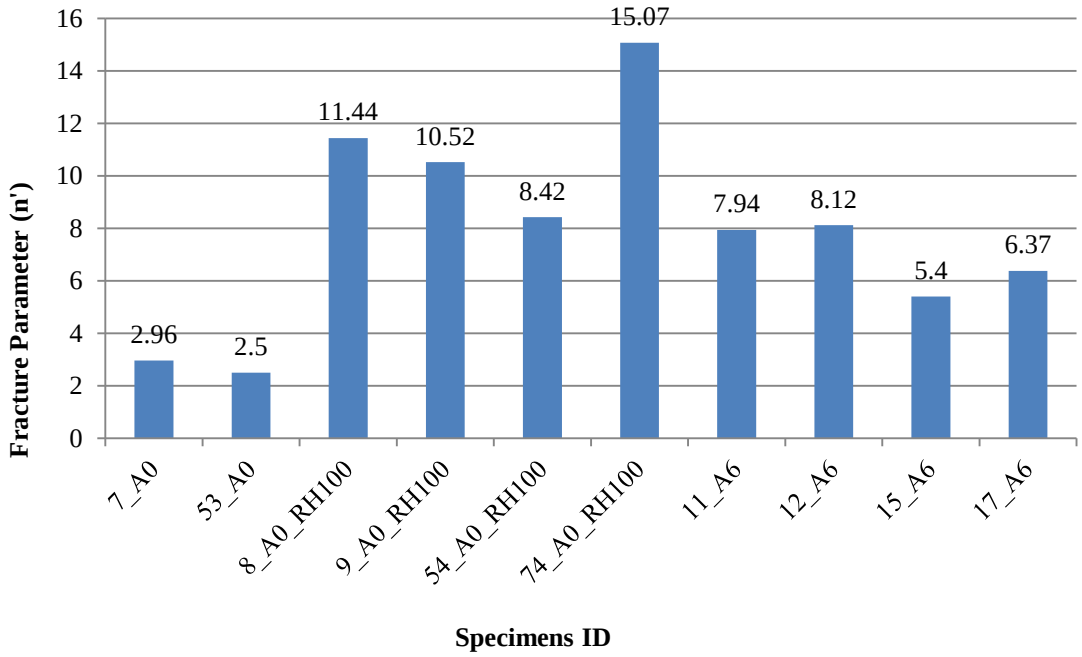

Figure 30. Fracture Parameter n' for Specimens with Valero Binder

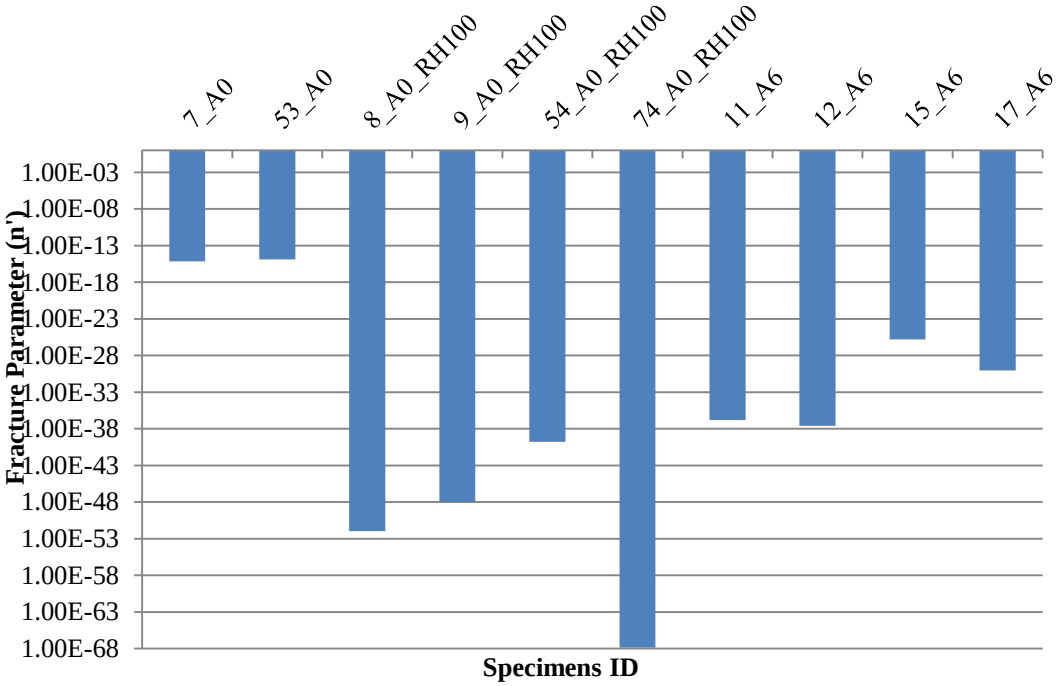

Figure 31. Fracture Parameter A' for Specimens with Valero Binder

The relation of log A' and n' was found to be highly linear, as illustrated in the Figure 32 and Figure 33, respectively. In general, the fracture parameter n' will increase if the $\log A'$ is decreasing, which indicates that A' and n' are highly correlated with each other.

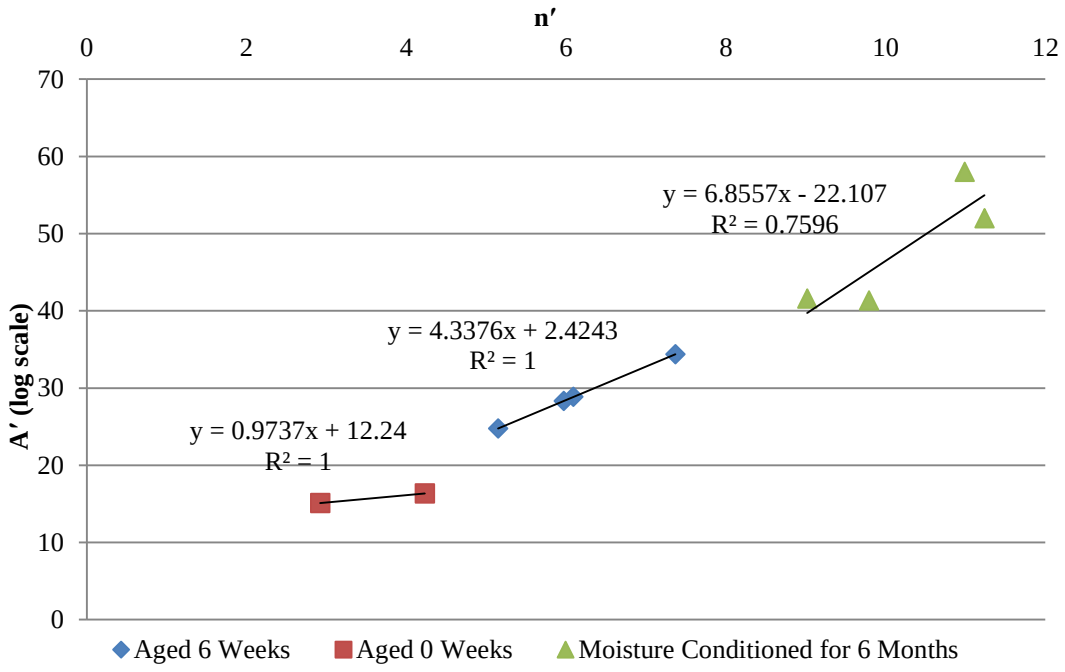

Figure 32. Plot of log A′ vs. n′ at Different Aging Time for NuStar Binder

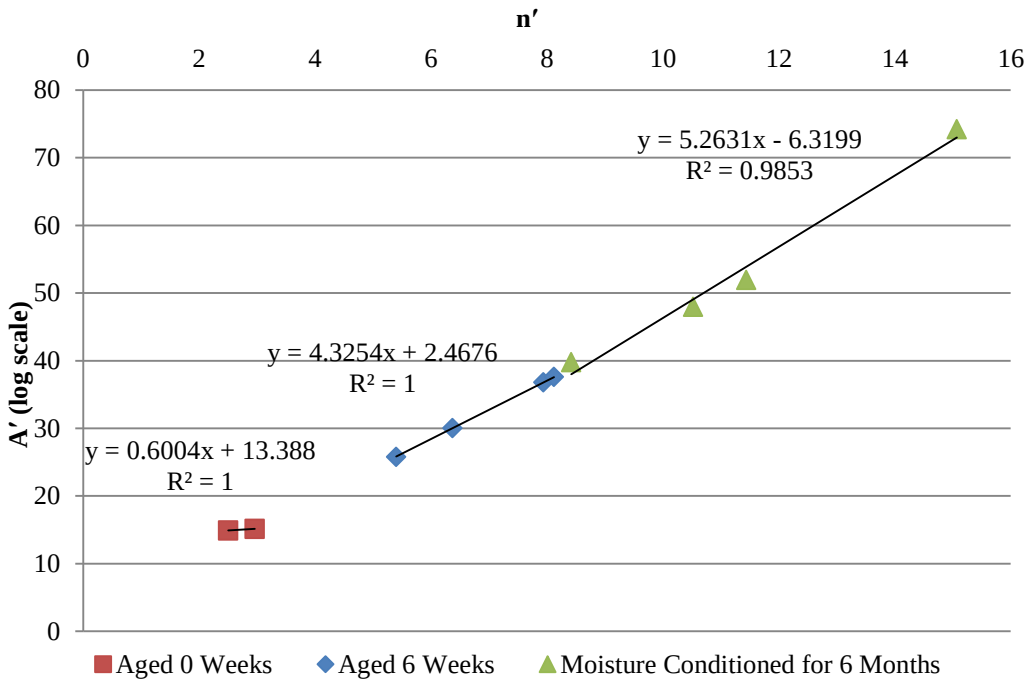

Figure 33. Plot of log A′ vs. n′ at Different Aging Time for Valero Binder

It was also observed, as shown in Figure 32 and Figure 33, that the slope of log A' vs. n' for the aged specimen was higher than the unaged specimens. The slope of $log\ A'$ *vs.* n' was higher for the moisture-conditioned specimens than the specimens aged for 6 weeks. Therefore, it could be concluded that both aging and moisture increase the fatigue potential of FAM significantly. Meanwhile, the water presence induced more damage in terms of fatigue than the specimens aged for 6 weeks.

WMA Test Results

As is observed in Figure 34, as the conditioning relative humidity increased to 100 percent, the fracture parameter n' tended to increase for both HMA and WMA

specimens, which indicates that the saturated vapor pressure in the specimens significantly increased the fatigue potential of the asphalt mix material. The modified Paris' law parameter A' tended to decrease as the relative humidity condition increased and this decrease is not adequate to offset the increase. Therefore, it is concluded that the moisture presence in the asphalt due to vapor diffusion increases the fatigue crack of the asphalt mix significantly. It is also concluded that the aging increases the rate of asphalt fatigue cracking of both warm asphalt mix and hot asphalt mix. Another finding is that the n' is higher for the moisture conditioned specimens than that for aged specimens, which demonstrates that the water presence induces more damage than aging. These findings demonstrate that cracks grow faster in specimens with a higher upward RH level for both warm and hot asphalt mix. This fact indicates that the diffusion of subsurface water vapor into the asphalt layer accelerates the deterioration of the asphalt layer of flexible pavement faster than the aging. As a result, the RH level must be taken into consideration when predicting the fatigue life of any asphalt mixture and when designing asphalt pavements.

It is also observed that the WMA performs better in terms of fatigue resistance when there is no moisture existed in the material. The reason is that WMA is usually produced at temperatures 20 C° to 50 C° lower than that of a typical hot-mix asphalt, which means the WMA has less binder aging. Hence, the less the binder ageing, the higher the bond energy between the asphalt and aggregate. However, WMA is more susceptible to moisture as demonstrated in the Figure 34. The possible reason is that the WMA has less binder absorption into aggregate due to the lower production temperature

and thus it is much easier for the moisture to reach into the interface between the asphalt and the aggregate in the asphalt mixture, which induced more deboning and led to the less resistance to fatigue.

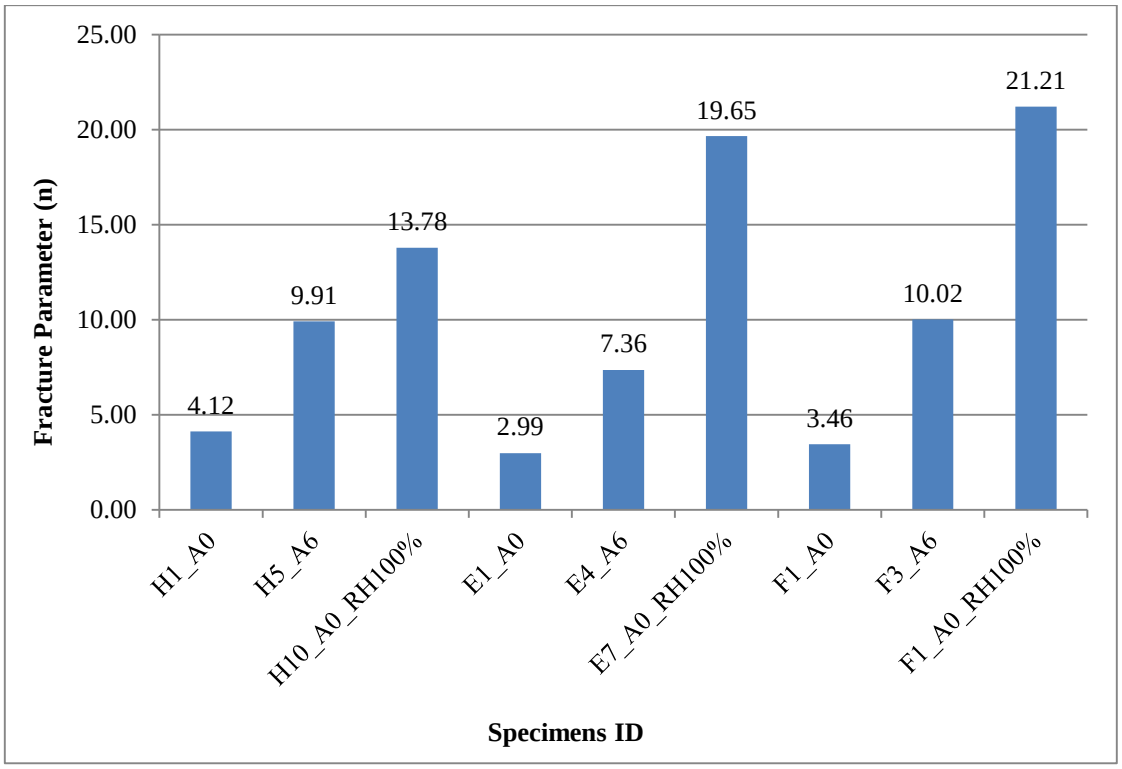

Figure 34. Test Results for HMA and WMA

CHAPTER VI

VALIDATION OF THE DMA TEST RESULTS*

In this chapter, a set of WMA specimens with full gradation aggregate was tested using an experimental method developed at TAMU to verify the efficiency of the DMA test results. Xue et al (2012) developed a controlled-strain repeated direct tension test to characterize fatigue cracking with the presence of permanent deformation of asphalt mixtures. This RDT test is conducted in the controlled-strain mode rather than the controlled-stress mode. The reasoning is that the plastic deformation resulting from yielding of the bulk material is small and the localized plastic deformation around cracks is significant under the controlled-strain mode. It is well documented in the literature that this localized plastic deformation affecting the cracking process, so the controlled-strain mode is more advantageous compared to the stress-controlled

The controlled-strain RDT test is conducted using the Material Test System (MTS) at the temperature of 20°C. The asphalt mixture specimen is cylindrical with a dimension of 102 mm in diameter by 150 mm in height. Two consecutive controlled-strain RDT tests are performed on the same asphalt mixture specimen: 1) Nondestructive

* "Modeling Water Vapor Diffusion in Pavement and Its Influence on Fatigue Crack Growth of Fine Aggregate Mixture" by Y. Tong, R. Luo, and R. L. Lytton. Presented at the 92nd Annual Meeting of the Transportation Research Board, January 2013, Washington, D.C., and accepted for publication in the 2013 series of the Transportation Research Record: Journal of the Transportation Research Board (forthcoming).

RDT tests with 100 load cycles at low loading levels; and 2) Destructive RDT test with 1,000 load cycles at the higher loading level. The loading frequency is 1 Hz in both tests, which is the same compared to the DMA test. The nondestructive RDT tests are performed to determine the critical undamaged state of the asphalt mixture specimen, which is the reference state from which the damage introduced into the asphalt mixture could be quantified.

Data Analysis

Since this is a controlled-strain RDT test, its stress always contains a tensile portion and a compressive portion in each loading cycle when the strain is controlled as a standard havesine shape that has only a tensile portion. Xue et al (2012) defined the situation with a tensile stress and a tensile strain as "tension portion"; the situation with a compressive stress and a tensile strain as "quasi-compression portion". The FFT was conducted separately to reduce the noise for both the tension portion and the quasi-compressive portion transforming. Using the Excel spreadsheet developed by Xue at TAMU, the results of the controlled-strain RDT can be used for the analysis for fatigue resistance of asphalt mixture

Mechanical Modeling

This method uses an energy based approach to characterize the fatigue resistance of the asphalt material. As summarized in the Figure 35, the energy calculated from the measured stress and measured strain is thus assumed to be distributed in the entire specimen, including the intact material and cracks. The measurement from the test is an apparent representation of what actually happens inside the asphalt mixture specimen.

Three equivalence equations are established between the apparent measurement and the true circumstance according to the mechanics principles.

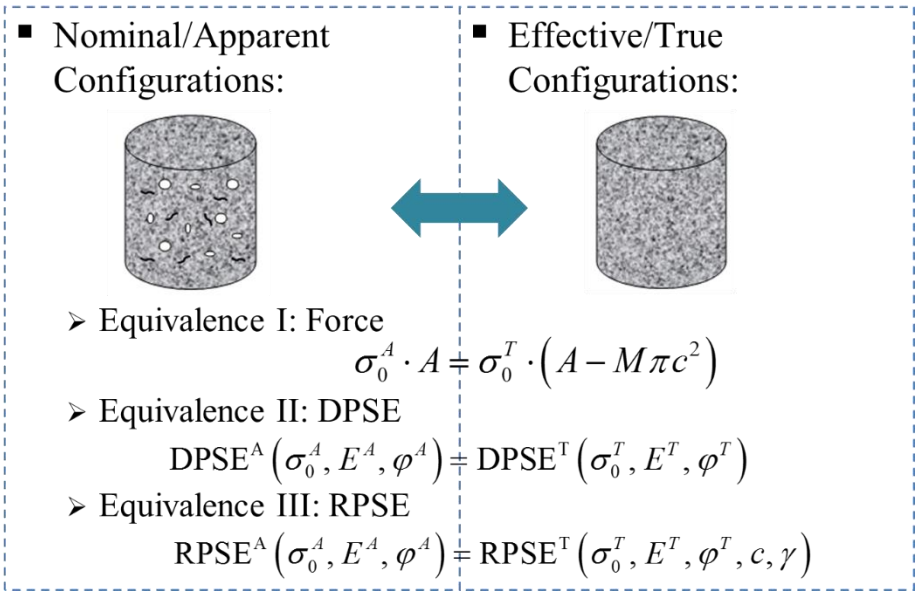

Figure 35. Mechanistic Modeling Demonstration for Fatigue Crack

The σ^A is apparent stress measured from the test, the superscript "A" standing for "apparent"; A is the area of the entire cross section of the specimen; σ^T is true stress in the intact material, the superscript "T" standing for "true"; and M is average area of cracks on the cross section of the specimen.; c is the average crack size of the specimens.

Results

Using the mechanical approach described, the average crack size and number of cracks versus the number of loading cycles can be obtained. As discussed in the Chapter V, using the modified Paris' law, the damage density versus the number of loading cycles was used to achieve the fracture parameters A' and n'. It is clearly observed in Figure

36, as the conditioning relative humidity increased to 100 percent, the fracture parameter n' tended to increase for both the HMA control and the WMA specimens, which indicates that the saturated vapor pressure in the specimens significantly increased the fatigue potential of the asphalt mix material.

It is also observed that the aging increases the rate of asphalt fatigue cracking of both warm asphalt mix and hot asphalt mix. Another finding is that the n' is higher for the moisture conditioned specimens than that for aged specimens, which indicated that WMA is more susceptible to moisture compared to the HMA. All those finds are comparable to the findings in the Chapter V, Therefore, this newly developed DMA test can be used an efficient and accurate test method to characterize the fatigue properties of asphalt mixture.

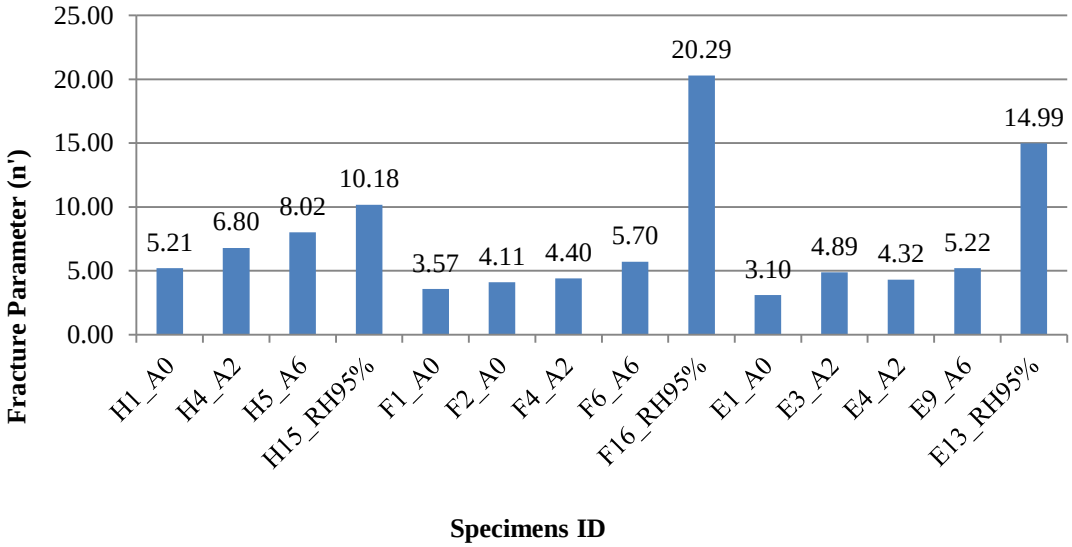

Figure 36. Fracture Parameter n' for Different Specimens

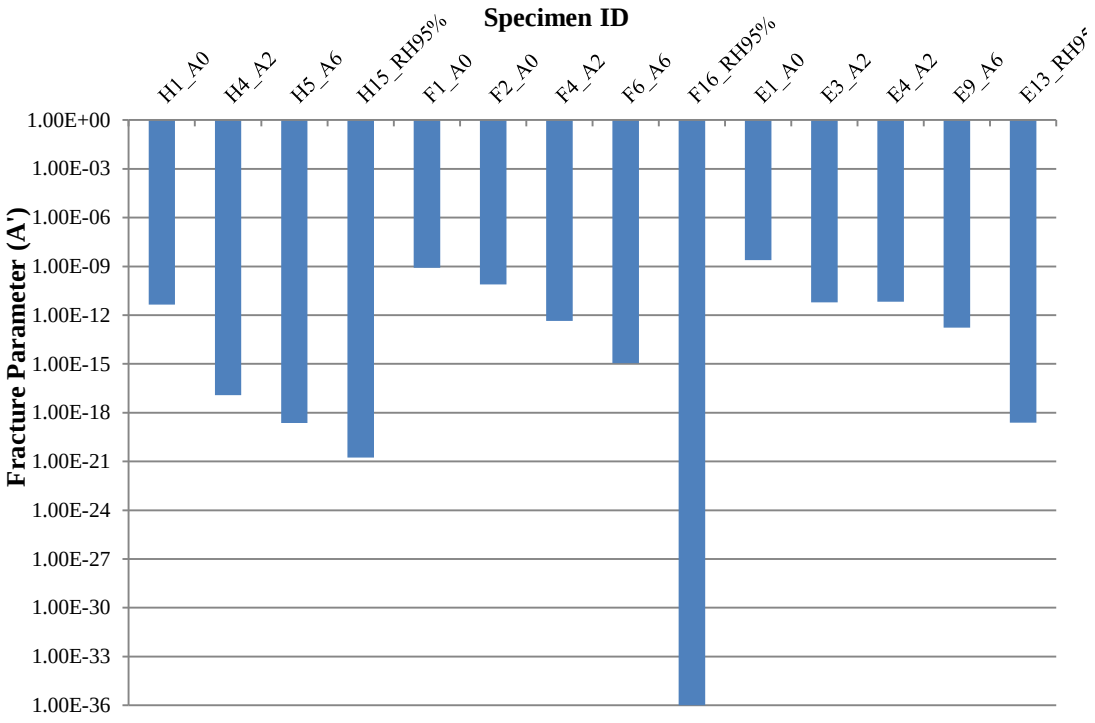

Figure 37. Fracture Parameter A' for Different Specimens

CHAPTER VII

CONCLUSIONS, RECOMMENDATION AND FUTURE RESEARCH

Highway system is of essential influence on the welfare of the economy. However, the national infrastructure rating received an overall grade of D-plus, an average pulled down by one of the biggest problem areas – roadways. The FHWA reported that restoring it to good working order will require an investment of $3.6 trillion by 2020. Currently, United States only spent less than 2% on average as a percentage of GDP into the transportation infrastructure since 1980 and the ASCE concluded, and if the current level of spending continues it will fall short by $1.6 trillion. It is reported that thirty-six percent of America's major urban highways are congested. Congestion costs drivers more than $63 billion a year in wasted time and fuel costs. Americans spend 3.7 billion hours a year stuck in traffic. And while their car engines are idling, they are pumping thousands of tons of pollution into the air every day. If we fail to increase investment, more senseless deaths will be see on the roadway system. It should be noticed that 33% of U.S. major roads are in poor or mediocre condition. Poor road conditions result in $67 billion in extra vehicle repairs and operating costs per year. The astonishing fact is that the degradation of asphalt pavements induced by the moisture in the U.S. results in additional vehicle costs over $54 billion annually, which is around 80% of the total extra vehicle cost and operating costs per year. More important, poorly maintained roads contribute to a third of all highway fatalities. That's more than 14,000 deaths every year.

Hence, worsened by the poor highway condition, the current highway capacity is unable to meet the rate of the economy development.

Facing the great pressure of transportation funding shortage, sustainable transportation systems stands out as a hot topic in the agencies of U.S. It start with building roadways in intelligent and innovative ways, which enhance riding quality and safety to meet the mobility requirement for economic growth, protect environment by minimizing consumption of non-renewable resources, and reduce cost. Due to the high temperature requirement during the process of production, the price of the asphalt mix is substantially affected by the cost of fuel consumption. As a result, the paving industry is always searching for more cost-effective and energy-efficient ways of building roads. Warm mix asphalt (WMA), originating as an effective measure to reduce cost and emissions, represents a group of technologies that allow reduced mixing and placement temperatures thereby enabling reduced fuel consumption, enhanced compaction, increased economical haul distances and an extended paving season. WMA is usually produced at temperatures 20 C° to 50 C° lower than that of a typical hot-mix asphalt (HMA). Hence, the fuel consumption used for heating asphalt and aggregate can be cut down by 10 to 20 percent. The implication is a substantial reduction of carbon dioxide emission and much less worker exposure to asphalt fumes. The literature review suggests that WMA has great potential in overcoming environmental challenges and reducing production costs. However, there are only limited performance studies available up to the present. Particularly, the current WMA performance evaluation methods, such as the Overlay Tester tests, torsional tests using the Dynamic Mechanical

Analyzer (DMA) and four-point beam fatigue tests, yield incompatible results with field performance. Therefore, for the purpose of accurately evaluating the performance of WMA and later incorporating it as a sustainable pavement strategy. Considering the increased pressure that the DOT agencies are dealing with, the demand for the asphalt pavement to perform as expected with minimal moisture related premature failure becomes more and more pressing. Conversely, more than 42 million tons of WMA have been placed in 2011 without a fundamental understanding of its moisture-related performance.

This study addresses the significant effect of water vapor on asphalt pavement materials. The water vapor diffusion model developed in this research clearly illustrates that the water vapor accumulates in the pavement at a rapid rate and it reaches nearly saturated vapor pressure within a period of 6 months. Moreover, wetting processes in the pavement layer brought by the subsurface water vapor diffusion is occurring day and night. Therefore, the water presence due to vapor diffusion in the asphalt surface layer is one of the major water movement mechanisms in pavement and it greatly accelerates the deterioration of the asphalt mixture.

This dissertation also presents a new test and data analysis protocol based on the pseudo strain energy equivalence theory to characterize the fatigue crack growth of FAM specimens that were conditioned at different RH levels. Compared to the previous torsional test, the newly proposed RDT test protocol greatly reduces the stress state complexity within the specimens by evenly distributing stress over the cross section area of the cylindrical specimen. This RDT test protocol is much more efficient than the

torsional test in terms of characterizing the fatigue crack growth of FAM. The results show that RH gradients existing in pavement layers are important in driving the diffusion of water vapor through the connected air voids into the surface asphalt layers and eventually to degrade the integrity of the asphalt material.

Water Vapor Transport Mechanism

Water vapor movement in the pavement structure is a diffusion process. The coefficient of water vapor diffusivity was obtained by monitoring the overall mass increase of the specimens for 6 month. Water vapor movement within the pavement layers was simulated using the laboratory experiment as detailed in the Chapter III. The conclusion are summarized as follows:

- Subgrade soil vapor pressure is generally near 100% relative humidity and the soil beneath the pavement can be treated as water vapor saturated material. In cold weather, the temperature gradients facilitate the vapor movement upward from underlying layers and thus produce nearly saturated vapor pressure in the pavement surface layer. In hot weather, although the pavement surface temperature is higher than the underlying layer, a temperature gradient which tends to drive the water vapor moving downward, the existing RH gradients override the tendency of the downward movement of water vapor driven by the temperature gradient.
- Vapor movement within the pavement layers is a diffusion process and occurs along the concentration gradients. And the variations in atmospheric temperature

and relative humidity might also influence the rate of vapor transport within pavement systems.

- The water vapor diffusion model developed in this paper clearly illustrates that the water vapor accumulates in the pavement at a rapid rate and it reaches nearly saturated vapor pressure within a period of 6 months. Moreover, wetting processes in the pavement layer brought by the subsurface water vapor diffusion is occurring day and night. Therefore, the water presence due to vapor diffusion in the asphalt surface layer is one of the major water movement mechanisms in pavement and it greatly accelerates the deterioration of the asphalt mixture. In order to simulate the water vapor diffusion process in the field, a new moisture conditioning method was developed using vacuum desiccators. Furthermore, water vapor diffusive coefficient was obtained by monitoring the overall mass increase of the specimens for 4 month using a simple diffusion model.
- Wind is another factor that needs to be addressed on the water vapor diffusion process in the pavement. When there is no wind, the RH in the air above the pavement surface remains steady. However, if there is a wind blowing across the pavement surface, it removes the water vapor rapidly in the air above the pavement surface. This generates a steeper RH gradient between the air and the asphalt surface layer, and increases the rate with which the RH increases in the asphalt layer.

Fatigue Resistance Affected by Water Vapor and Aging

Moisture and aging are two major factors that can significantly increase the fatigue cracking in the asphalt mixture. As the conditioning relative humidity increased to 100 percent, the fracture parameter n' tended to increase for FAM specimens, which indicates that the saturated vapor pressure in the specimens significantly increased the fatigue potential of the asphalt mix material. Therefore, it was concluded that the moisture presence in the asphalt due to vapor diffusion did increase the fatigue crack of the asphalt mix significantly. These findings demonstrate that cracks grow faster in specimens with a higher RH level. This fact indicates that the diffusion of subsurface water vapor accelerates the deterioration of the asphalt layer of flexible pavement. As a result, the RH level must be taken into consideration when predicting the fatigue life of any asphalt mixture and when designing asphalt pavements. The detailed summary is listed as follows:

1. The WMA Evotherm DAT and foaming technologies improves the fatigue crack growth of WMA compared to the HMA slightly when there is no moisture presence in the material. The reason is that WMA is usually produced at temperatures 20 C° to 50 C° lower than that of a typical hot-mix asphalt, which means the WMA has less binder aging. Hence, the less the binder ageing, the higher the bond energy between the asphalt and aggregate
2. The results shown that there is direct correlation between fatigue crack resistance and binder absorption. As the absorbed binder increases, the fatigue crack of asphalt decreases.

3. After 6 weeks of aging period at the temperature 60 C°, the fatigue crack growth of WMA increases substantially and there is no significant difference between HMA and WMA.
4. WMA is more susceptible to moisture as discussed in the Chapter V. The possible reason is that the WMA has less binder absorption into aggregate due to the lower production temperature and thus it is much easier for the moisture to reach into the interface between the asphalt and the aggregate in the asphalt mixture, which induced more deboning and led to the less resistance to fatigue.

Recommendations

1. As discussed in the research, water enters a pavement system by three major mechanisms: 1) surface water percolates into the pavement system, 2) subsurface water is drawn up into a pavement system by capillary rise, and 3) water vapor diffusion. This research only focus on the water vapor diffusion and it might be for the best of pavement engineer if a combined model can be developed to account all three mechanism at the same time.
2. The conditioning method developed in this research did not consider the freeze and thaw influence on the fatigue life of asphalt mixture. However, in the cold area, the moisture buildup could lead to the development of ice lenses and frost heave, which would lead to thaw weakening of base and subgrade soils when thaw occurs.

3. It is still unknown whether the WMA additive trap water into the material or not. Further forensic investigation of the moisture presence in WMA should be conducted.
5. The major problem in this vapor diffusion model using the approximation solution method is the two different boundary assumptions. Therefore, a numerical method was can be adopted to improve the previous models. Crank-Nicolson is a popular method for solving parabolic partial differential equations because it is unconditionally stable and second-order accurate. The simplest and well-known implicit Crank-Nicholson scheme is obtained by a combination of the forward time differencing and an averaging over time of the second-order, centered-space derivative operator. It is based on the central difference in space and the trapezoidal rule in time, giving second-order convergence in time. A preliminary model was established and discussed in the Appendix C.

Future Research

There are two major areas that will need future research in the future study. The first is related to the crack growth model and the second is related to the model of water vapor diffusion.

The results from this newly developed control-stress test demonstrated very repeatable results in evaluating the fatigue cracking of FAM. Since there are many other variables that need to be considered in evaluating the fatigue crack of asphalt material such as air void structure and additives so on. Therefore, it is recommend that more

FAM samples should be studied to further validate the effectiveness of the model, especially for mixes and mixes with known field performance.

Secondly, in the procedure of modeling the water vapor diffusion, the moisture diffusion coefficients measured in FAM samples by monitoring the weight of specimens varies significantly, which is mainly because of the complexity and heterogeneity of the material. Therefore, how to ensure the consistency of the FAM specimens is of great importance to the RH profile in the pavement. It is also essential to reduce the moisture conditioning time for the FAM specimens, which probably could be realized by increase the condition pressure in the dissectors.

It is believed that the completion of this research will provide a solid basis for understanding the water vapor diffusion in the pavement and its influence performance on the performance of asphalt mixture from the aspect of mechanics.

REFERENCES

Arambula, E., S. Caro and E. Masad (2010). "Experimental Measurement and Numerical Simulation of Water Vapor Diffusion Through Asphalt Pavement Materials." Journal of Materials in Civil Engineering 22(6): 588-598.

Arambula, E., E. A. Masad and A. E. Martin (2007). "The Influence of Crack Growth Distribution on the Moisture Susceptibility of Asphalt Mixes." Journal of materials in civil engineering, ASCE 19(8): 655-664.

Bhasin, A. and D. N. Little (2007). "Characterization of Aggregate Surface Energy Using the Universal Sorption Device." Journal of Materials in Civil Engineering 19(8): 634-641.

Bhasin, A., E. Masad, D. Little and R. Lytton (2006). "Limits on Adhesive Bond Energy for Improved Resistance of Hot-Mix Asphalt to Moisture Damage." Journal of the Transportation Research Board(1970): 3-13.

Caro, S., E. A. Masad, A. Bhasint and D. N. Little (2008a). "Moisture Susceptibility of Asphalt Mixtures, Part 1: Mechanisms." International Journal of Pavement Engineering 9(2): 81-98.

Caro, S., E. A. Masad, A. Bhasint and D. N. Little (2008b). "Moisture Susceptibility of Asphalt Mixtures, Part 2: Characterisation and Modelling." International Journal of Pavement Engineering 9(2): 99-114.

Carpenter, S. H., R. L. Lytton and J. A. Epps (1974). "Environmental Factors Relevant to Pavment Cracking in West Texas. " 18-1, Texas Transportation Institute, Texas A&M University System.

Cheng, D., D. Little, R. Lytton and J. Holste (2002). "Moisture Damage Evaluation of Asphalt Mixtures by Considering Both Moisture Diffusion and Repeated-Load Conditions." Transportation Research Record: Journal of the Transportation Research Board 1832(1): 42-49.

Cheng, D., D. N. Little, R. L. Lytton and J. C. Holste (2001). "Surface Free Energy Measurements of Aggregates and its Application to Adhesion and Moisture Damage of Asphalt Aggregate Systems." 9th Symposium of International Center for Aggregates Research.

Copeland, A. (2005). "Moisture in Asphalt Pavements in the United States: A financial Perspective." First International Workshop on Moisture Damage.

Dijk, V. W. and W. Visser (1977). "Energy Approach to Fatigue for Pavment Design." Association of Asphalt Paving Technologists Proc: 1-40.

Estakhri, C., J. Button and A. E. Alvarez (2010). "Field and Laboratory Investigation of Warm Mix Asphalt in Texas." Texas Transportation Institute.

Fowkes, F. M. (1964). "Attractive Forces at Interfaces." Industrial Engineering &. Chemistry 56 (12): 40-52.

Hicks, R. G., Santucci, L. and Ashchenbrener, T. (2003). "Introduction and Seminar Objectives. Moisture Sensitivity of Asphalt Pavements, Transportation Research Board National Seminar." San Diego, California. 3-19.

Ghuzlan, K. A. and S. H. Carpenter (2002). "Traditional Fatigue Analysis of Asphalt Concrete Mixtures Transportation Research Board Annual Meeting." Washington D.C.

Goss, K.-U. and M. Madliger (2007). "Estimation of Water transport Based on In-situ Measurements of Relative humidity and Temperature in a Dry Tanzanian Soil." Water Resources Research 43 W05433.

Hefer, A. (2004). "Adhesion in Bitumen-Aggregate Systems and Quantification of the Effects of Water on the Adhesive Bond." Ph.D., Texas A&M University.

Hefer, A., A. Bhasin and D. N. Little (2006). "Bitumen Surface Energy Characterization Using a Contact Angle Approach." Journal Materials Civil Engineering 18(6): 759-767.

Hefer, A., D. N. Little and R. L. Lytton (2005). "A Synthesis of Theories and Mechanisms of Bitumen-aggregate Adhesion Including Recent Advances in Quantifying the Effects of Water." Association of Asphalt Paving Technologists 74: 139-196.

Hicks, G. R. (1991). "Synthesis of Highway Practice 175: Moisture Damage in Asphalt Concrete." Transportation Research Board, National Research Council, Washington, D.C.

Howson, J. E. (2011). "Relation Between Suface Free Energy and Total Work of Fracture of Asphalt Binder and Asphalt Binder-Aggregate Interfaces." Doctor of Philosophy, Texas A&M University.

Kandhal, P. S., C. W. Lubold and F. L. Roberts (1989). "Water Damage to Asphalt Overlays: Case Histories. " NCAT 89-1, National Center for Asphalt Technology.

Kandhal, P. S. and I. J. Rickards (2001). "Premature Failure of Asphalt Overlays from Stripping: Case Histories." NCAT 01-01, National Center for Asphalt Technology.

Kanitpong, K. and H. U. Bahia (2006). "Evaluation of HMA Moisture Damage in Wisconsin as it Related to Pavement Performance." Transportation Research Board 85th Annual Meeting. WAshington D.C., Transportation Research Board: 25p.

Kassem, E., E. A. Masad, R. Bulut and R. L. Lytton (2006). "Measurements of Moisture Suction and Diffusion Coefficient in Hot-Mix Asphalt and Their Relationships to Moisture Damage." Transportation Research Record: Journal of the Transportation Research Board 1970(1): 45-54.

Kiggundu, B. M. and F. L. Roberts (1988). "Stripping in HMA Mixture: State of the Art and Critical Review of Test Methods." NCAT Report No. 88-2, National Center for Asphalt Technology.

Kringos, N., T. Scarpas and A. D. Bondt (2008). "Determination of Moisture Susceptibility of mastic-stone Bond Strength and Comparison to Thermodynamical Properties." 2008 Annual Meeting of the Association of Asphalt Paving Technologists, AAPT, April 25, 2008 - April 30, 2008, Philadelphia, PA, United states, Association of Asphalt Paving Technologist.

Little, D. N. and A. Bhasin (2006). "Using Surface Energy Measurements to Select Materials for Asphalt Pavement." NCHRP 9-37, National Cooperative Highway Research Program.

Lytton, R. L., E. A. Masad, D. Zollinger, R. Bulut and D. N. Little (2005). "Measurements of Surface Energy and Its Relationship to Moisture Damage. 0-4524-2." Texas Transportation Institute, Texas A&M University System.

Lytton, R. L., J. Uzan, E. G. Fernando, R. Roque, D. Hiltunen and S. M. Stoffels (1993). Development and Validation of Performance Prediction Models and Specifications for Asphalt Binders and Paving Mixes. SHRP-A-357. Washington, DC, National Academy of Sciences.

Marek, C. R. and M. Herrin (1968). "Tensile Behavior and Failure Characteristics of Asphalt Cements in Thin Films." Association of Asphalt Paving Technologists 37: 386-421.

Masad, E. A., E. Arambula, A. R. Abbas, R. A. Ketcham and A. E. Martin (2007). "Nondestructive Measurement of Moisture Transport in Asphalt Mixtures." Journal of the Association of Asphalt Paving Technologists 76: 919-952.

Masad, E. A., C. Zollinger, R. Bulut, D. N. Little and R. L. Lytton (2006). "Characterization of HMA Moisture Damage Using Surface Energy and Fracture Properties." Journal of the Association of Asphalt Paving Technologists 75: 713-754.

Mitchell, P. W. (1980). "The Structural Analysis of Footings on Expansive Soil." Kenneth W.G. Smith & Associates, Adelaide, Australia.

Monismith, C. L., J. A. Epps and D. A. Kasianchuk (1971). "Asphalt Mixture Behavior in Repeated Flexure." University of California, Berkeley.

Oss, C. J. V., M. K. Chaudhury and R. J. Good (1988). "Interfacial Lifshitz-van der Waals and Polar Interactions in Macroscopic Systems." Chemical Review 88: 927.

Pocius, A. V. (1997). Adhesion and Adhesives Technology, Hanser/ Gardner Publications, Inc.

Rashid K. Abu Al-Rub, Eyad A. Masad and M. A. Graham (2010). "Physically Based Model for Prediction the susceptibiltiy of Asphalt Pavements to Moisture-Induced Damage." SWUTC/10/476660-00012-1, Texas Transportation Institute: 73.

Sasaki, I., A. Moriyoshi, Y. Hachiya and N. Nagaoka (2006). "New Test Method for Mositure Permeation in Bituminous Mixtures." Journal of Japan Petroleum Institute 49(1): 33-37.

Schapery, R. (1975). "A Theory of Crack Initiation and Growth in Viscoelastic Media." International Journal of Fracture 11(1): 141-159.

Solaimanian, M., D. Fedor, R. Bonaquist, A. Soltani and V. Tandon (2006). "Simple Performance Test for Moisture Damage Prediction in Asphalt Concrete " Journal of the Association of Asphalt Paving Technologists 75: 345-380.

Sood, E. (2005). "Determination of Diffusion Coefficient for Unsaturated Soils." Master's Thesis, Texas A&M University.

Thornthwaite, C. W. (1948). "An Approach Toward a Rational Classification of Climate." Soil Science 66(1).

TxDOT (2004). Standard Specifications for Construction and Maintenance of Highways, Streets, and Bridges. Test Procedure for Design of Bituminous Mixtures, TxDOT Designation: Tex-204-F.

Vasconcelos, K. L., A. Bhasin, D. N. Little and R. L. Lytton (2011). "Experimental Measurement of Water Diffusion through Fine Aggregate Mixtures." Journal of Materials in Civil Engineering 23(4): 445-452.

Wilson, W. G. (1990). "Soil Evaporative Fluxes for Geotechnical Engineering Problems." Doctor of Philosophy, University of Saskatchewan.

APPENDIX A

TESTING PROTOCOLS OF RDT USING DMA

Related References

1. AASHTO T 85, Specific Gravity and Absorption of Coarse Aggregates.
2. AASHTO T 166, Bulk Specific Gravity of Compacted Hot Mix Asphalt Using Saturated Surface-Dry Specimens.
3. AASHTO T 209, Theoretical Maximum Specific Gravity and Density of Bituminous Paving Mixtures.
4. AASHTO T 312-04, Preparing and Determining the Density of the Hot Mix Asphalt (HMA) Specimens by Means of the Superpave Gyratory Compactor.

Applications

These experiments are designed to evaluate the effects of moisture, aging, air voids, and different additives on the asphalt mixture fatigue resistance. Materials, specimen fabrication, aging conditions, and laboratory testing for each experiment are discussed in this section. The protocol refers mainly to two different tests that can be performed using the DMA apparatus: (a) repeated direction tension, and (b) creep test. These tests provide relevant information regarding the behavior of the HMA fine matrix, which is composed of fine aggregates (particles passing the No. 16 [1.18-mm] sieve) and asphalt binder. The results from these procedures can be used to:

1. Determine the undamaged properties from creep tests at different temperatures.
2. Determine the fracture properties of FAM at different test conditions

3. Characterize the continuous damage of the sample in terms of the dissipated pseudo strain energy as a function of the number of cycles.
4. Evaluate the moisture susceptibility of FAM using the fracture mechanics model.

Test Methods

The DMA test provides fundamental information regarding the fatigue properties of the fine matrix portion of asphalt mixtures. The design methodology of DMA mixtures attempts to obtain a representative sample of the FAM of a complete asphalt mixture. For this reason, a previously established HMA design is required for this process. The design procedure considers the granular material of the HMA mixture passing the No. 16 sieve. The percent of asphalt is estimated by the surface area method.

When the binder content of a FAM is determined, the FAM specimens are fabricated following three main steps: (1) the gradation of FAM is the fine portion of the full aggregate mixture; (2) the FAM is compacted as a specimen with a diameter of 6 inches and height of 2.75 inches using a Superpave gyratory compactor; and (3) a number of DMA samples are cored with a diameter of 0.5 inch and a height of 2 inches from the big cylindrical specimens. The DMA specimens that are cored from the outer circle of the 6 inches diameter specimen have more air voids than those cored from the inner circle. This pattern, well-documented by other researchers, has been found in samples made with both the AAD binder and the AAM binder.

The RDT test is conducted on an average of two DMA specimens (depending on the coefficient of variation). The test is conducted in controlled-stress modes and has two main parts: (1) 50 load cycles at low constant stress amplitude, and (2) a fatigue test

at higher constant stress amplitude. Both tests are performed at a fixed frequency. The low stress should guarantee that the material's behavior is in the linear viscoelastic region, and the high stress amplitude should produce an initial damage behavior of the material.

Apparatus

1. DMA (as see in Figure A-1)—the machine has the following characteristics:
    - Maximum load should be greater than 450 N.
    - Environmental chamber is needed.
    - Force and displacement measurement should have the desired accuracy.

Figure A-1. DMA Test Instrument

2. Calipers: digital or analog calipers with an accuracy of ±0.01mm
3. Glue (as see in Figure A-2) must be able to withstand force applied to the sample by a machine and must bond well to the cylindrical sample and end caps.

Figure A-2. Glue Need for Specimens

4. End caps or holders—stainless steel pieces used to secure the sample in the DMA attachments for testing. They must be slightly larger than 0.5 mm inch diameter and 0.08 inch depth.

Figure A-3. End Caps with Specimens

Other apparatus—other apparatus required to perform the procedures described in this document include an oven, SGC, vacuum desiccators for moisture conditioning, temperature-controlled room for aging conditioning, and ignition oven furnace and its accessories.

Mixture Preparation

An aggregate surface area method is used to determine the asphalt content of a FAM with the assumption that the asphalt binder is proportionally distributed on the aggregate surface area.

$$CR_i = 3\left(\frac{1}{r_i D_i} + \frac{1}{r_{i-1} D_{i-1}}\right) \quad \text{(A-1)}$$

where CR_i = specific surface area of the particles with diameters in the range between sieve sizes D_i and D_{i-1}; and r_i = effective density of aggregate, kg/m^3.

The assumption of a perfectly spherical aggregate is calibrated using a volume factor K, which is obtained using the equation as follows:

$$V_i = KM\frac{4}{3}\pi\left[\frac{1}{2}(D_i + D_{i-1})\right]^3 \quad \text{(A-2)}$$

where V_i = measured volume of aggregate retained on the i_{th} sieve; M = number of aggregate particles retained on the i_{th} sieve; and K = volume factor.

The volume factor K is then used to calibrate the CR_i :

$$CR_i = 3K\left(\frac{1}{r_i D_i} + \frac{1}{r_{i-1} D_{i-1}}\right) \quad \text{(A-3)}$$

It can be seen that the specific surface area factor is related to aggregate particle size, effective density of aggregate, and volume factor. Once the binder content is determined, then the fabrication of asphalt mixture should follow the corresponding specification in each state.

The preparation of cylindrical specimens for use in DMA tests consists of four steps:

1. Prepare a 150-mm (6-inch) compacted sample of the fine aggregate portion asphalt mixture in the SGC. In this step, the job formula for the HMA mixture, the binder properties (for determining the amount of binder, and the mixing and compacting temperatures), and the value of the theoretical maximum specific gravity of the FAM are required. The mixing and compacting temperatures should be calculated from the results of viscosity according to the corresponding specification.

2. Saw the upper and lower parts of the cylindrical sample to obtain a new cylinder with the same diameter (150 mm) but with a 50-mm height (as shown in the Figure A-4).

Figure A-4. Specimens Trimming

3. Core the DMA (as shown in the Figure A-5), as cylindrical specimens that are 50 mm in height and 12 mm in diameter. The velocity used during the coring process is a relevant parameter in determining the quality of the sample.
4. Immediately after each specimen is obtained, label it as A, B, or C (or any other way to identify specimens), where A corresponds to the inner concentric zone of the core, B to the intermediate zone, and C to the outer zone in this case. Also include a number for each sample in each zone. Each sample should also contain a mark indicating the border that corresponds to the upper part of the original compacted specimen.

Figure A-5. Cored DMA Specimens

Allow the samples to dry completely for at least 24 h, and then calculate the air void content for each specimen.

Test Procedure

As shown in the Figure A-6, the FAM specimens should be glued to the caps.

Figure A-6. DMA Specimens Glued with Caps

Then, the DMA specimens can be clamped using the apparatus shown in the Figure A-7.

Figure A-7. Cored DMA Specimens

Finally, the specimens is mounted to the DMA matching for testing as shown in the Figure A-8.

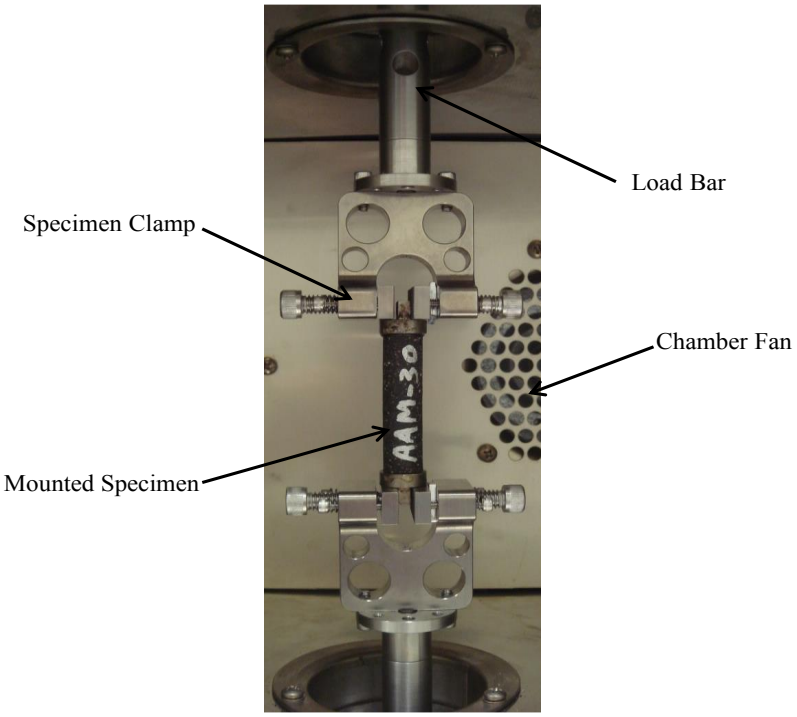

Figure A-8. Cored DMA Specimens

APPENDIX B

CREEP TESTING PROTOCOLS USING DMA

The DMA can also be used to run creep test and obtain the related material properties. The specimens preparation should follow the procedure as discussed in the Appendix A. The creep test is a nondestructive procedure. The test method uses a uniaxial tensile creep test to estimate the dynamic modulus and the phase angle of the FAM. The tests are conducted on asphalt mixture specimens at three temperatures (10, 23, and 30°C, for example) to determine the tensile properties at each temperature and then to construct the master curve. The determined properties include magnitude and phase angle of the tensile complex modulus.

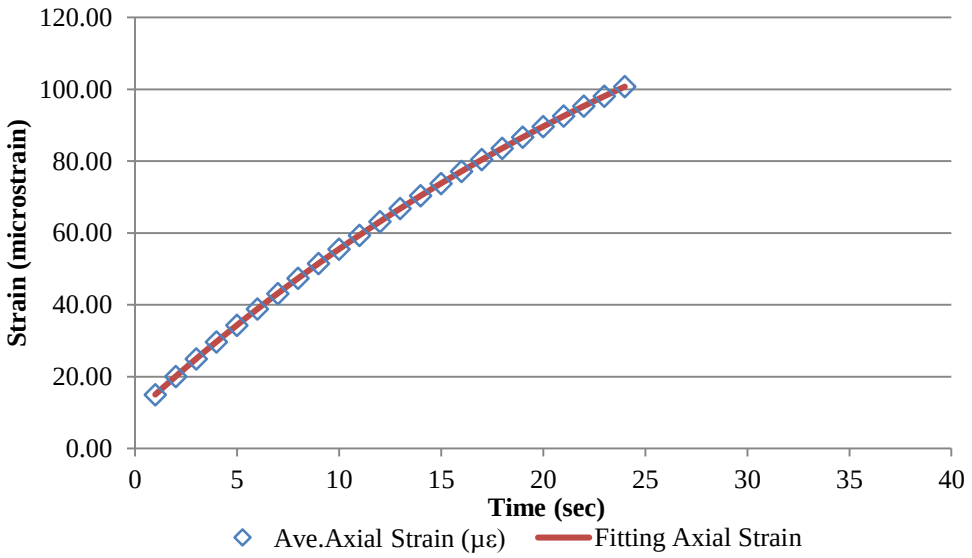

Figure B-1. Measured Strain vs. Fitted Strain for NuStar_51 Aged 4 Weeks at 10°C

First, an undamaged creep test is conducted by controlling the tensile strain level to 100 micro-strains, as shown in the Figure B-1, and the strain response is collected and then fitted using the model shown as follows:

$$\varepsilon = a*(1-\exp(-b*t))+c \tag{B-1}$$

where a, b, and c are the fitting parameters; and t is the time, s.

The Laplace transformations of the relaxation modulus and the stress and strain have the following relationship:

$$\overline{E}(s) = \frac{\overline{\sigma}(s)}{s\overline{\varepsilon}(s)} \tag{B-2}$$

By applying inverse Laplace transforms, the relaxation modulus can be obtained. Then based on the relationship between the complex modulus and the relaxation modulus, the following equation is established:

$$E^*(\omega) = i\omega L\{E(t)\}_{s=i\omega} = \left[s\overline{E(s)}\right]_{s=i\omega} \tag{B-3}$$

By using Equation B-3, the complex modulus and the phase angle are calculated, respectively. In order to construct the master curve of the FAM, the Christensen Anderson Marasteanu (CAM) model is used to achieve this goal.

$$\left|E^*(\omega)\right| = \frac{E_g}{\left\{1+\left[\frac{\omega_c}{\omega\cdot 10^{C_E(T-T_r)}}\right]^{\frac{\log 2}{R_E}}\right\}^{\frac{R_E}{\log 2}}} \tag{B-4}$$

where E_g = glassy modulus of the asphalt mixture, MPa; ω_c = crossover frequency of the asphalt mixture for modulus, rad/s; R_E = rheological index of the asphalt mixture for

modulus; C_E = slope of the temperature shift factor for modulus; and T_r = reference temperature.

As recommended, the Williams-Landel-Ferry (WLF) function is recommended to calculate the time-temperature shift factor for Bahia's model for the phase angle of the FAM master curve.

$$\varphi = \frac{\varphi_m}{\left\{1+\left[\frac{\log\left(\frac{\omega_m}{\omega \cdot 10^{\frac{C_1(T-T_r)}{C_2+(T-T_r)}}}\right)}{R_\varphi}\right]^2\right\}^{\frac{m}{2}}} \quad \text{(B-1)}$$

where φ_m = the maximum phase angle for modulus, degrees; ω_m = the frequency rad/s; *m*, *Rφ* = fitting parameters for modulus phase angle; *Tr* = reference temperature; and *C1* and *C2* = regression constants in the WLF function.

Figure B-2 illustrates the magnitude of the tensile dynamic modulus at different temperatures. Since the FAM has an asphalt content of 10.3 percent, it is found that the phase angle of the specimens tested ranges from 40 to 70 degrees, as shown in the Figure B-3, which is much higher than its corresponding coarse aggregate mixture. Furthermore, the 4-week aged specimen of NuStar_51 has a higher magnitude of complex modulus than the unaged specimens of NuStar_88, as shown in Figure B-4. If the stress can be well controlled without significant variations, and the strain can be collected to the desired level of 1μm rather than 0.001 mm, this creep test is an efficient and reliable way to construct the master curve of FAM. However, it is found that the

built-in linear variable differential transformer precision of the DMA machine cannot achieve the desired strain precision. Therefore, the current creep testing results will only be used as a reference to back-check the dynamic cyclic loading testing results until the desired strain precision is achieved. Figure B-5 shows the magnitude of the tensile phase angles at different temperatures for the specimen aged 4 weeks. Figure B-6 shows the tensile modulus master curve for both aged and unaged specimens with the NuStar binder.

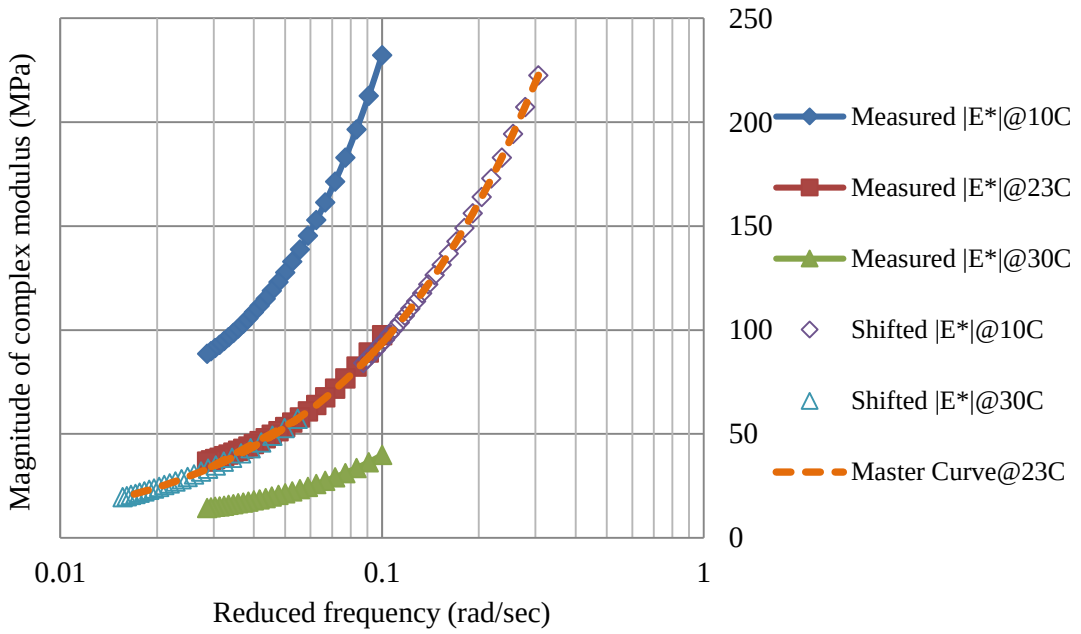

Figure B-2. Magnitude of Tensile Dynamic modulus at Different Temperatures and master Curve at 23°C for Specimen NuStar_88 Unaged

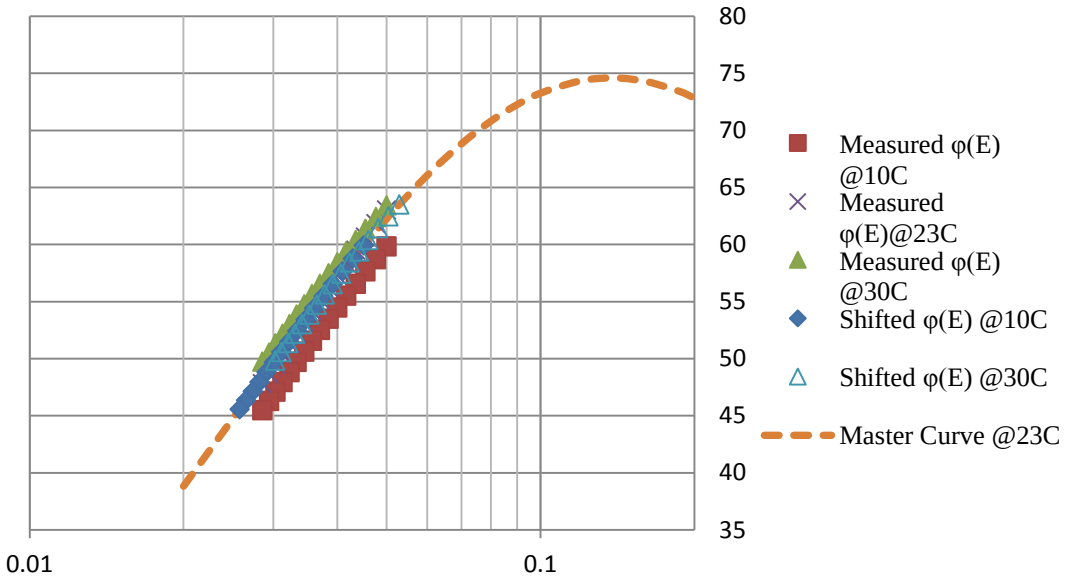

Figure B-3. Magnitude of Tensile Phase Angle at Different Temperatures and Master Curve at 23°C for Specimen NuStar_88 Unaged

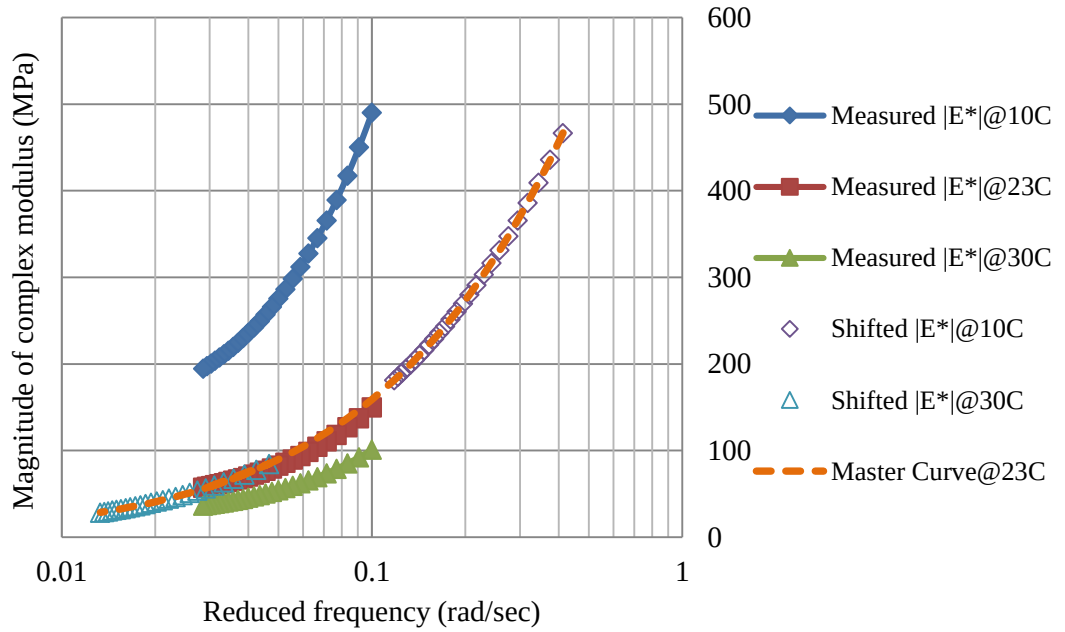

Figure B-4. Magnitude of Tensile Dynamic Modulus at Different Temperatures and Master Curve at 23°C for Specimen NuStar_51 Aged 4 Weeks

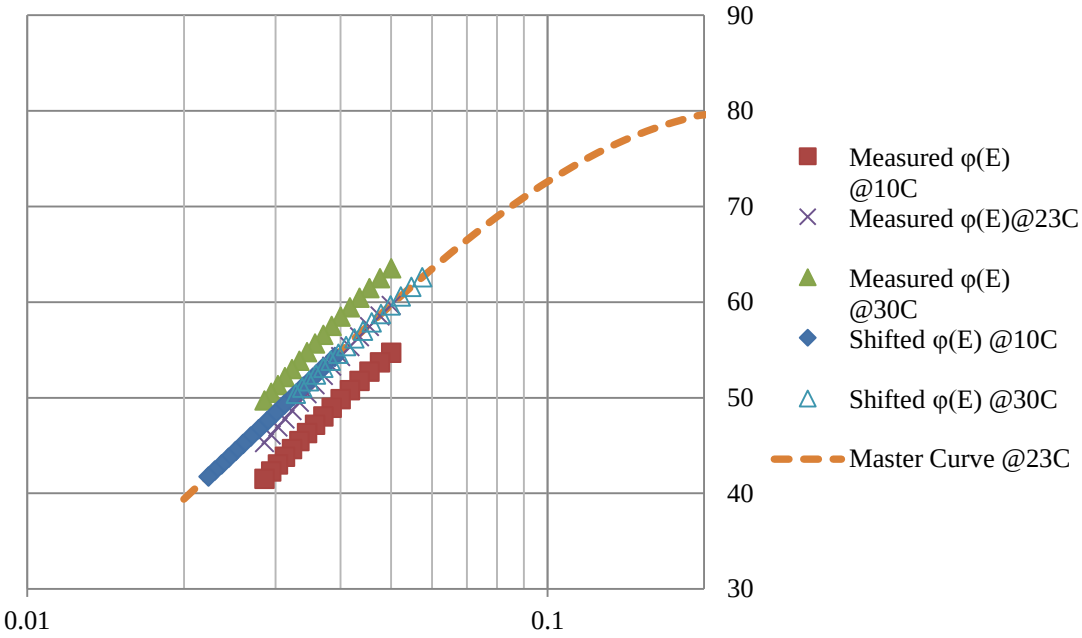

Figure B-5. Magnitude of Tensile Phase Angle at Different Temperatures and Master Curve at 23°C for Specimen NuStar_51 Aged 4 Weeks

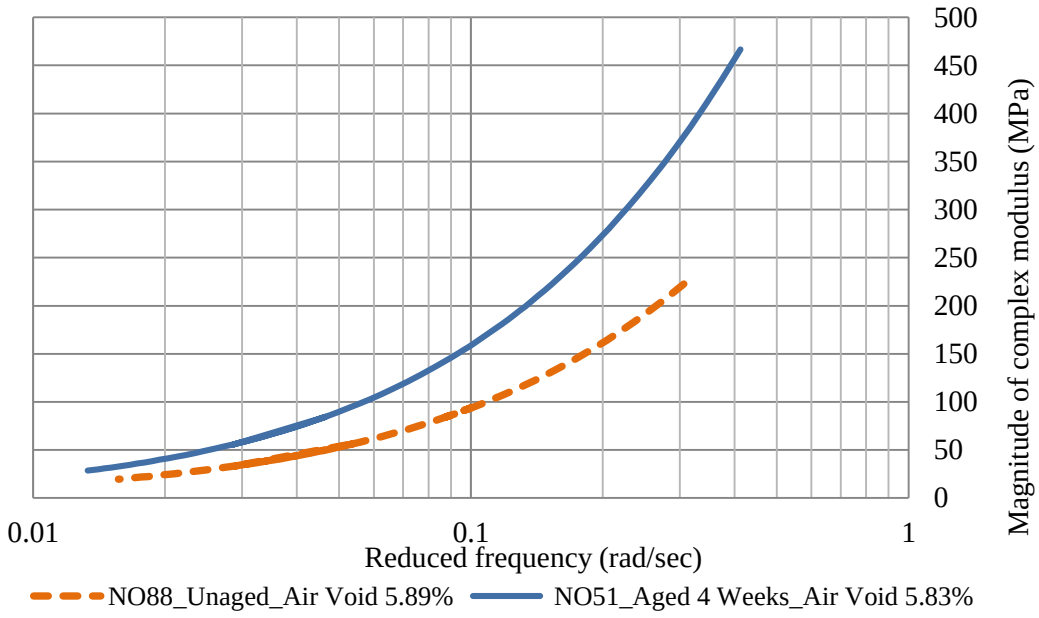

Figure B-6. Magnitude of Tensile Modulus at Different Temperatures and Master Curve at 23°C for Specimen NuStar_51 Aged 4 Weeks

APPENDIX C

NUMERICAL METHOD TO MODEL WATER VAPOR DIFFUSION IN PAVEMENT

The major problem in the previous modeling using the approximation solution method is the two different boundary assumptions. Therefore, a numerical method was adopted to improve the previous models. Crank-Nicolson is a popular method for solving parabolic partial differential equations because it is unconditionally stable and second-order accurate. The simplest and well-known implicit Crank-Nicholson scheme is obtained by a combination of the forward time differencing and an averaging over time of the second-order, centered-space derivative operator. It is based on the central difference in space and the trapezoidal rule in time, giving second-order convergence in time.

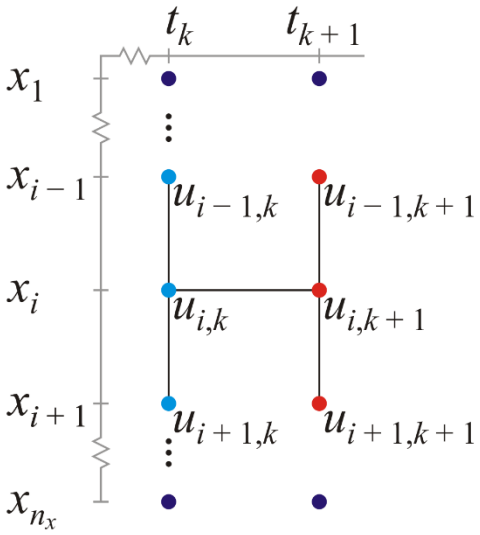

Figure C-1. Illustration of Crank-Nicolson Method

Given the general diffusion formulated as Fick's law, the finite-difference equation can be generated using the equation as follows:

$$2u_{i,k+1} = 2u_{i,k} + \frac{D\Delta t}{h^2}\left(u_{i-1,k} - 2u_{i,k} + u_{i+1,k}\right) + \frac{D\Delta t}{h^2}\left(u_{i-1,k+1} - 2u_{i,k+1} + u_{i+1,k+1}\right) \qquad \text{(C-1)}$$

where h = the distance steps upward from the subgrade soil to the surface of the HMA layer, cm; and Δt = time steps for this scheme, s.

$$r = \frac{\kappa\Delta t}{h^2} \qquad \text{(C-2)}$$

The equation in C-3can be reformulated as follows by removing all unknowns to the left and all known to the right:

$$-ru_{i-1,k+1} + 2(r+1)u_{i,k+1} - ru_{i+1,k+1} = 2u_{i,k} + r\left(u_{i-1,k} - 2u_{i,k} + u_{i+1,k}\right) \qquad \text{(C-3)}$$

Since there are n-2 unknowns, it is necessary to set up a system of n-2 linear equations to solve. Combining all the equations, this can be written in the form Mx = b as follows:

$$\begin{pmatrix} 2(1+r) & -r & & & & \\ -r & 2(1+r) & -r & & & \\ & -r & 2(1+r) & \ddots & & \\ & & \ddots & \ddots & -r & \\ & & & -r & 2(1+r) & -r \\ & & & & -r & 2(1+r) \end{pmatrix} \begin{pmatrix} u_{2,k+1} \\ u_{3,k+1} \\ u_{4,k+1} \\ \vdots \\ u_{n_x-2,k+1} \\ u_{n_x-1,k+1} \end{pmatrix} = \begin{pmatrix} 2u_{2,k} + r\left(u_{1,k} - 2u_{2,k} + u_{3,k}\right) + ra_{\text{bndry}}\left(t_{k+1}\right) \\ 2u_{3,k} + r\left(u_{2,k} - 2u_{3,k} + u_{4,k}\right) \\ 2u_{4,k} + r\left(u_{3,k} - 2u_{4,k} + u_{5,k}\right) \\ \vdots \\ 2u_{n_x-2,k} + r\left(u_{n_x-3,k} - 2u_{n_x-2,k} + u_{n_x-1,k}\right) \\ 2u_{n_x-1,k} + r\left(u_{n_x-2,k} - 2u_{n_x-1,k} + u_{n_x,k}\right) + rb_{\text{bndry}}\left(t_{k+1}\right) \end{pmatrix} \qquad \text{(C-4)}$$

For the convenience of programming, the equation can be further simplified as follows:

$$\begin{pmatrix} 2u_{2,k}+r\left(u_{1,k}-2u_{2,k}+u_{3,k}\right) & +ra_{\text{bndry}}\left(t_{\ell+1}\right) \\ 2u_{3,k}+r\left(u_{2,k}-2u_{3,k}+u_{4,k}\right) & \\ 2u_{4,k}+r\left(u_{3,k}-2u_{4,k}+u_{5,k}\right) & \\ \vdots & \\ 2u_{n_x-2,k}+r\left(u_{n_x-3,k}-2u_{n_x-2,k}+u_{n_x-1,k}\right) & \\ 2u_{n_x-1,k}+r\left(u_{n_x-2,k}-2u_{n_x-1,k}+u_{n_x,k}\right)+rb_{\text{bndry}}\left(t_{\ell+1}\right) & \end{pmatrix} = 2\begin{pmatrix} u_{2,k} \\ u_{3,k} \\ u_{4,k} \\ \vdots \\ u_{n_x-2,k} \\ u_{n_x-1,k} \end{pmatrix} + r\begin{pmatrix} u_{1,k}-2u_{2,k}+u_{3,k} \\ u_{2,k}-2u_{3,k}+u_{4,k} \\ u_{3,k}-2u_{4,k}+u_{5,k} \\ \vdots \\ u_{n_x-3,k}-2u_{n_x-2,k}+u_{n_x-1,k} \\ u_{n_x-2,k}-2u_{n_x-1,k}+u_{n_x,k} \end{pmatrix} + \begin{pmatrix} ra_{\text{bndry}}\left(t_{k+1}\right) \\ \\ \\ \vdots \\ \\ \\ rb_{\text{bndry}}\left(t_{k+1}\right) \end{pmatrix} \quad \text{(C-5)}$$

Boundary conditions are set as follows:

$$1.\quad u\left(x=d,t\right)=u_d \quad \text{(C-6)}$$

$$2.\quad \frac{\partial u}{\partial x}\left(x=0,t\right)=0 \quad \text{(C-7)}$$

where u_d = the suction in the granular base material, which is a constant.

Thus, given the initial state at time t_1, we create a system of equations with $k = 1$ to solve for $u_{2,2}$ through $u_{n_x-1,2}$. By applying the same theory to the following time and spatial steps, all the unknowns, as shown in the schematic illustration as shown in the Figure C-2, can be solved.

$u_{init}(x_1)$	$a_{bndry}(t_2)$	$a_{bndry}(t_3)$	$a_{bndry}(t_4)$	$a_{bndry}(t_5)$	$a_{bndry}(t_6)$	$a_{bndry}(t_7)$	$a_{bndry}(t_8)$	$a_{bndry}(t_9)$	$a_{bndry}(t_{10})$	$a_{bndry}(t_{11})$	$a_{bndry}(t_{12})$
$u_{init}(x_2)$	?	?	?	?	?	?	?	?	?	?	?
$u_{init}(x_3)$	?	?	?	?	?	?	?	?	?	?	?
$u_{init}(x_4)$	?	?	?	?	?	?	?	?	?	?	?
$u_{init}(x_5)$	?	?	?	?	?	?	?	?	?	?	?
$u_{init}(x_6)$	?	?	?	?	?	?	?	?	?	?	?
$u_{init}(x_7)$	?	?	?	?	?	?	?	?	?	?	?
$u_{init}(x_8)$	?	?	?	?	?	?	?	?	?	?	?
$u_{init}(x_9)$	$b_{bndry}(t_2)$	$b_{bndry}(t_3)$	$b_{bndry}(t_4)$	$b_{bndry}(t_5)$	$b_{bndry}(t_6)$	$b_{bndry}(t_7)$	$b_{bndry}(t_8)$	$b_{bndry}(t_9)$	$b_{bndry}(t_{10})$	$b_{bndry}(t_{11})$	$b_{bndry}(t_{12})$

Figure C-2. Illustration of Crank-Nicolson Formulation

The wind speed effect is considered in modeling the vapor diffusion process in pavement by using the Crank-Nicolson numerical method. The flux boundary condition, including wind speed at the pavement surface, is formulated as follows:

$$\frac{\partial u}{\partial x} = f(u)*(u_a - u_s) \tag{C-8}$$

where $\frac{\partial u}{\partial x}$ is the rate of potential evaporation (PE); u_a is the suction in the air; u_s is the suction at the pavement surface; and $f(u)$ is a function that depends on the wind above the surface of pavement and can be expressed as follows:

$$f(u) = h*(1+\alpha_m) \tag{C-9}$$

where *h* is the coefficient of vapor transfer at the boundary surface; and α_m is the mass exchange coefficient of water vapor due to the wind at the surface. Specifically, this indicates that the wind speed increases the water vapor mass exchange at the surface, α_m:

$$\alpha_m = K\sqrt{\frac{V}{L}} \tag{C-10}$$

where *V* is the wind speed, m/s; and *L* is the length over which the wind blows. The largest α_m occurs if the wind blows across the width of the highway, m. *K* can be expressed as:

$$K = 0.662\lambda_m (P_{rm})^{1/3} (\frac{1}{\upsilon})^{1/2} \tag{C-11}$$

where P_{rm} is the Prandtl number for air; υ is the kinematic viscosity of air, m^2/s; and λ_m is a constant at the air temperature of 20°C and is $2.54\times10^{-3} kg/(s^{-1}\cdot m^2)$.

By substituting the Equation C-11 into the Equation C-12, α_m was calculated based on wind data available for Texas from the National Climatic Data Center. The wetting process of a pavement using the numerical method is illustrated in the Figure C-3. As the service time increases, the asphalt surface layer gradually wets up after placement due to the moisture movement from the subgrade soil into the base course and then into the surface layer. The closer to the pavement surface, the lower the relative humidity in the asphalt layer. The moisture builds up in the asphalt mixture at such a fast rate that the RH in the surface asphalt layer reaches 95 percent in approximately 180 days, and this RH level remains within the asphalt layer. These modeling results illustrate that the pavement surface layer attains nearly saturation vapor pressure within a relatively short period of 180 days. This high RH level may lead to an accelerated pavement deterioration rate. The wind tends to drive faster vapor movement from the subsurface compared to the pavement without wind. The results are consistent with the previous findings.

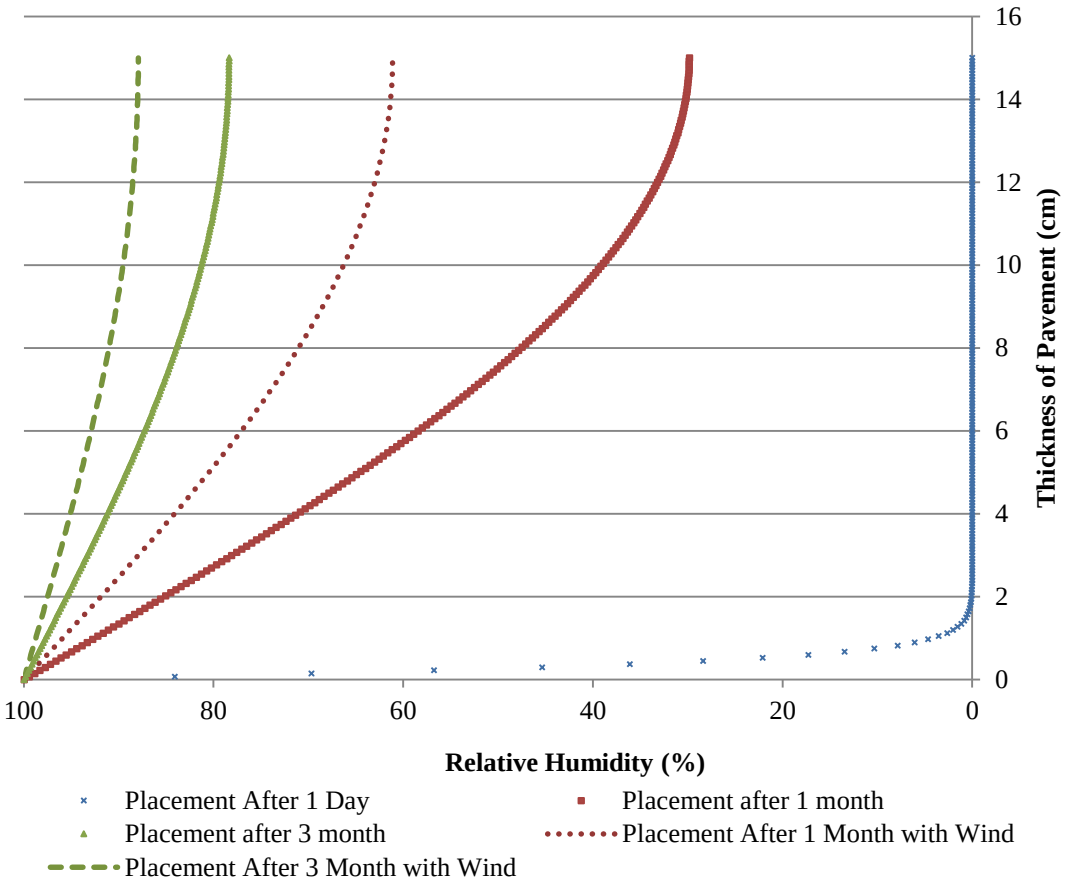

Figure C-3. Chart. Wind Effect on Water Vapor Diffusion in Pavement

APPENDIX D:

SURFACE ENERGY MEASUREMENTS

Surface energy of aggregates is measured using the Universal Sorption Device (USD), while surface energy of binder is measured using the Wilhelmy plate. The USD indirectly determines the aggregate surface energy by using gas adsorption characteristics of three probing vapors. The Wilhelmy plate determines the surface energy of binder by using the contact angle between a thin plate coated with binder immersed and withdrawn from a liquid with a known surface energy components. Both USD and Wilhelmy plate have been thoroughly researched and well documented at TAMU (Cheng et al. 2001, Hefer et al. 2005 and 2006, Little and Bhasin 2006, Bhasin and Little 2007, Howson 2011)

Universal Sorption Device

The aggregates are dry sieved passing the 4.75 mm sieve and retained on the 2.36 mm sieve. The aggregate size is controlled by the aggregate sample holder used in the USD made of aluminum mesh. Approximately 40 grams of aggregates retained on the 2.36 mm sieve are washed with potable water to remove dust particles. The aggregates are then put through a washing cycle for final preparation. The washing cycle consists of rinsing the aggregate with distilled water, then methanol, then hexane, then methanol again. After washing, the aggregates are placed in an oven and dried for at least 4 hours. After drying, the aggregates are cooled down to room temperature by being placed in a

desiccator. Once cooled the aggregates are placed in the aluminum mesh sample holder to be put in the USD.

The Universal Sorption Device testing protocol at Texas Transportation Institute was developed by Cheng, and improved by many others since then. A picture of the main components of the USD is provided in Figure D-1. The aggregate sample is placed in a sealed vacuum chamber, while the pre-selected solvent is released into the chamber at a specific vapor pressure. The amount of solvent on the aggregate surface is measured using a magnetic suspension balance, while also measuring vapor pressure. The vapor pressure is increased and stabilizes to the steady-state at 10 different stages while the mass of solvent is measured. The sample is tested in the following order with three solvents: *n*-Hexane, methyl propyl ketone (MPK), and water. A washing cycle is performed in between each solvent.

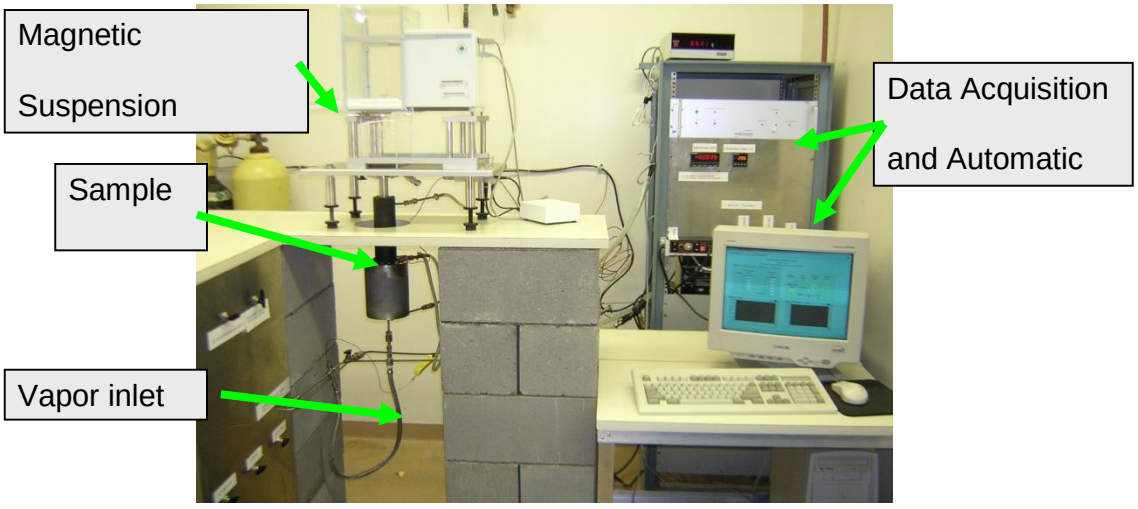

Figure D-1. Universal Sorption Device

The USD testing protocol requires inserting vapor into the chamber in 10 states until reaching the saturation vapor pressure as seen in Figure D-2. The adsorbed solvent mass is also measured for each stage and shown in Figure D-3. Figure D-4 illustrates how this data can be used to construct an isotherm of the amount of solvent adsorbed versus relative pressure at constant temperature.

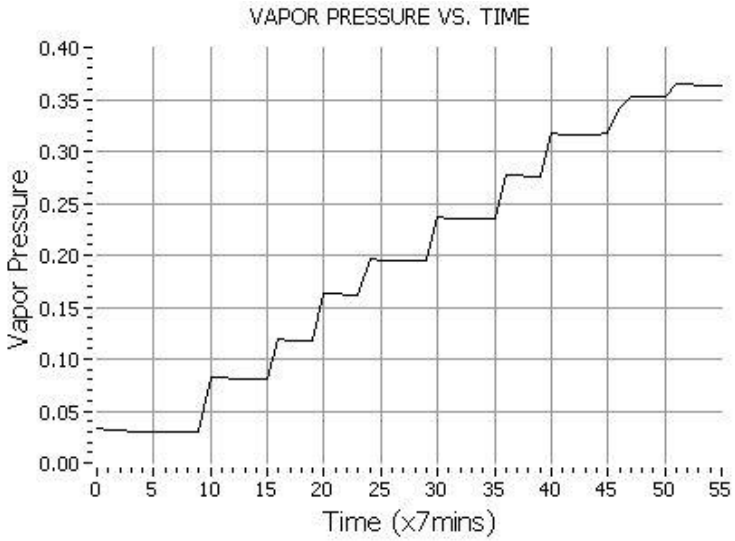

Figure D-2. Vapor Pressure verses Time Plot from USD

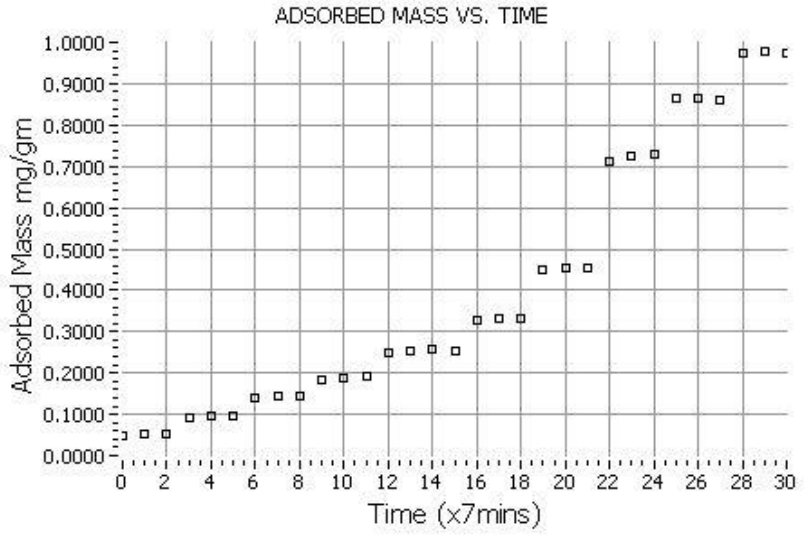

Figure D-3. Absorbed Solvent Mass verses Time from USD

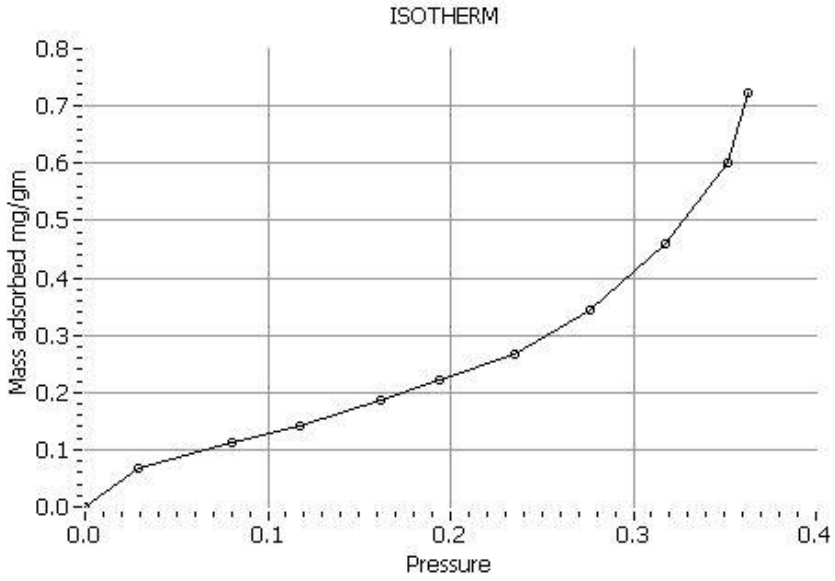

Figure D-4. Typical Adsorbed Solvent Mass verses Vapor Pressure Isotherm

The 10 stages of increasing vapor pressure and mass of solvent are used to calculate the specific surface area of the aggregate. The two-parameter BET (Brunauer,

Emmett, and Teller) model is applied to the isotherm data to obtain the specific surface area of the aggregate sample for the three solvents adsorbed. According to the BET theory, adsorption can be represented by the following linear equation,

$$\frac{P}{n(P_O - P)} = \left(\frac{c-1}{n_m c}\right)\frac{P}{P_O} + \frac{1}{n_m c}(32) \qquad \text{(D-1)}$$

where, P_0 is the saturated vapor pressure of the solute, P is the vapor pressure, *n* the specific amount adsorbed on the surface of the absorbent, n_m is the monolayer capacity of the adsorbed solute on the absorbent, and c the parameter theoretically related to the net molar enthalpy of adsorption. The monolayer capacity of the adsorbed solute on the absorbent can be obtained from the slope and the intercept of the straight line that fits the plot *P/n(P-Po)* versus *P/Po* best as illustrated in Figure D-5.

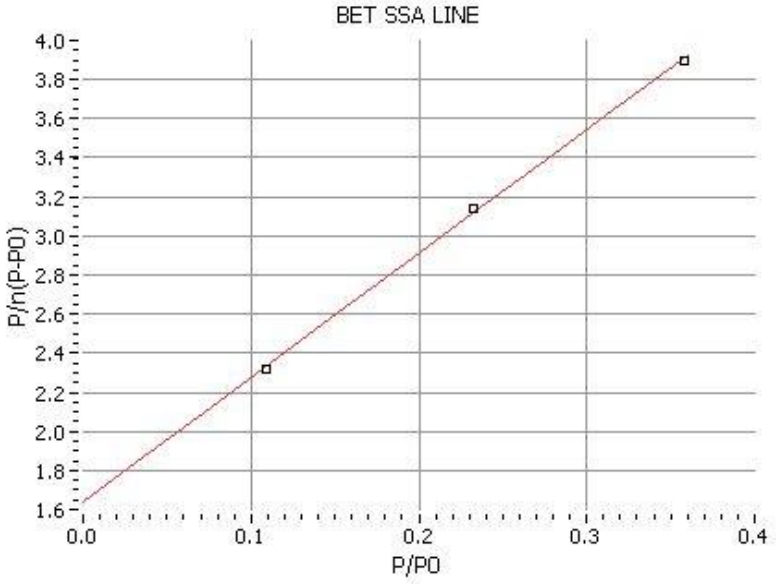

Figure D-5. Plot for Determining Monolayer Capacity

At the saturation vapor pressure, the spreading pressure is computed for all three solvents. With the components of surface energy for the three solvents known, the components of surface energy for the aggregate are then computed.

Specific Procedure for Testing

- If test was run the previous day, close the USD Test window on the computer and turn the gas valve (water, hexane, or MPK) to the CLOSED position.

Figure D-6: Black Knob Be Horizontal in the OFF Position

- Open the VV Valve (marked with a VV sign)

Figure D-7: VV Valve in the CLOSED Position before Changing Aggregate

- Changing the aggregate sample:
    - Place the metal stand below the sleeve
    - Loosen the bolt on the bottom on the sleeve while supporting the sleeve with your opposite hand
    - Lower the sleeve down onto the stand
    - Loosen the bolts on the top of the cylinder: keep the front and back bolts tight at first while loosening the other 3 using a 9/16” box wrench, then loosen the back and front bolts while supporting the cylinder with your opposite hand
    - Slide the cylinder down into the sleeve resting on the stand
    - Remove the aggregate sample basket, discard the tested aggregate, and refill the basket with new aggregate

- Hang the basket back on the hook, slide the cylinder back up, and re-tighten the bolts (front and back bolts first)

- On the computer desktop, double-click on the Manual Balance icon

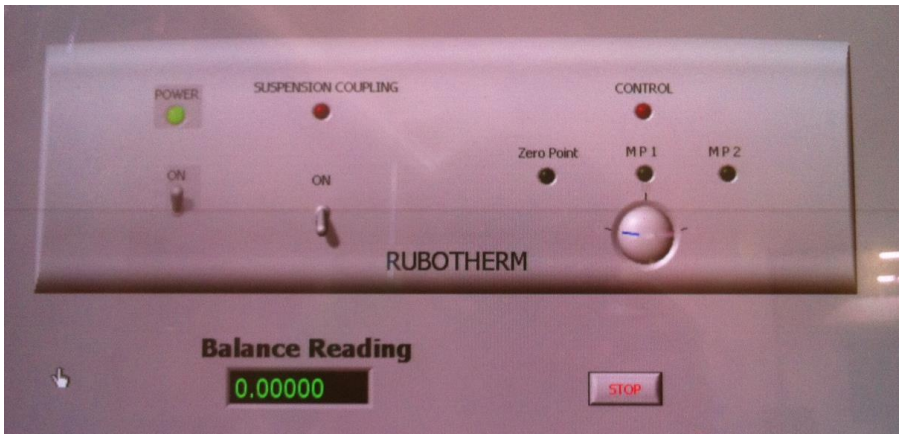

Figure D-8: Manual Balance Control Interface

- Turn ON the suspension coupling and wait for the Zero Point "Balance Reading" to stabilize (should stabilize around 12)
- Move dial on right side to MP1 and wait for the "Balance Reading" to stabilize (around 30 usually)
- Move dial back to Zero Point and wait for the "Balance Reading" to stabilize again
- Move back up to MP1 and wait for the "Balance Reading" to stabilize again

- Make sure that the readings for MP1 and Zero Point are fairly consistent (this may take several iterations of the previous steps) and stable
- Once readings have stabilized, move back to Zero Point and turn OFF the suspension coupling
- Close the Manual Balance window

- Level vertically and tighten the test cylinder using the level and box wrench
  - Be careful not to over-tighten the bolts
- Slide the sleeve back up over the test cylinder and replace the bolt and washer at the bottom to the support the sleeve.
- On the computer desktop, double-click on the Degassing icon
  - Degassing procedure when begin automatically when you open this program

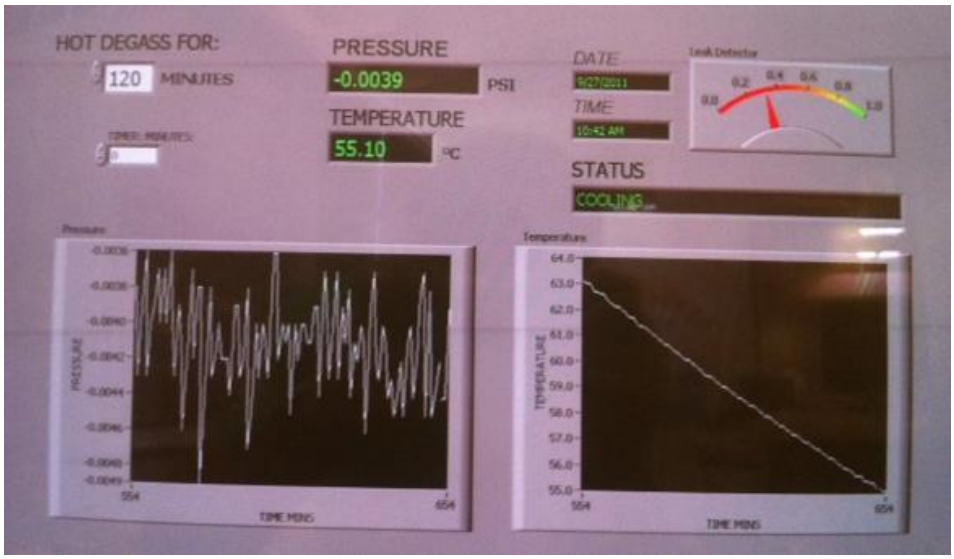

Figure D-9: Degassing Program Interface

- Close the VV Valve (refer back to *Figure 2* for the CLOSED position)
- Turn the main pump valve to the OPEN position

Figure D-10: Main Pump Valve Shown in the OPEN Position

- Switch the pump ON

Figure D-11: Arrow Points to the Power Switch

- Hot degassing procedure will not begin until the pressure reading has dropped below a certain threshold
- If pressure does not drop below the threshold within a timely manner (usually after testing Hexane), manually override the degassing program by scrolling down, and setting the “Start Hot” option to 0.002

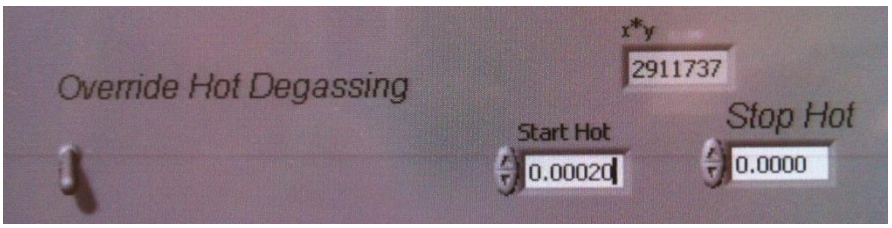

Figure D-12: Override the Hot Degassing Program

- Once the Hot Degassing procedure has begun, double-click on the Auto Balance icon on the computer desktop
    - Set the time to 3.5 hours
    - Click the “Start Horizontal Centering” button

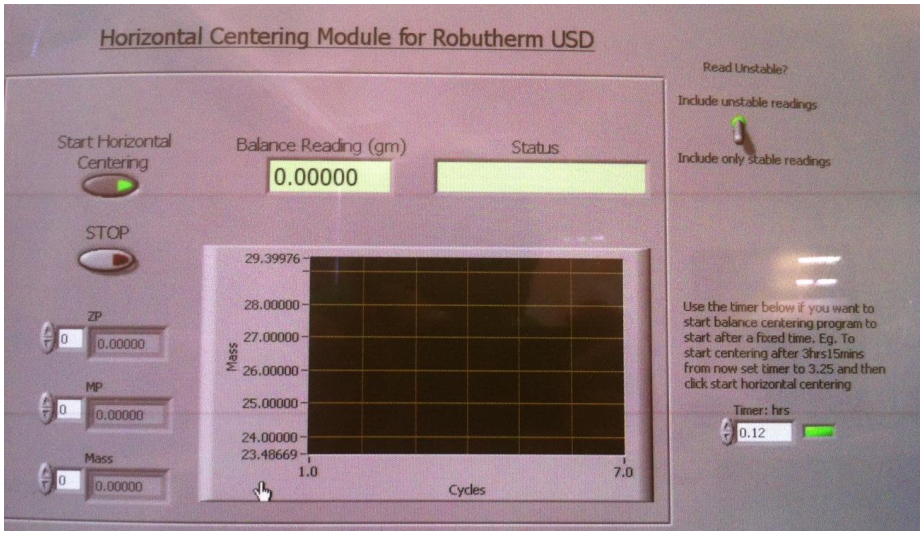

Figure D-13: Auto Balance Interface

- The hot degassing procedure will now take about 4 hours to complete.
- After 4 hours, check that the Auto Balance readings are relatively stable and then close the Auto Balance program
- Check that the status of the Degassing program now reads “COOLED” and then close the Degassing program
- On the computer desktop, double-click the Reboot Initialize icon

- After Reboot Initialize has opened, close the window
- On the computer desktop, double-click the USD Test icon

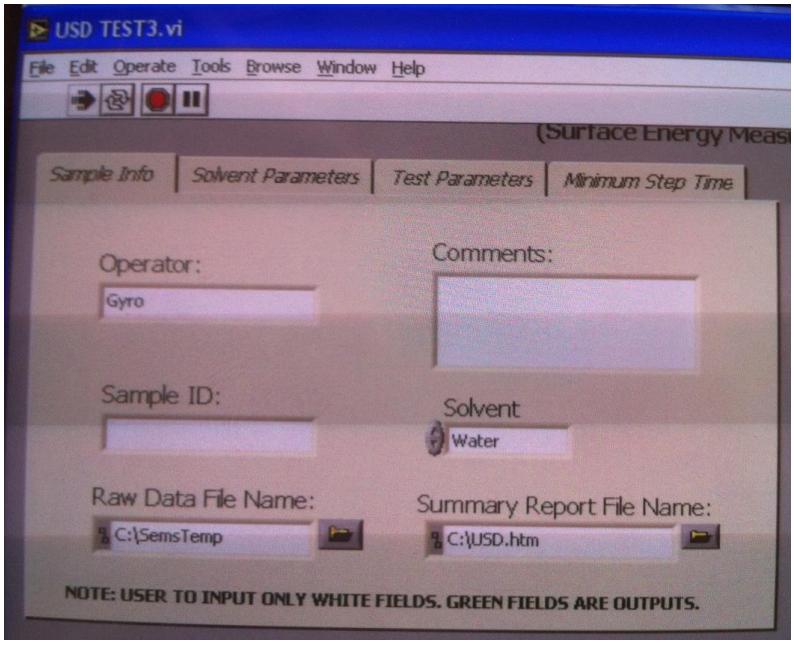

Figure D-14: Part of the USD Test Interface

  - Go to "Sample Info" tab
  - Type in the Sample ID in the following format:
    - Aggregate – Liquid – Test #
  - Under the "Raw Data File Name" and "Summary Report File Name" sections, click on the folder button and save the files in the desired location under the Sample ID file name
    - For example: Hanson Limestone – Water – 4

- Under the “Solvent” section, choose the solvent that the test will be run
- Click the START TEST button

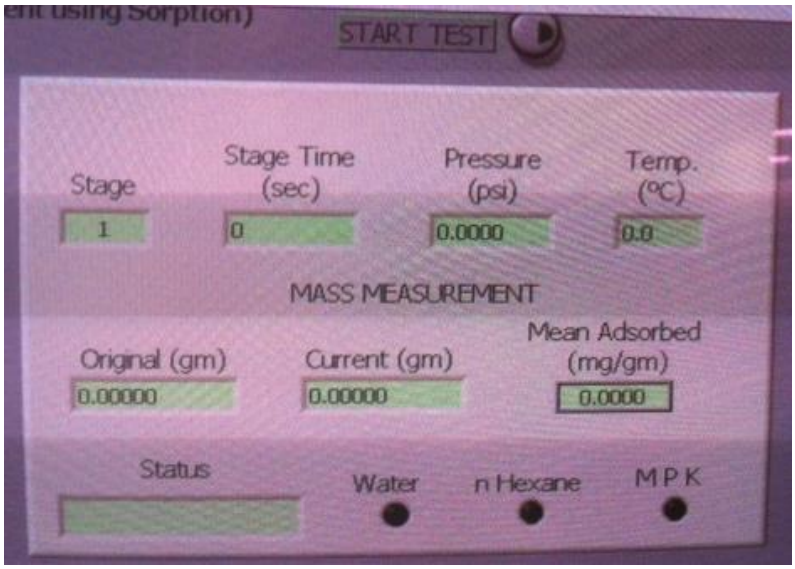

Figure D-15: Part of the USD Test Interface

- Wait until the Status displays: Stepping Pressure
    - This step may take a while depending on how accurate the mass readings are
- Once the test has reached stepping pressure:
    - Close the main pump valve
    - Turn off the pump
    - Turn on the lamp

- Place the screen back over the box
- Open the valve for the liquid that will be tested

- The status box should then display: Measuring
- Let the test run overnight.

Figure D-16: Liquid Containers behind the Machine

Wilhelmy Plate

The asphalt surface energy is determined by dipping thin micro glass slides coated with thin asphalt into three pre-selected solvents with known surface energy components.

Figure D-6 shows the Dynamic Contact Angle (DCA) system comprising a data acquisition system, and a Cahn Balance used to measure the force data. Twelve glass slides (50 mm by 24 mm by .15 mm) are cleaned using acetone and distilled water. Once the glass slides are dried, the asphalt is heated to a liquid state at a temperature depending on the asphalt grade. The glass plate is immersed into the liquid asphalt approximately 30 mm and then removed. The asphalt covered plated is turned over, and while cooling the excess asphalt is allowed to drip off, creating a smooth surface. The dimensions of the asphalt covered plate are measured, and the plate is placed in the desiccator overnight.

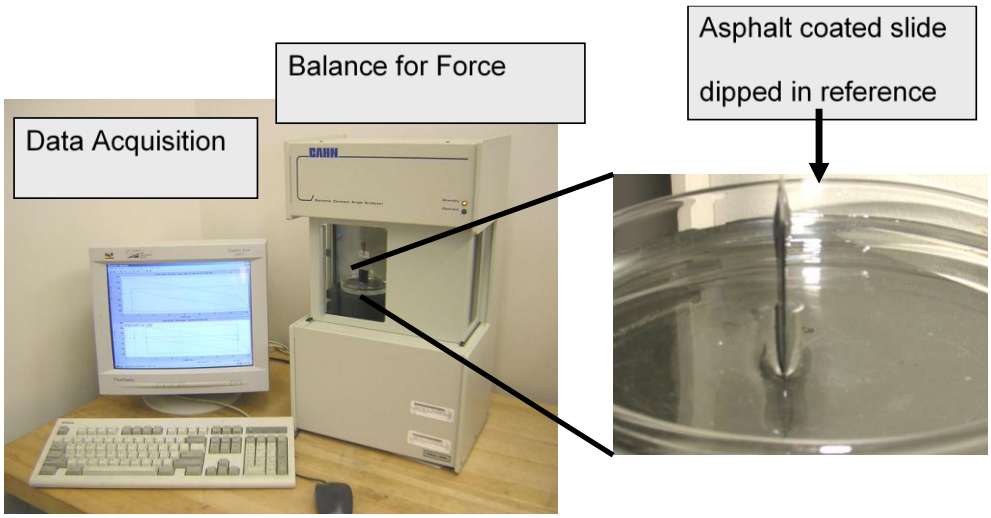

Figure D-17. Dynamic Contact Angle System

For each solvent, the contact angle is measured for three separate plates. The three solvents used in this project were: water, glycerol, and methylene iodide. The

asphalt coated plate is attached to the Wilhelmy plate device. The Wilhelmy plate immerses the plate into each solvent and then withdraws it. The contact angle measured during the immersion process is called the advancing contact angle, and the contact angle measured during the withdrawal process is known as the receding contact angle as illustrated in Figure D-7.

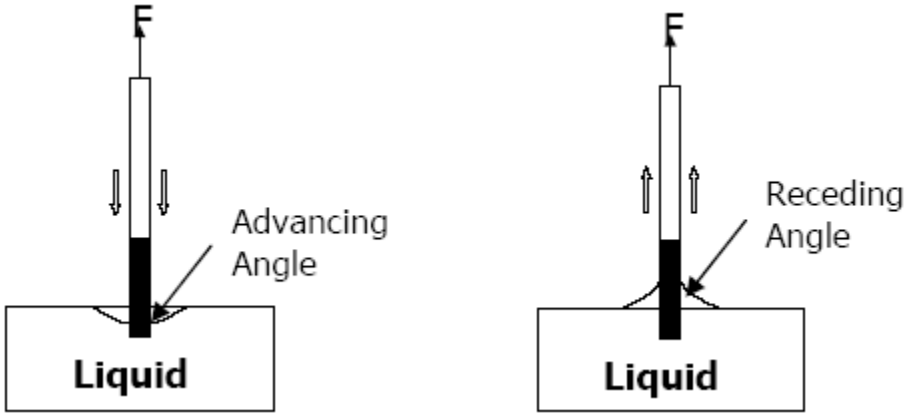

Figure D-18. Schematic Illustration of Wilhelmy Plate Technique.

The surface energy determined from the advancing contact angle is known as the surface free energy of wetting and has been associated with the fracture healing process. The surface energy determined from the receding contact angle is known as the surface free energy of dewetting and has been associated with the fracture mechanism process. The Wilhelmy plate measures the contact angle by constantly measuring the weight of the plate as it is immersed and withdrawn from the solvent. Before the plate is immersed, the dry plate mass is known. As the plate is immersed, the force applied to

the plate is affected by the perimeter of the plate, surface energy of the solvent, contact angle between plate and solvent, and the volume of immersed plate. Typical output from the DCA data acquisition system is show in Figure D-8. The advancing contact angle is represented in the bottom portion of the hysteresis loop, while the receding contact angle is represented in the top portion. Knowing the contact angles between the solvents and asphalt, combined with the surface energy components of the solvents, the surface energy components of the asphalt can be computed as described by Hefer and also in Appendix D (Hefer 2004).

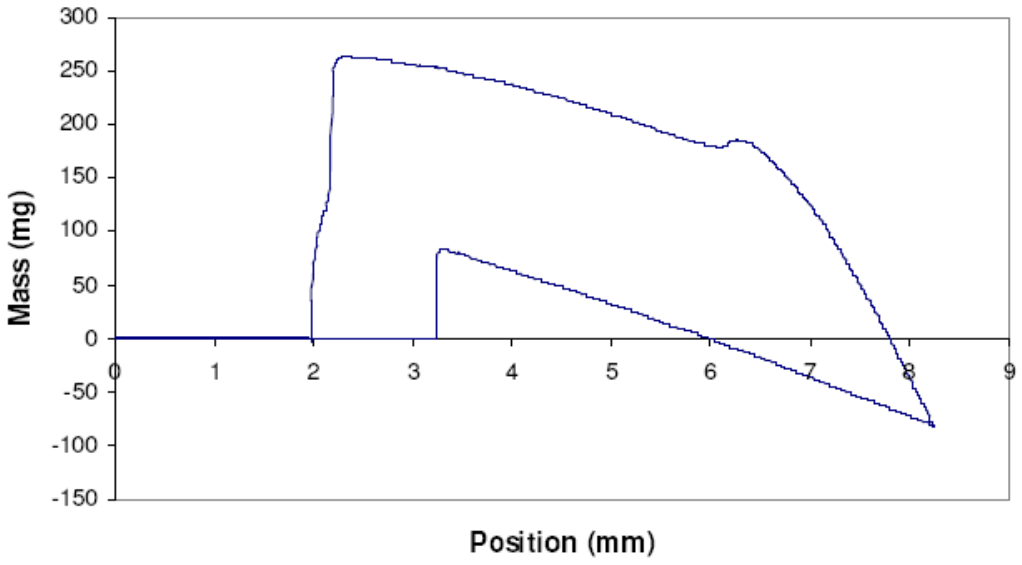

Figure D-19. Typical Output from the DCA Data Acquisition System

Specific Procedure for Testing

I. Oven

a. Turn on oven to about 135 ^{o}C (275 ^{o}F)

b. Heat bitumen sample in oven for 45 min to an hour.

c. 10 minutes before bitumen sample is ready to remove from oven, turn on hot plate and set to 150 ^{o}C (300 ^{o}F).

d. Ensure to stir bitumen at least once while it is heating in the oven.

II. Slide preparation (while bitumen is heating)

a. For each can of bitumen, at least 15 slides are needed (22 slides recommended).

b. Put on latex gloves.

c. Rinse glass slide with acetone on both sides.

d. Immediately after, rinse the slide on both sides with distilled water to remove acetone.

e. Dry slide with a lint-free cloth called a Kim-wipe (lint-free).

f. Place slide in a holder.

III. Coating slide with bitumen

a. Remove bitumen from oven and place can on hotplate.

b. Wait until bitumen starts circulating due to the heating.

c. Stir bitumen with a clean stirring rod (spatula).

d. Light propane torch.

    i. Attach nozzle to propane bottle.

    ii. Hold striker or lighter over the mouth of the nozzle.

    iii. Turn on the torch and strike flint and steel several times about a second later.

iv. If it won't light turn off torch and wait until fumes clear before trying again.

e. Take glass slide and quickly run it through the flame (twice on each side) to remove any particles and moisture from the glass.
f. Tilt bitumen container on its edge and dip slide about one inch into bitumen.
g. Remove slide from bitumen and let the excess bitumen drip from slide for five seconds.
h. Turn slide upside down (bitumen coated side pointing up) and place in holder.
i. Do not touch the bitumen coated part of the slide or bring into contact with anything. It will spoil the results.
j. After all slides are completed, place holder and slides in an oven at 130 ^{o}C for a few seconds to allow bitumen to evenly coat the slides. Ensure and check continually that the bitumen does not completely melt.

IV. Desiccator

a. After all slides are coated with bitumen, place them in the desiccator. Be careful not to hit the slides on the side of the container.
b. Ensure the DryRite rocks in the bottom of the desiccator are still blue. If they are completely purple, they need to be replaced with new ones.
c. Seal desiccator. The slides will not be ready to test for 24 hours, but cannot be in the desiccator for more than three days from time of preparation. This means there is a two day testing window.

V. Starting a Test

a. Decide which liquid you are going to test with (Water, Glycerol, Ethylene Glycol, Formamide, or Diiodomethane). Pour a small amount into a clean, washed beaker, *swish* it around and then discard the liquid. This is done to remove any foreign particles from the beaker. Next, pour 10 ml of the liquid into the beaker and place on platform. If using the diiodomethane, make sure to use a beaker wrapped in black electrical tape since diiodomethane is light sensitive; if not available run the test with lights turned off. The liquid will need to be replaced when you finish testing a set of slides (four slides).
b. Open up the program on the computer.
c. Load the appropriate template for the liquid you will be running the test with.
d. Go to the Edit tab to modify the labels, test number, and measurements for the test being run. Make sure to label the sample so that you will recognize it if you have to go back and look at it. (First letter of bitumen name, PG grade of bitumen, liquid being used. e.g. W6422di; Wright bitumen, PG 64-22 binder, and Diiodomethane). The program will automatically insert the slide number at the end of the file name, e.g. W6422di1.
e. Under Edit there will be a place to enter the dimensions of the slide being tested. It will ask for the width and thickness of the slide in millimeters. Be very careful when measuring the slide. Do NOT touch or measure the slide where the liquid will come in contact. This will alter the surface profile and cause the measured contact angles to change.
f. Once all the changes have been made for the new test, make sure to save them.

g. To set up the slide, take one of the copper clips and very carefully connect it to the center end of the slide (end with no bitumen). Hang slide from hook over probe liquid. Make sure slide is hanging level based on the surface of liquid.

h. Raise the platform the liquid is sitting on until it is almost touching the slide [6mm (1/4 inch) or less]. Ensure the slide and liquid are not allowed to touch. If you are not comfortable getting it that close then leave a larger gap. It will not affect the test, just prolong it. Ensure the slide is level with the probe liquid. This is very important for the test.

i. Replace cover on machine and wait until the slide has stopped moving before starting the test. Do not touch the machine or bump the counter while the test is running.

j. To start the test, click the Acquire Data button. The test will take 8 to 15 minutes depending on the height of the slide above the liquid.

k. After the test is done, record the advancing and receding angles along with the R^2 values for each in an Excel workbook.

l. The computer will default save all tests at the location where the last test was opened. So, the first test run will be saved in that folder. To make the program save the data in the folder you want, go to Open, see which folder the file was saved in, drag that file to your folder, and open it in the program. This should make the program save all subsequent files in your folder.